

TN 295

.U4

No. 9042





Bureau of Mines Information Circular/1985



Mine Subsidence Control

Proceedings: Bureau of Mines Technology
Transfer Seminar, Pittsburgh, PA,
September 19, 1985

Compiled by Staff, Bureau of Mines



UNITED STATES DEPARTMENT OF THE INTERIOR



BUREAU OF MINES TECHNOLOGY TRANSFER SEMINAR (1985:
" PITTSBURGH, Pa.)

Information Circular 9042

Mine Subsidence Control

**Proceedings: Bureau of Mines Technology
Transfer Seminar, Pittsburgh, PA,
September 19, 1985**

Compiled by Staff, Bureau of Mines



LCCN 85-600218

UNITED STATES DEPARTMENT OF THE INTERIOR
Donald Paul Hodel, Secretary

BUREAU OF MINES
Robert C. Horton, Director

TN295

.U4

no.9042

1930634

PREFACE

This Information Circular summarizes recent Bureau of Mines research aimed at improving technology for predicting and controlling mine subsidence. The four papers contained in this publication constitute a large portion, but not all, of the research being performed by the Bureau in this area.

The papers were presented at a technology transfer seminar on mine subsidence control in September 1985. Technology transfer seminars are sponsored frequently by the Bureau of Mines to direct the mineral industry's attention to research results that may be useful and helpful in solving problems. Those desiring more information about Bureau research programs should contact the Bureau of Mines, Branch of Technology Transfer, 2401 E St., NW, Washington, DC 20241.

CIP/BR 02 4 sec 85

8d0318 nov 85

CONTENTS

	<u>Page</u>
Preface.....	i
Abstract.....	1
Introduction.....	1
Longwall mine subsidence surveying--an engineering technology comparison, by Gary W. Krantz and John C. LaScola.....	2
Short-term effects of longwall mining on shallow water sources, by Noel N. Moebs and Timothy M. Barton.....	13
Comparison of the subsidence over two different longwall panels, by Paul W. Jeran and Timothy M. Barton.....	25
Precalculation of subsidence over longwall panels in the northern Appalachian coal region, by Vladimir Adamek and Paul W. Jeran.....	34

UNIT OF MEASURE ABBREVIATIONS USED IN THIS REPORT

cm	centimeter	mm	millimeter
deg	degree	mm/m	millimeter per meter
ft	foot	μm	micrometer
ft/d	foot per day	μmho/cm	micrometer per centimeter
gpm	gallon per minute	pct	percent
h	hour	ppm	part per million
in	inch	V ac	volt, alternating current
km	kilometer	V dc	volt, direct current
min	minute (time)	W	watt

MINE SUBSIDENCE CONTROL

Proceedings: Bureau of Mines Technology Transfer Seminar,
Pittsburgh, PA, September 19, 1985

Compiled by Staff, Bureau of Mines

ABSTRACT

This publication contains four papers presented at a seminar on mine subsidence control held in Pittsburgh, PA, on September 19, 1985. The seminar was designed to keep the mineral industry informed of new technology developed by the Bureau of Mines that permits reliable and accurate prediction of mine subsidence. The papers describe actual field studies undertaken by the Bureau to monitor surface subsidence over longwall panels. Topics discussed include the effects of subsidence on water table levels, the development of subsidence precalculation methodology suitable for use with the specific lithological conditions of the Pittsburgh coalbed, an engineering comparison of technologies used in surveying for longwall mine subsidence, and a comparison of the process of subsidence over two different longwall panels.

INTRODUCTION

To minimize damage caused by mining-related subsidence, a better understanding of the relationship between underground mining and subsequent surface movement is needed. Such an understanding, coupled with information gathered while researching this relationship, can be used advantageously by mine operators to predict when and where subsidence will occur. Mine subsidence prediction methods have been developed by European countries, but these methods are tailored to the mining and geologic conditions of those countries--conditions that often differ greatly from those of the United States. To fill the existing subsidence information and technology voids, the Bureau of Mines conducted in-depth research to develop techniques that permit accurate prediction of surface ground movements over underground mines. The investigation entailed an extensive data gathering effort to properly characterize the extent and nature of subsidence under various geologic conditions. Results of this research are presented in this Information Circular through four papers presented at a Technology Transfer Seminar on Mine Subsidence Control on September 19, 1985, in Pittsburgh, PA.

LONGWALL MINE SUBSIDENCE SURVEYING--AN ENGINEERING TECHNOLOGY COMPARISON

By Gary W. Krantz¹ and John C. LaScola²

ABSTRACT

A typical longwall mine subsidence survey monitoring grid was installed at the Bureau of Mines. Conventional and high-technology surveying systems, including an electronic distance meter-theodolite-level, (EDM-theodolite), an automatic recording infrared laser tacheometer, a global positioning system satellite

surveyor, aerial photography (photogrammetry), and a prototype inertial surveyor were developed over the grid during a 1-month period. A statistical analysis indicates that the average three-dimensional displacements from the base (EDM-theodolite) for both the tacheometer and photogrammetry were almost identical.

INTRODUCTION

This investigation evaluates and compares five surveying methodologies available for use in surface longwall subsidence monitoring. They include EDM-theodolite, tacheometer, and photogrammetry surveying. Inertial surveying systems are discussed, but an in-depth evaluation was impossible owing to on-site system failure.

Geodetic survey work is conducted to establish time-based deformational characteristics of the ground surface as the longwall mine face advances beneath. Surface monuments installed above the mine panel must be accurately and repetitively measured to determine the dynamic vertical and horizontal movements.

ACKNOWLEDGMENTS

The authors would like to acknowledge the assistance provided by the U.S. Army, Corps of Engineers, Huntington, WV, District and Ft. Belvoir, VA, Engineering Topographic Laboratory; Jan Stenstroem of Carl Zeiss, Inc., Thornwood, NY;

Geo-Hydro Inc., of Rockville, MD; the Tennessee Valley Authority, Chattanooga, TN; John W. Antalovich of Kucera & Associates, Inc.; Mentor, OH; and Robert M. Keddal of R. M. Keddal & Associates, Inc., Library, PA.

APPROACH

The purpose of this investigation was to compare conventional and high-technology geodetic surveying systems using a survey grid with physical characteristics typical of current longwall mine subsidence study sites. Since continued aberrant surface movement during the study would have masked the comparative measurements, the grid, as shown in figure 1, was installed on the Bureau of Mines Pittsburgh Research Center (PRC) grounds over a stable surface.

The grid was developed over gently rolling, well-drained topography with slopes approaching 30 pct and a maximum relief of approximately 150 ft (45 m). Figure 2 shows the grid layout on a topographic base map. The grid baseline, 1,750 ft (533.4 m) long, was oriented with two perpendicular cross profiles intersecting it at monuments 4+50 and 14+50. The profile at monument 4+50 is 1,200 ft (365.8 m) long; the other profile is 650 ft (198.1 m) long. This configuration is typical of actual subsidence grids since it allows cross-section capability both parallel and perpendicular to the direction of mining. The monuments were spaced every 25 ft (7.62 m)

¹Engineering geologist.

²Physical scientist.



FIGURE 1. - Aerial photograph of survey grid.

and consisted of 2-ft (0.6-m) sections of No. 5 reinforcement bars driven into the ground. Although the center of the grid was located in an open field, the ends of the baseline and profiles encountered thick vegetation.

Property boundaries forced control monument locations much closer to the grid than normal, but since the site was not being undermined, there was no danger of

subsidence alteration. The control monument coordinates were determined to a first-order accuracy horizontally, and to a second-order accuracy vertically.

The results and conclusions of this report should be interpreted in light of the prerequisites and requirements of surveying for this particular application.

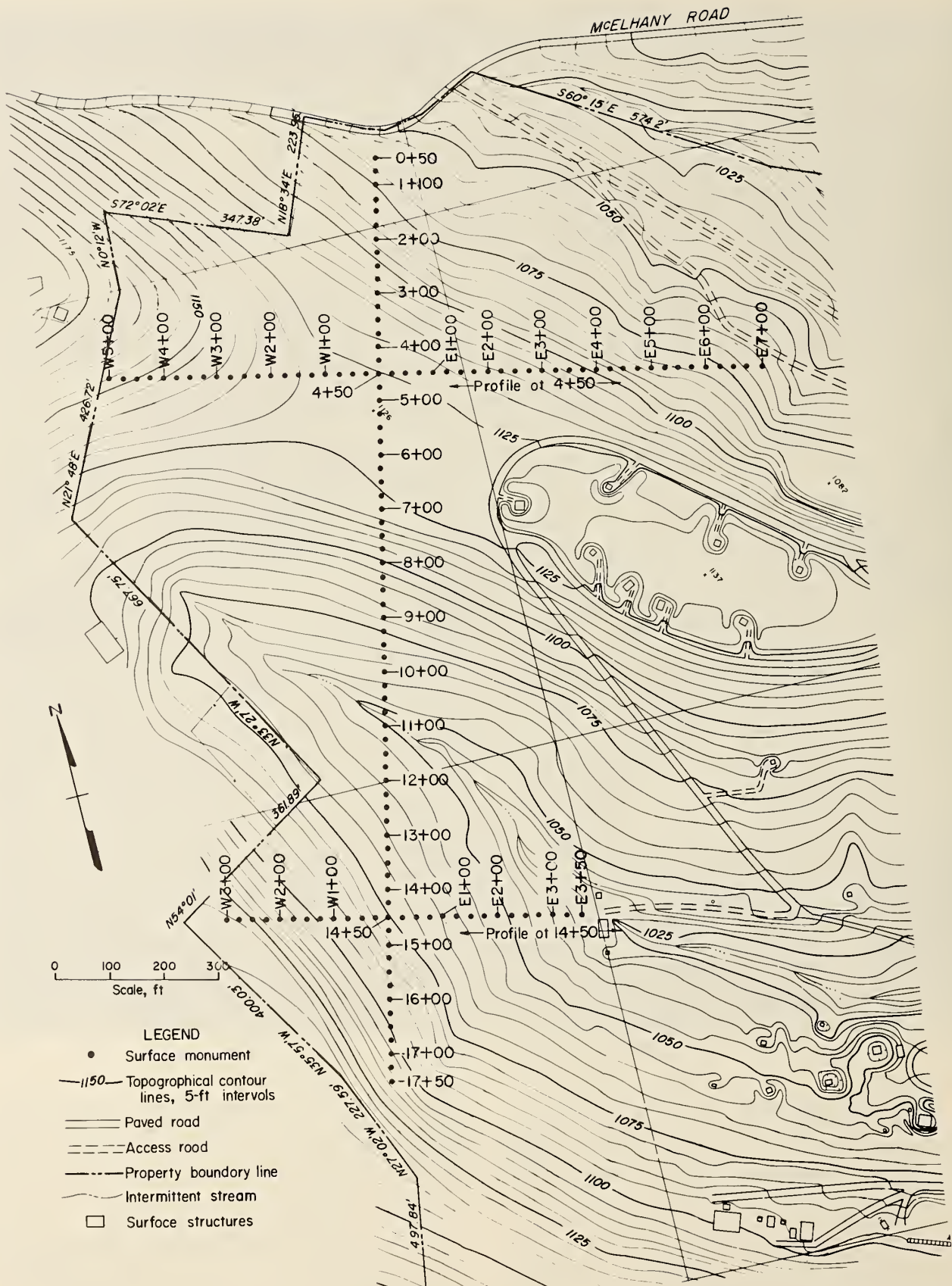


FIGURE 2. - Survey grid on topographic base map.

SURVEY STUDY

ELECTRONIC DISTANCE
METER-THEODOLITE-LEVEL SURVEY

The grid was installed using conventional optical alignment procedures and two different EDM-theodolite systems, a Wild T1-A³ and a Topcon GTS-2 semitotal station, plus a steel tape. All control and grid monuments were then surveyed with a precision (second-order) Zeiss NI-1 level. The field data were hand-tabulated. Computations were performed on a Radio Shack TRS-80 model 1000 micro-computer. The data were later transformed using global positioning values, a Hewlett-Packard HP41CX calculator, and a Stevenson Transformation software program.

The EDM-theodolite surveying system and equipment are extremely portable, rugged, and relatively simple to operate when used by a trained engineering surveyor. Strict field procedures and data tabulation (compilation) are required for precise work. Since the data are hand-tabulated and compiled, the human factor can result in error. In fact, an analysis of the grid data indicates that such an error may have occurred.

The grid was resurveyed with the EDM-theodolite after all other survey systems had been developed to detect any possible monument movements.

Environmental constraints imposed on the EDM-theodolite system are customary and standard. Windy, rainy conditions cause a variety of problems including lens fogging, survey rod movement, and hand tabulation errors. The EDM-theodolite is particularly susceptible to wet weather downtime, primarily in an effort to protect the system, and to heat turbulence on bright, clear sunny days.

SATELLITE-BASED GLOBAL
POSITIONING SYSTEM (GPS)

The NAVSTAR GPS is a space-based, worldwide, all-weather system designed to

provide extremely accurate three-dimensional navigational and/or positioning capability. Present plans call for the system to be fully operational in 1989 (1).⁴ The system, at that time, will consist of a constellation of 18 active space satellites, plus 3 or more passive satellites, orbiting approximately 20,000 km above the earth in 6 different orbital planes. When the entire constellation is in place, an observer any place on the earth will be able to receive signals from a minimum of four satellites at any time and determine his position instantaneously (2). At present, only 6 of the 18 satellites have been successfully placed in orbit.

The GPS receiver system demonstrated on the grid was the Macrometer interferometric surveying system, which is capable of receiving NAVSTAR satellite signals but is not capable of decoding the special military "P" and "S" codes. The system is advertised as having three-dimensional relative positioning capability to 5 mm over a 1-km baseline and 5 cm capability over a 10-km baseline with 2 h of recorded data. The system requires two or more receivers, one of which must be located over a precisely known survey control monument, and the other(s) located on unknown monuments or point(s). Survey points can be separated by considerable distances (miles) and do not have to be intervisible.

The GPS survey was performed on July 9 and 10, 1984. The survey was designed to accomplish three objectives:

1. Establish first-order horizontal and vertical control on the grid datum and four control monuments.
2. Establish coordinates on at least two randomly selected grid monuments for comparison with other survey data.
3. Perform repeat observations on a minimum of three monuments for comparison purposes.

³Reference to specific products does not imply endorsement by the Bureau of Mines.

⁴Underlined numbers in parentheses refer to items in the list of references at the end of this paper.

Unfortunately, repeat observation data were not provided by the contractor, although four monuments were occupied in more than one session.

The Macrometer Interferometric Survey System includes the field unit V-1000 receiver, a remote control-display unit, a DEC TU-58 tape drive, and an antenna assembly. The office-based equipment includes a P-1000 data processor, computer terminal (monitor), disk drive unit, and line printer. A unique, proprietary software package is provided with the system for data analysis. The field system requires power both from a 115-V-ac inverter and from high-amperage 12-V-dc batteries. The battery system must

provide constant power to the precision clock system and other systems. The entire system requires 350 W of power.

Approximately 2-1/2 h of observation time is required to secure first-order-accuracy data. The observation window, therefore, permitted each survey instrument to occupy two monuments per day since they were close enough to permit relocation of the receiver and antennae system within 15 to 20 min. The layout of the GPS survey is shown in figure 3.

A tripod is centered over the monument to be measured, and an optical plummet is used to precisely align and level the center of the antenna coupler over the center of the monument. An acrylic dome

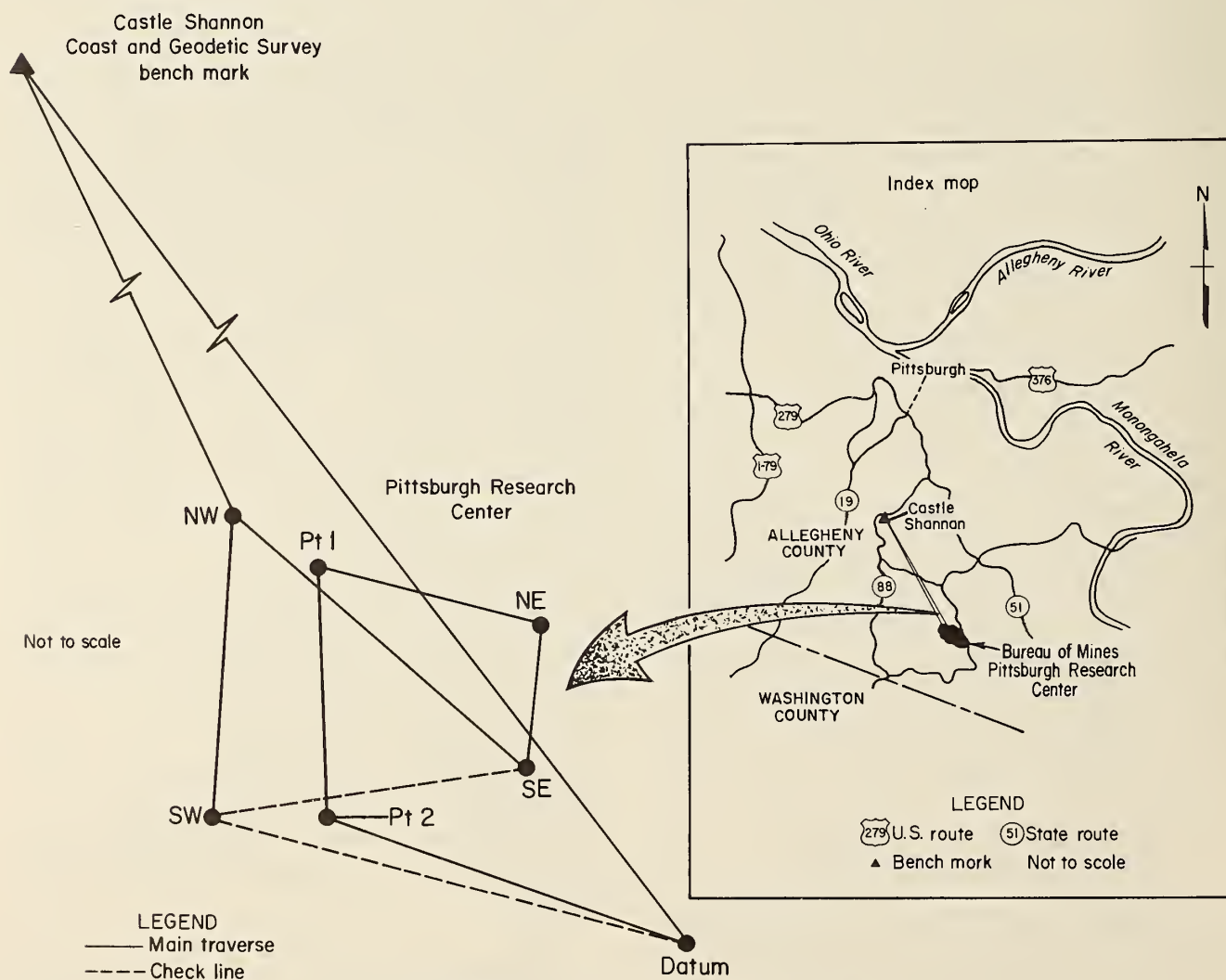


FIGURE 3. - Layout of the GPS survey.

protects the antennae from rain, dew, or frost without affecting the reception performance significantly.

Although the GPS survey control monument sites were very carefully selected so as to have open sky above a 20° zenith angle and within the azimuth range of the known satellite observation sectors, a loss of data on one control monument was reported by the contractor. The data loss also reportedly prevented the computation of individual survey session results from which repeat-reading comparisons could have been documented. Accordingly, the survey site selection process may be the system's primary environmental constraint. If the system can only be used in open fields, as was the case for three of the four subsidence grid control monuments, the constraint would seriously limit the use of the system for establishing subsidence survey control.

The GPS equipment apparently functions satisfactorily in rainy weather. Although light showers occurred during the survey, high winds, thundershowers, and lightning were not observed.

The high-amperage requirement of the GPS equipment and its sensitivity to temperature variations may impose a measure of environmental constraint. The system requires a stable ac power system plus massive batteries for the dc requirements.

AUTOMATIC RECORDING TACHEOMETER SURVEY

The automatic recording survey instrument used in measuring the PRC subsidence grid was a Zeiss Elta 2 electronic tacheometer with digital precision theodolite, electro-optical range finder, microcomputer, program module, and recording unit. The tacheometer was capable of computing, processing, and storing the x, y, and z coordinates of the monuments instantaneously as they were being measured, either in metric, feet, or survey "chains" format. Additionally, the zenith angle, slope distance, and horizontal azimuth could be recorded or computed into horizontal distance, direction, and difference in elevation and

then recorded. The smallest range finder display unit is 1 mm. Distances of up to 5 km can reportedly be measured in one shot.

Data acquired and computed in the field over the grid during the daytime were printed out in easting, northing, and elevation format within 1 h after collection. The tacheometer survey was performed July 24 and 25, 1984.

All of the raw data acquired during the survey were collected in an arbitrary "relative" positioning format. Since horizontal and vertical controls were not available at the time of the tacheometer survey, angular and vertical assumptions had to be made. Survey data transformation was later performed on the collected data using first-order GPS-acquired coordinates for two control monuments.

The data were transformed using a survey data transformation software package on a Hewlett Packard 9845B computer system, HP9885 flexible disk drives, and an HP2631B printer.

Owing to scheduling obligations, the tacheometer survey had to be terminated abruptly on the second day before a survey closure could be completed back to the point of origin. Had closure been completed, errors could have been spread out through the data points using computational procedures, rendering the final data slightly more precise than those contained in this comparative analysis. Another control monument was surveyed by the tacheometer as the last point measured in the lengthy traverse.

For a short period at the beginning of the survey, there were two reflector rodmen. Using two rodmen, the instrument operator was able to survey seven or eight monuments every 3 min. This rate includes instrument positioning on the reflectors and a rodman positioning on monuments in an open field.

The tacheometer system used had essentially the same environmental constraints as the EDM-theodolite, discussed previously. The system was repeatable and easy to operate when used by an experienced surveyor trained on the system. Since the system contains a sophisticated computer system, function setting, system

programming, and calibration are more involved than for conventional systems. The basic operational procedures, however, were straightforward, easily understood, and well labeled on the instrument. A person with basic surveying knowledge could produce accurate data with a minimum of instruction and training. The time required to survey the entire subsidence grid, consisting of 145 monuments plus the instrument traverse points, with 1 instrument operator and 1 rodman was approximately 14 h. Since each instrument move and/or setup in traverse mode requires precise leveling and adjustment, the selection of traverse instrument station locations is very important. Good selection of traverse stations for maximum grid monument visibility can result in rapid advancement of the survey. Poor traverse station selection can result in survey time increases. Data processing was performed immediately after data collection.

The important factor to consider when using the tacheometer is that human error involved in the computation is reduced essentially to zero. Hand tabulations or computations are not performed. Field errors can only be made if the instrument operator incorrectly sets a function or incorrectly tags a data point; in this case compiled data will be printed correctly but will be incorrectly labeled. One such error was made and easily detected.

On extremely clear, bright, hot, sunny days, the process of setting up, adjusting, leveling the instrument, and making readings across bright reflective surfaces was considerably more difficult and time consuming than on overcast cool days. These factors may be the most serious environmental constraints and are characteristic of laser surveying equipment. Other constraints that customarily apply to surveying equipment relate to the use of the system in windy, rainy weather.

AERIAL PHOTOGRAMMETRY SURVEY

Photogrammetry is frequently employed as a precise, noncontact measuring method

in geotechnical engineering and mining, particularly for measuring ground displacements such as subsidence.

Conventional survey methods commonly take days to gather data. Since subsidence is a dynamic phenomenon, during active periods it is possible to miss significant pieces of information by monitoring the surface as if it were static. Photogrammetric surveying eliminates this problem because all data are simultaneously recorded on photographs. The actual measurement process takes a certain amount of time, but since all the work is done on photographs, the surface conditions are frozen in time and the monument positions are computed for the instant of the photograph.

Photogrammetry offers two other advantages over conventional surveys under certain conditions. First, a survey can be conducted in remote, inaccessible areas without significant additional cost. However, a ground survey might be required to establish a few control points outside the subsidence area if no existing control data are available.

Second, the survey will provide much greater detail of the visible surface area. This offers two valuable options: the interpreter may use any visible, discrete natural object as a monitoring point whether originally planned or not; and the interpreter may utilize the techniques of remote sensing to determine the effects of subsidence on vegetation or other facets of the surface environment. This is possible because once the photographs exist, they can be reevaluated, remeasured, and checked for new information (3).

The survey was conducted on July 31, 1984. The plane was equipped with a Wild model RC-8 camera fitted with a 6-in-focal-length lens. To make the 1/2-in-diam rebar grid monuments visible from the air, reflective 13-in-diam disposable aluminum pans were installed over each monument. To make the photogrammetric analysis more accurate, the distance between the top of the rebar monument and its marker was measured and recorded for adjusting the elevations.

Aerial photographs were taken at 1,200, 3,000, and 6,000 ft. Photogrammetric analysis, however, was performed only on the 1,200-ft-elevation stereo photographs. The targets were observable on the 3,000- and 6,000-ft-elevation photographs but could not be measured to the same accuracy.

The analysis of the aerial photography was performed on a first-order-accuracy Matra Traster stereo plotter. The instrument has a reported 1- μ m interpretation accuracy in both horizontal and vertical directions. The system was interfaced with a Data General model 5/130 Eclipse computer. Coordinates for each target were read three distinct times using the system floating mark. The computer converts the Traster machine stage coordinates into precise ground coordinates.

Photo point coordinates can be read off stereo (60-pct overlay) photographs using a space coordinate system and either mechanically or mathematically intersecting the coordinate lines. Although mechanical intersection is performed in conventional mapping (stereoplotting), mathematical intersection or analytical aerotriangulation and/or stereocompilation can be performed. The analytical technique permits data refinement and statistical adjustment for extremely accurate photo point identification. Additionally the procedure permits error correction in camera calibration, film emulsion deformation, camera platen flatness, tangential lens distortion, atmospheric refraction, and earth curvature (3).

The primary environmental constraint in photogrammetric surveying is the ground visibility requirement. Obviously a point must be seen in the photograph if it is to be surveyed and its position computed. This necessitates clearing away any ground cover that might obscure the target from the air and making the target visible. Photogrammetric surveys must generally be conducted in early spring and late fall when ground cover is at a minimum. However, normal subsidence monitoring continues through all seasons.

In addition, photographs must be taken in a clear atmosphere and with a proper sun angle for exposure. The problem of target visibility is probably the limiting factor when deciding whether or not photogrammetry can be used (3).

INERTIAL SYSTEM SURVEY

The technology began in the early 1970's when the Department of Defense declassified an older version of an inertial navigation system used in early space ventures and in high-technology aircraft. Prototype inertial surveying equipment has been greatly improved and is now reportedly accurate enough for geodetic survey work over large traverses in rough terrain. The equipment is normally placed in four-wheel-drive surface vehicles; however, it can be flown in fixed wing or helicopter-type aircraft. The system is moved from established control points to unknown monuments and returned to the original control point or to a known second control point. The electrostatic gyro inertial system used was built by Litton. The system had been retrofitted with high-precision accelerometers for use in research and development by the U.S. Army Corps of Engineers Topographic Laboratories. The equipment permits survey data accumulation with only one operator.

The sources of noise or error can be assigned to three major categories: (1) accelerometer measurement error, (2) platform drift rate, or (3) environmental effects. Measurement errors associated with the accelerometer are induced by thermal or vibration effects during a survey traverse. Platform drift rate occurs because of vibration variations and thermal transients. Environmental noise includes variations in the earth's gravity field, temperature variations, and other causes (4).

The inertial surveying was conducted on October 3 and 4, 1984. Data obtained during the survey were erroneous, however, owing to system computer malfunctions. The system could not be repaired and was returned.

System accuracies have been reported to be in the range of 0.33 to 0.82 ft for horizontal components. Vertical accuracy has been reported to range from 0.03 to 0.39 ft (5).

OTHER HIGH-TECHNOLOGY SURVEY METHODS

A variety of other remote-sensing technologies have been used to detect and delineate mine subsidence (6). Studies conducted in the Northern Anthracite Coalfields of Pennsylvania included Earth Resources Technology Satellite imagery (ERTS-1), side-looking airborne radar

(SLAR) imagery, and multispectral scanner imagery for 11 spectral bands including thermal infrared, color, color infrared, and black and white photography. The multispectral scanning work was conducted to observe subsidence-related moisture patterns in bare soil areas. The aircraft imagery was used in the detection of faults, fractures, and other features related to subsidence. Since these techniques are not of sufficient accuracy or resolution to be useful for subsidence surveys, they will not be discussed further in this report.

SURVEY DATA ANALYSIS

Statistical analyses were performed for the EDM-theodolite, tacheometer, and photogrammetric surveys since the values of northing, easting, and height data were available for a majority of the monuments. The GPS system data, however, were not used because survey data were available for only a few select monuments. The EDM-theodolite data were used as the base for comparison because this is a most commonly used method for making subsidence measurements.

Since only a limited number of surveys were made using each type of system, the ultimate question of accuracy cannot be addressed as part of this study. However, the difference in monument positions can be examined. The statistical analyses were therefore performed on the difference in individual monument positions as identified by a survey method as compared to the base (EDM-theodolite). All statistical parameters were calculated using the absolute value of the differences. This approach was used because the sign of the difference in monument position relative to the base were

not nearly as important as the magnitude of the number. Furthermore, if the actual difference values are used, they tend to mask the real variation in monument position.

Various statistical parameters are shown in table 1. For the tacheometer survey comparison, the mean and its standard deviation of the northing values are approximately twice those of the easting values. However, for the photogrammetric comparison, the mean and its standard deviation of the northing and easting values are almost identical. While the tacheometer's mean elevation is 1/4 to 1/2 that of its horizontal values, the photogrammetric mean elevation is approximately 2 times its horizontal values. Furthermore, the photogrammetric elevation shows the largest mean and dispersion observed, approximately 4 times those of the tacheometer values. The total three-dimensional displacement from the base for both the tacheometer (0.25 ft) and photogrammetry (0.24 ft) is almost identical.

SUMMARY AND DISCUSSION

A typical longwall mine subsidence survey grid was installed over stable ground to compare conventional and high-technology survey systems. Five systems were employed: inertial, GPS, EDM-theodolite, tacheometer, and photogrammetry. Highlights of the systems follow:

Inertial - Extremely portable in that it can be placed in surface vehicles and aircraft. Sources of error include accelerometer measurement caused by thermal effects, platform drift rate caused by vibration variations and thermal transients, and environmental effects such as

TABLE 1. - Statistics on the absolute value of the difference in measurements

Statistic	Northing	Easting	Vertical
TACHEOMETER-THEODOLITE			
Count (N).....	138.00	138.00	138.00
Sum.....	31.58	12.12	6.53
Mean.....	.23	.09	.05
Standard error of the mean.....	.01	.01	.00
Median.....	.22	.08	.05
Variance.....	.01	.00	.00
Standard deviation.....	.09	.06	.04
Maximum.....	.51	.34	.44
Minimum.....	.08	.00	.00
Range.....	.43	.34	.44
Skewness.....	1.08	1.24	5.83
Kurtosis.....	1.00	2.44	52.66
PHOTOGRAMMETRY-THEODOLITE			
Count (N).....	127.00	127.00	127.00
Sum.....	12.22	10.97	25.64
Mean.....	.10	.09	.20
Standard error of the mean.....	.01	.00	.01
Median.....	.09	.07	.17
Variance.....	.00	.00	.03
Standard deviation.....	.07	.05	.16
Maximum.....	.25	.26	.67
Minimum.....	.00	.00	.00
Range.....	.25	.26	.67
Skewness.....	.32	.55	.94
Kurtosis.....	-.98	-.26	.22

variations in the earth's gravitational field and temperature variations. Survey data could not be used in this study owing to computer malfunction.

GPS - When completed, will be able to determine receiver position instantaneously. Constraints are the high amperage required to power the field system and sensitivity to temperature variations and site selection. This system was used to accurately determine the position of the control monuments, but the expense and time required to survey precluded its use over the entire grid.

EDM-theodolite - Portable, rugged, and relatively simple to operate. Sensitive to windy and/or rainy conditions and subject to errors due to hand tabulations and computations. Utilized as the base for this comparison because it is the

most commonly used method for making subsidence measurements.

Tacheometer - Completely automated for rapid recording, computing, and data generation. Subject to the same environmental constraints as the theodolite system.

Photogrammetry - Can be used for inaccessible areas. All data are gathered simultaneously, providing a permanent photographic record that can be reevaluated. Surveys cannot be conducted during inclement weather, data for control points must be available, and targets must be visible on the photographs.

A statistical analysis indicates that the three-dimensional displacements from the base (EDM-theodolite) were almost identical for the tacheometer and photogrammetry.

REFERENCES

1. Hothem, L. D., and C. J. Fronczek. Report on Test and Demonstration of Macrometer Model V-1000 Interferometric Surveyor. Fed. Geod. Control Comm., Rep. 15-83-2, May 1983, 36 pp.
2. Collins, J. A Satellite Solution to Surveying. Prof. Surv., Nov.-Dec. 1982, pp. 13-17.
3. Sendlein, L. V., Y. Hasan, C. L. Carlson, and K. R. Herbert (eds.). Surface Mining Environmental Monitoring and Reclamation Handbook (U.S. Dep. Energy, Asst. Sec. Energy Tech., Off. Coal Mining, contract DE-AC-2280-ET-14146). Elsevier, 1980, 750 pp.
4. Huddle, J. R. Theory and Performance for Position and Gravity Survey With an Inertial System. J. Guidance and Control, v. 1, No. 3, May-June 1978, pp. 183-188.
5. Roof, E. F. Inertial Survey Applications to Civil Works. U.S. Army Corps Eng., Eng. Topog. Lab., ETL-0309, Jan. 1983, 63 pp.
6. Earth Satellite Corp. (Washington, DC). Use of Photo Interpretation and Geological Data in the Identification of Surface Damage and Subsidence. Appalachian Reg. Comm. Rep. ARC-73-111-2554, 1973 (final rep. 1975), 113 pp.

SHORT-TERM EFFECTS OF LONGWALL MINING ON SHALLOW WATER SOURCES

By Noel N. Moebs¹ and Timothy M. Barton²

ABSTRACT

The Bureau of Mines monitored surface subsidence, water table levels, and stream flow above a longwall panel in southwestern Pennsylvania, for about 6 months prior to mining and 12 months afterward. Only water levels within the boundary of the longwall showed a

precipitous decline as a result of mining. Water levels 500 ft or more outside the panel rib line were unaffected. No evidence of mining effects on the small streams or springs located within 1,200 ft of the panel was detected.

INTRODUCTION

Federal regulations controlling subsidence are intended to ensure that underground mining is conducted so as to protect the health and safety of the public, minimize damage to the environment, and protect the rights of landowners (1).³ These regulations furthermore require the applicant for a mining permit to "...identify the extent to which the proposed underground mining activities may proximately result in contamination, diminution, or interruption of an underground or surface source of water within the proposed mine plan or adjacent area for domestic, agricultural, industrial, or other legitimate use" (2).

This is not easily accomplished because of the lack of documented quantitative information regarding the effects of underground mining on surface or underground sources of water. Throughout the northern Appalachian bituminous coal region, numerous instances of springs, streams, or domestic wells going dry because of underground coal mining have been reported, but without documentation or allowances for the effect of seasonal changes or precipitation.

Two recent studies, however, have provided some urgently needed information on the relation between mining and ground

water resources. The first study, by Owili-Eger (3), was conducted in the Dunkard Basin of the northern Appalachian bituminous coal region. The effects of longwall mining on well yields and water quality were assessed, and conclusions were reached as follows:

1. Water levels in aquifers located at least 330 ft above the mine horizon usually recovered after mining.
2. There was a general lowering of the piezometric levels.
3. There was no major lasting deterioration in the quality of ground water systems studied.

In a second study, Hill, Burgdorf, and Price (4) monitored the short-term effects of longwall mining on ground water aquifers in western Pennsylvania. Eleven wells ranging in depth from 75 to 250 ft were monitored. Some of the general conclusions resulting from this study follow:

1. Only minor water level declines of 12 to 31 ft occurred in shallow wells less than 100 ft in depth. Water levels rebounded to near premining levels within 2 months after the face had passed beneath a well.
2. Water level declines of 20 to 211 ft occurred in wells 160 to 250 ft deep. The most precipitous water level declines occurred during the 2- to 3-week period of maximum surface subsidence, when the face still was less than 200 ft beyond a well.
3. Water level declines were greater over the center of the longwall panel than near the edge or beyond.

¹Geologist.

²Mining engineer.

Pittsburgh Research Center, Bureau of Mines, Pittsburgh, PA.

³Underlined numbers in parentheses refer to items in the list of references at the end of this paper.

The diminution or interruption of water sources, especially of shallow domestic wells, springs, and small streams, has occurred largely as a result of room-and-pillar mining, which accounts for about 93 pct of all underground coal production in the Appalachian region. However, longwall mining, a more uniform method of extraction, is providing an increasing portion of underground coal production, and interest in environmental effects and damage prevention is shifting toward this method.

In rural areas, such as much of the northern Appalachian coal region, the degree of subsidence damage to frame structures generally is not as devastating as even a temporary loss of water sources, especially in farming. While a certain amount of water can be hauled for household use, the requirements for watering farm animals or washing are substantial and heavily dependent on a local supply. Therefore, it is essential that the effects of mining on local water supplies can be assessed and general predictive guidelines developed.

Cautions must be exercised, however, in applying general conclusions drawn from disparate results to specific mining situations, for as Waite (5) admonishes "...there really is no such thing as a 'typical' underground coal mine. Individual mines, even in close proximity to one another, often exhibit dramatic differences in relation to ground water." It is highly probable, also, that no two individual water wells, even in close proximity, will respond identically to mining and subsidence.

The Bureau of Mines currently is monitoring surface deformations over longwall panels as part of a long-range program to improve the prediction of longwall subsidence and ultimately to control damage to surface structures. At one longwall

monitoring site in southwestern Pennsylvania (fig. 1), where the first longwall panel in the area was mined, the Bureau also arranged for the measuring of water levels in five 6-in-diam wells, each drilled to a depth of 150 ft. These wells were located along a survey monitoring profile which extends from the centerline of the longwall panel, where the first well is located (fig. 2), to a distance of 1,270 ft outside the rib line, where the outermost hole was located.

The purpose of this study was to determine the short-term effects of mining the longwall panel on the water levels in the five wells, which were intended to simulate a fairly typical domestic water well in the region. Wells of this depth (150 ft) penetrate the shallow water table aquifer but do not reach any of the deeper confined aquifers. The term "water table" is used here to designate the surface below which the overburden is saturated. The water table aquifer extends from the water table down through the saturated zone to the first layer of relatively impermeable rock that does not transmit ground water rapidly enough to supply a well or spring. In the Appalachian region water wells rarely are drilled to the several-hundred-foot depths where the deeper aquifers occur because these aquifers commonly are of very low yield and may be highly saline in character.

Weekly measurements were made of water levels in the five wells, and weirs were installed on three small streams and one spring in the vicinity of the longwall panel for measuring flow rates.

The long-term effects of mining, such as the postmining recovery of water levels, will be reported later, along with an assessment of the effects of mining an adjacent longwall panel.

ACKNOWLEDGMENTS

The author is grateful for the cooperation of EMway Resources Inc., operators

of the mine, and to landowners Carl E. Tustin and John T. Gaskill.

SITE DESCRIPTION

The study site at which the water sources and subsidence were monitored is

is near Waynesburg, Greene County, PA, in the hilly terrain typical of the

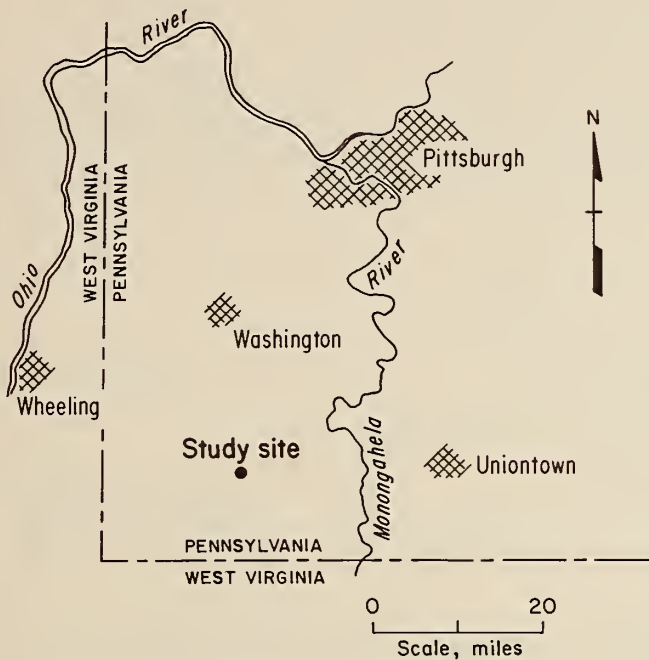


FIGURE 1. - Index map.

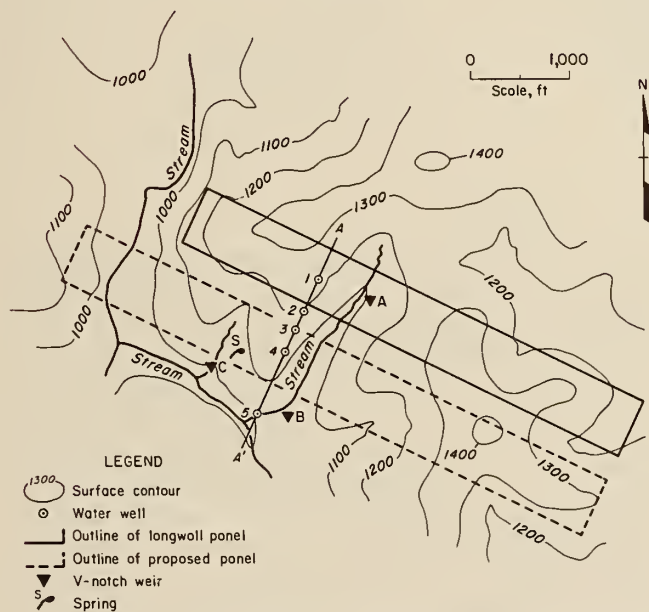


FIGURE 2. - Surface features and longwall panel.

Appalachian Plateau province. Land use is chiefly for grazing and hay crops; very little is wooded. Bedrock at the site is overlain by 7 to 11 ft of residual soil consisting of clay and weathered shale fragments. There is evidence of

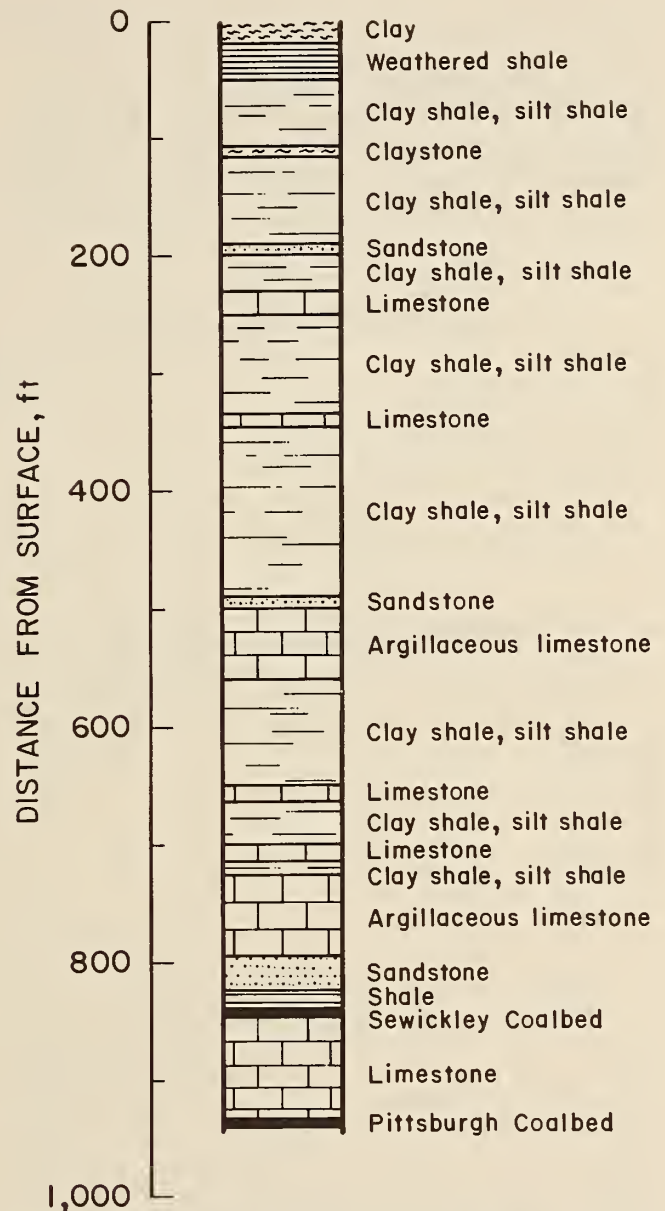


FIGURE 3. - Generalized columnar section.

weathering in the bedrock to a depth of about 50 ft.

The geologic character of the strata in the overburden is shown in figure 3 and consists of interbedded clay shale, silt shale, claystone, limestone, sandstone, and coal. Mine overburden above the Pittsburgh coalbed ranges from 750 to 1,000 ft thick, and the strata dip about 1° SE.

SITE MONITORING

All measurements of surface deformations above the longwall panel were conducted by a local commercial firm familiar with the site. These surface deformations are summarized in transverse

profiles (fig. 4), in longitudinal profiles (fig. 5), and as the final subsidence contours in the vicinity of water wells 1-4 (fig. 6).

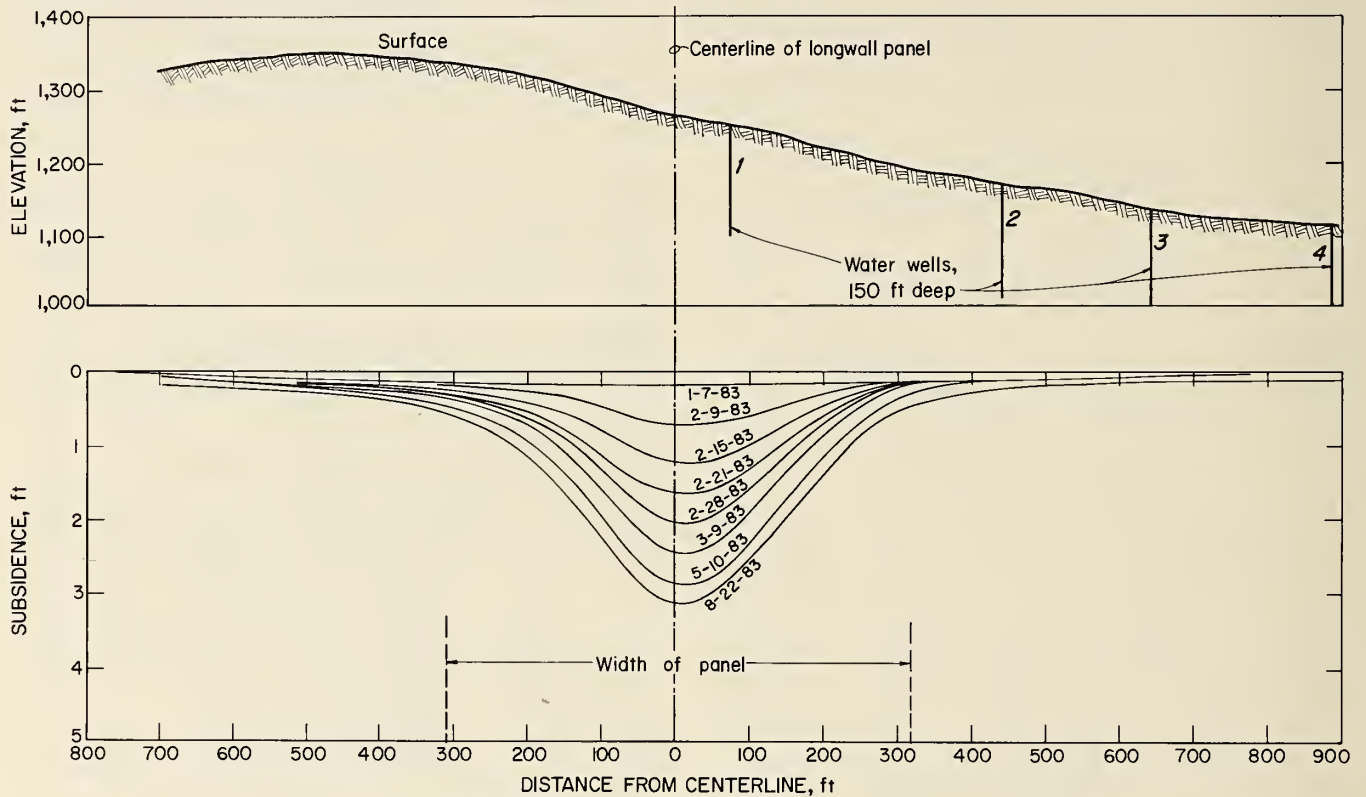


FIGURE 4. - Transverse subsidence profiles.

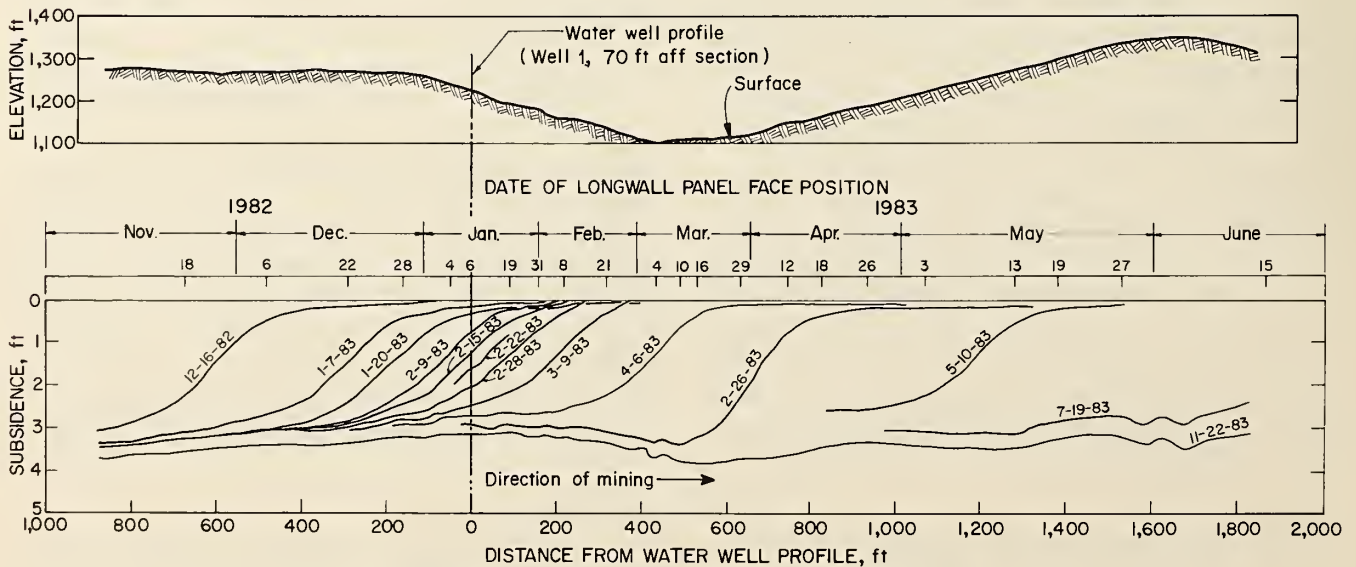


FIGURE 5. - Longitudinal subsidence profiles.

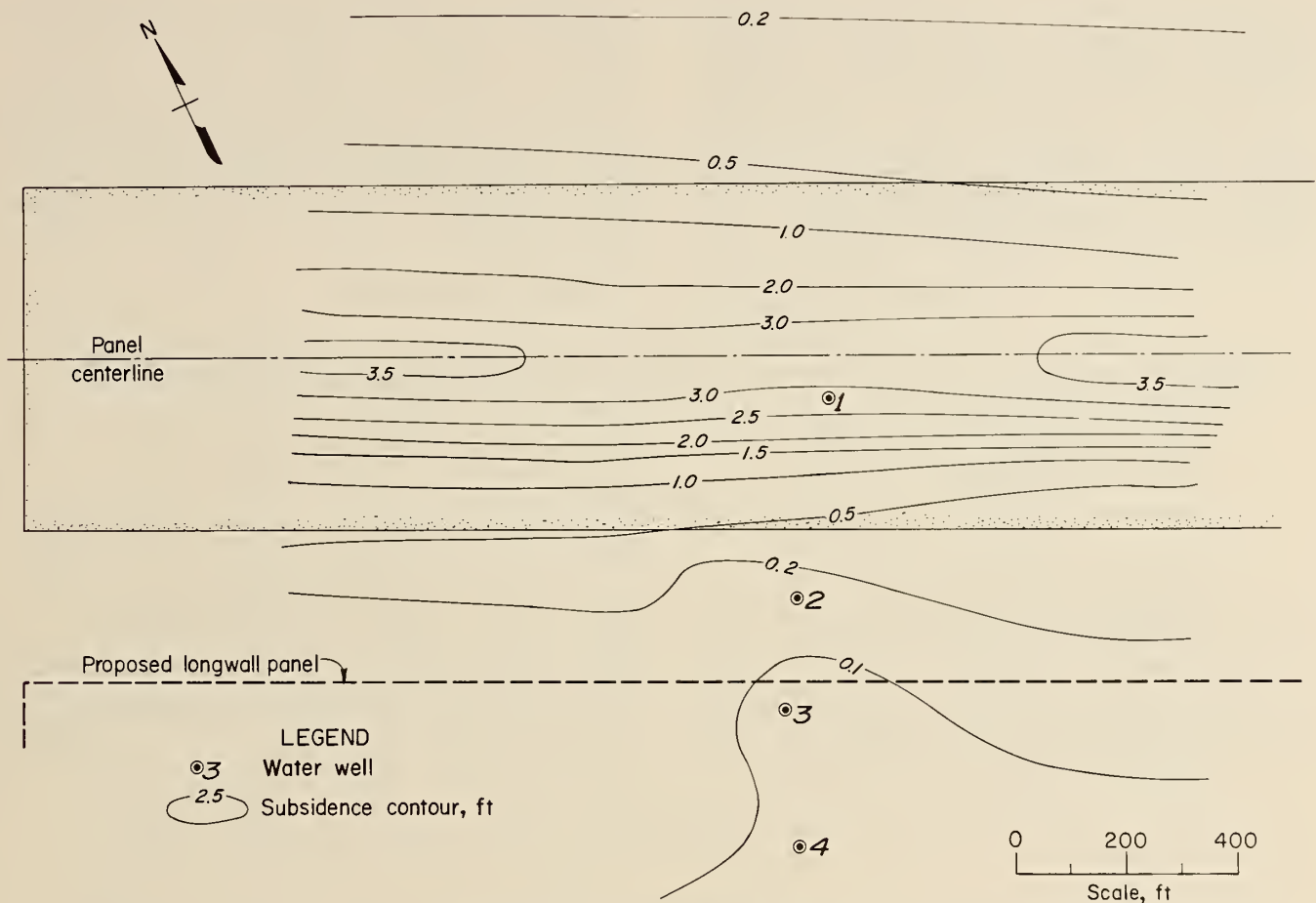


FIGURE 6. - Subsidence contours.

Measurements of water levels in the five water wells and flow rates at the three weirs and one spring were conducted by the Bureau on a weekly schedule as nearly as possible. It is recognized that, ideally, observations to establish premining hydrologic conditions should be conducted for a full year to determine seasonal variations. This, however, was impossible to accomplish at this site, and hence observation water well records in the vicinity were examined for seasonal variations. The wells on the site

were completed as soon as possible, in the second quarter of 1982, the water levels were allowed to stabilize for several weeks, and regular measurements were begun in July 1982.

Weirs A and B were installed in May 1982, and weir C in January 1983. Measurements of the spring overflow were initiated in May 1982. This information on surface water sources was compiled to supplement that obtained from the water wells.

WELL WATER QUALITY

Water samples were bailed from each of the five water wells at the study site prior to mining of the longwall panel. These samples were analyzed, and the results are shown in table 1.

The analysis of well water samples collected about 12 months after mining had reached the profile is shown in table 2.

It is apparent from comparing tables 1 and 2 that there is no pronounced change in overall water quality between premining and 1 year after the longwall face passed the water well profile. In each well the pH has increased slightly and the alkalinity has decreased a small amount. The dissolved solids changed

very little; some increased and some decreased slightly. These minor changes could be natural variations, or could be attributed to a lowered water table, the effects of cascading⁴ and a fluctuation in water level, or possibly altered channels of flow in the overburden as a result of the subsidence process. No

correlation could be made between water quality and the water levels in the wells.

⁴Cascading is ground water entering a water well above the water level in the well, indicating a hydraulically unstable condition.

TABLE 1. - Well water analyses, premining

	Well 1	Well 2	Well 3	Well 4	Well 5
Analysis, ppm:					
Alkalinity as CaCO ₃	211	207	252	176	218
Calcium as CaCO ₃	245	184	197	157	101
Chloride as NaCl.....	17	17	23	12	29
Chromium as Cr.....	0.2	0.2	0.2	0.2	0.2
Dissolved solids.....	502	207	252	176	218
Ferrous iron as Fe.....	0.4	1.2	ND	ND	0.7
Manganese as Mn.....	0.1	0.2	0.2	0.1	0.1
Magnesium as CaCO ₃	80	94	80	43	38
Nickel as Ni.....	ND	ND	ND	ND	ND
Nitrate as NO ₃	1.0	1.6	2.4	2.5	4.4
Potassium as K.....	2	2	2	2	2
Sodium as Na.....	13	11	12	21	53
Sulfate as SO ₄	101	57	48	62	12
Total iron as Fe.....	0.4	1.2	0.4	0.7	0.7
Zinc as Zn.....	0.5	0.2	0.1	0.1	0.2
pH.....	6.8	7.0	7.0	7.4	7.3
Specific conductance.....µmho/cm..	410	600	600	350	560

ND Not detected.

TABLE 2. - Well water analyses, postmining

	Well 1	Well 2	Well 3	Well 4	Well 5
Analysis, ppm:					
Alkalinity as CaCO ₃	161	164	162	166	193
Calcium as CaCO ₃	195	155	155	176	117
Chloride as NaCl.....	20	25	25	33	45
Chromium as Cr.....	ND	ND	ND	ND	ND
Dissolved solids.....	386	236	210	250	256
Ferrous iron as Fe.....	ND	ND	ND	ND	ND
Manganese as Mn.....	ND	ND	ND	ND	ND
Magnesium as CaCO ₃	88	62	50	36	38
Nickel as Ni.....	ND	ND	ND	ND	ND
Nitrate as NO ₃	2.1	2.2	1.7	2.5	1.8
Potassium as K.....	ND	ND	ND	ND	ND
Sodium as Na.....	9	8	7	17	41
Sulfate as SO ₄	89	41	36	48	29
Total iron as Fe.....	1.3	0.2	0.2	0.2	0.3
Zinc as Zn.....	ND	ND	ND	ND	ND
pH.....	7.9	7.4	7.4	7.5	7.7
Specific conductance.....µmho/cm..	440	440	390	440	450

ND Not detected.

ANALYSIS OF RESULTS

Figure 7 illustrates the general situation along profile A-A' of figure 2, including the amount of surface subsidence and the depression of the water levels (water table) that occurred after the longwall panel had been completely extracted. Figure 8 illustrates the relation of well water levels with respect to longwall face advance.

The most pronounced surface effect from the mining is the formation of the subsidence trough with a maximum subsidence of 3.4 ft. Analysis of survey data indicates a 15° angle of major surface deformation and a 24° angle to the limit of detectable surface deformation (commonly referred to as the angle of draw).

The most pronounced effect of mining on the water table aquifer was indicated by well 1, which went dry, and by wells 2 and 3, in which the water levels dropped 10 and 25 ft, respectively. It is noteworthy that water levels in wells

4 and 5, located beyond the 24° limit of surface deformation, were unaffected by the mining.

The effects of mining, if any, on the streams and spring in the vicinity of the longwall panel (fig. 2) were not detectable over the short term of this study, partly because of normal seasonal variations.

Further details on the results of monitoring the wells, streams, and spring are discussed in the following sections.

WATER WELLS

Well 1

After remaining fairly stable for a month after monitoring began, the water level in well 1, located near the centerline of the longwall panel (fig. 2), began an unexplained rise in late August 1982 (fig. 9), when the longwall face was

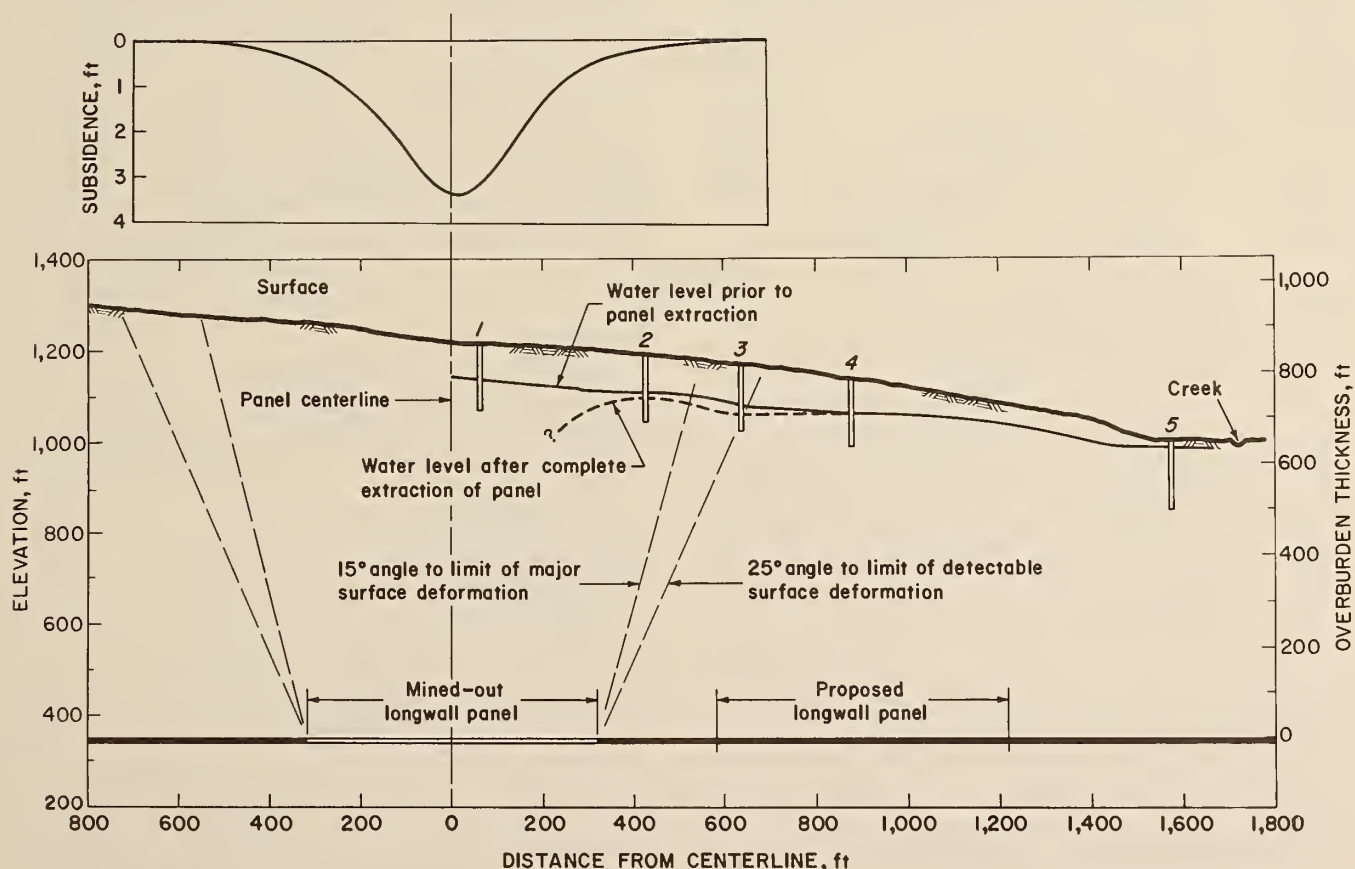


FIGURE 7. - Subsidence and water well profiles.

DISTANCE OF FACE FROM
WATER WELL SECTION, ft

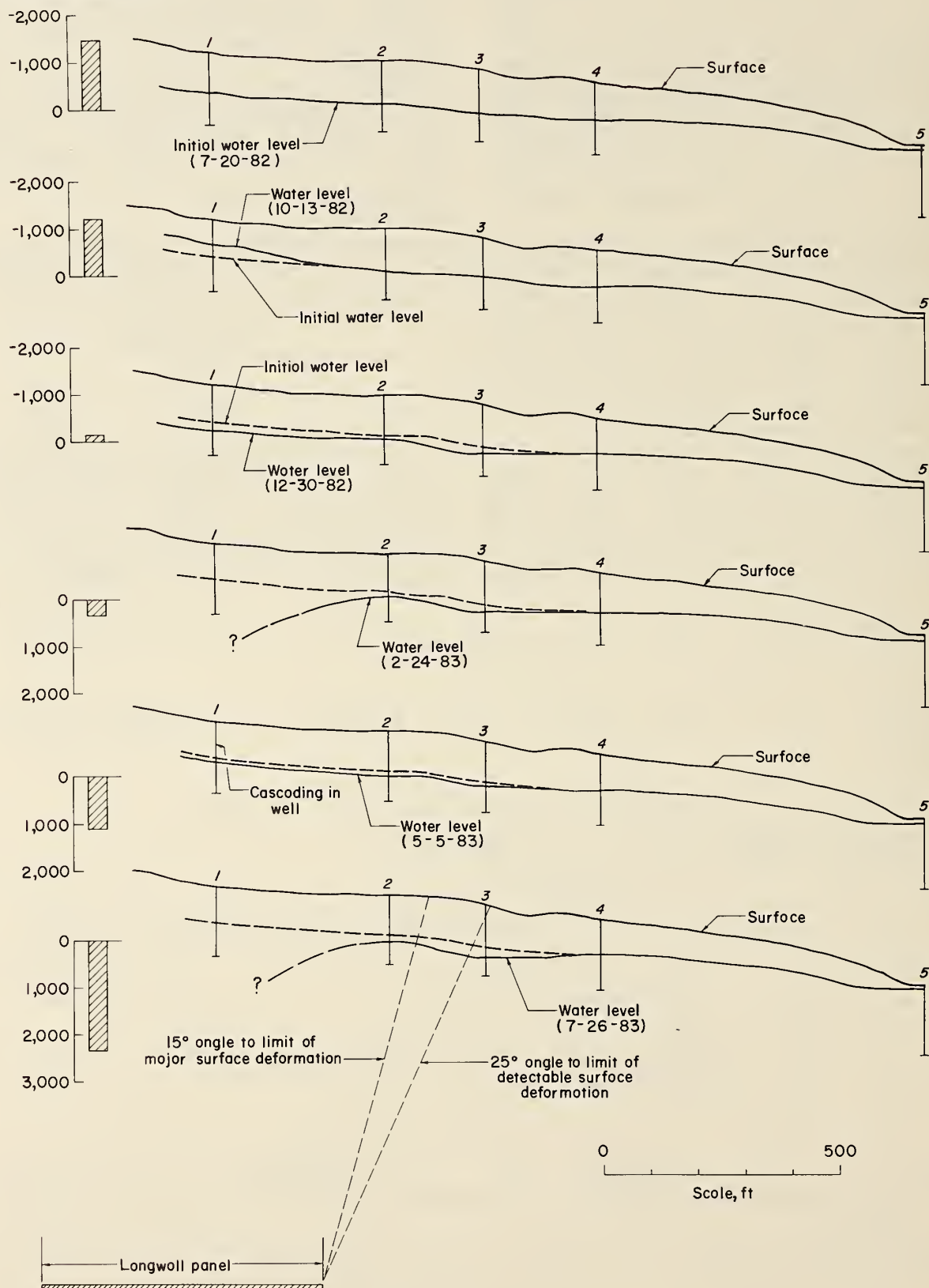


FIGURE 8. - Relation of water levels to longwall face advance.

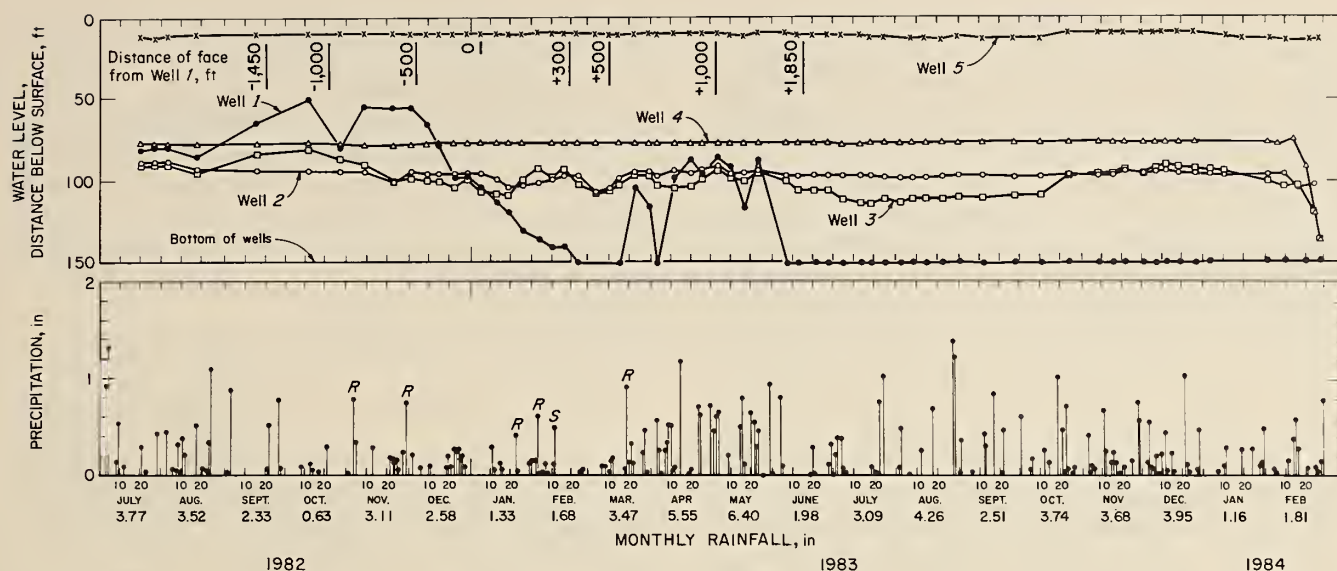


FIGURE 9. - Graph of water well levels. Significant precipitation during the winter months is designated as either rain (R) or snow (S).

over 1,450 ft away and mining had not yet begun. This rise continued for 3 months. A similar but less pronounced rise was detected in well 3. The rise cannot be explained by precipitation, which was below average for the 3-month period, nor can it be attributed to seasonal effects because in this region stream and water table levels generally continue to decline through October and sometimes November. This is because of the high evapotranspiration rates prevailing in the summer and fall.

A declining trend began about December 2, 1982, when the longwall face was 500 ft from the well. This trend continued for 3 months to February 24, when the well went dry. At this time the longwall face had progressed to 400 ft past the well.

It is worth noting at this point that at this study site the first detectable surface subsidence commonly occurs when the face has approached to within 500 to 700 ft of a survey monument, and the first major surface subsidence, defined here as 10 pct of maximum subsidence, occurred when the face was about 200 ft from the monument (fig. 10). These relations are a function of the character and thickness of the overburden and the thickness of the coalbed and vary from site to site.

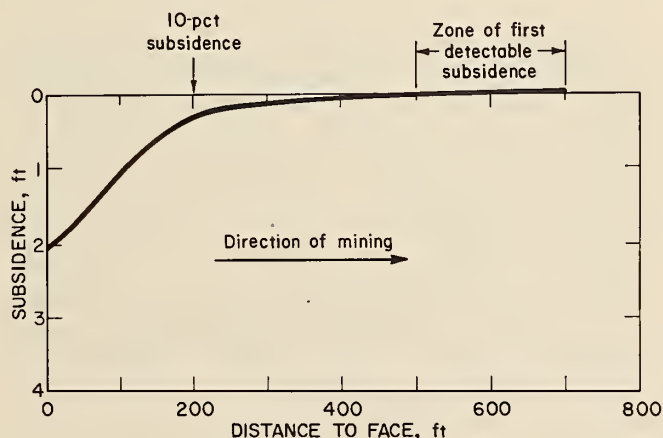


FIGURE 10. - Longitudinal subsidence profile.

At this site, then, both the land surface and the water table showed the first detectable effects of mining when the longwall face had approached to within 500 ft. At 200 ft, 10 pct of maximum subsidence had occurred and the water level in the well was falling at a rate of 1.6 ft/d.

Well 1 went completely dry on February 24, 1983, and remained dry for 3 weeks. Cascading then occurred, and water levels rebounded for about 2-1/2 months, finally dropping below the well bottom and remaining there for the remainder of 1983.

Well 2

The water in well 2, located over the chain pillars 440 ft from the longwall panel centerline (fig. 2), remained at a relatively constant level throughout most of the monitoring. Some minor fluctuations occurred for an interval of 4 months from January 6, 1983, when the longwall face was directly even with the well profile, to May 10, 1983, when the face had progressed 1,250 ft past the well profile (fig. 5). These fluctuations probably can be attributed to mining because wells 4 and 5, located much farther away from the panel (fig. 7), remained unchanged for the same interval (fig. 8). Also, well 2 lies within the 15° angle of major deformation where some effects were anticipated.

Well 3

The water level in well 3, located 320 ft beyond the rib line of the longwall panel (fig. 7), was unstable throughout most of the 17-month interval of monitoring from July 1982 to December 1983 (fig. 9). Water levels varied up to 33 ft. While no pronounced effects could be attributed with certainty to mining, water levels during the interval of January 6 to May 10, 1983, were somewhat more unstable than at other times. Also, well 3 was within the 24° angle of detectable surface deformation, so that some effects were anticipated.

The low level of June 8 to October 25, averaging 110 ft below the surface, can be attributed to the summer season effects of high evapotranspiration, after which the levels recovered to premining levels of about 90 ft.

Wells 4 and 5

Wells 4 and 5 are located 580 ft and 1,270 ft, respectively, outside the rib line of the longwall panel and 230 ft and 920 ft, respectively, beyond the 24° limit of detectable surface subsidence (fig. 7).

Neither well showed any detectable seasonal or mining effects. Water levels

remained stable throughout the 17 months of monitoring (fig. 9).

Precise comparisons of results of this study with those of a similar test site, such as that described by Hill, Burgdorf, and Price (4), should be avoided. Nonetheless, general similarities in the water level depression resulting from longwall mining were noted in three wells at each site, as follows:

Well location	Water level depression, ft	
	Bureau site	Other site
Near panel centerline	-150 (dry)	108-211
Outside panel:		
350 ft.....	-21	-14
1,250 ft.....	0	Nap
4,000 ft.....	Nap	0

Nap Not applicable.

The comparison of wells near the margins of the panels at these sites yielded only erratic results.

STREAMS

One very small perennial stream flows across the longwall panel about 450 ft southeast of the monitoring profile A-A' (fig. 2). The stream flow rate was measured at two points, weir A and weir B, to establish flow rate characteristics and to detect the effects of mining.

The most outstanding features of the hydrograph for weir A (fig. 11) are the sharp peak flows of February through May and November through December 1983, characteristic of winter and early spring seasons when evapotranspiration is low and infiltration rates are high. Between peak flows a base flow of about 1 gpm was measured for mid-June to mid-November 1983 due to high evapotranspiration. While the peak flows of February through May 1982 might have obscured any effects from mining activity, which brackets that interval (fig. 11), similar peaks recur in November through December 1983, indicating the response of the stream to similar episodes of precipitation is about the same and the effects of mining must be minimal.

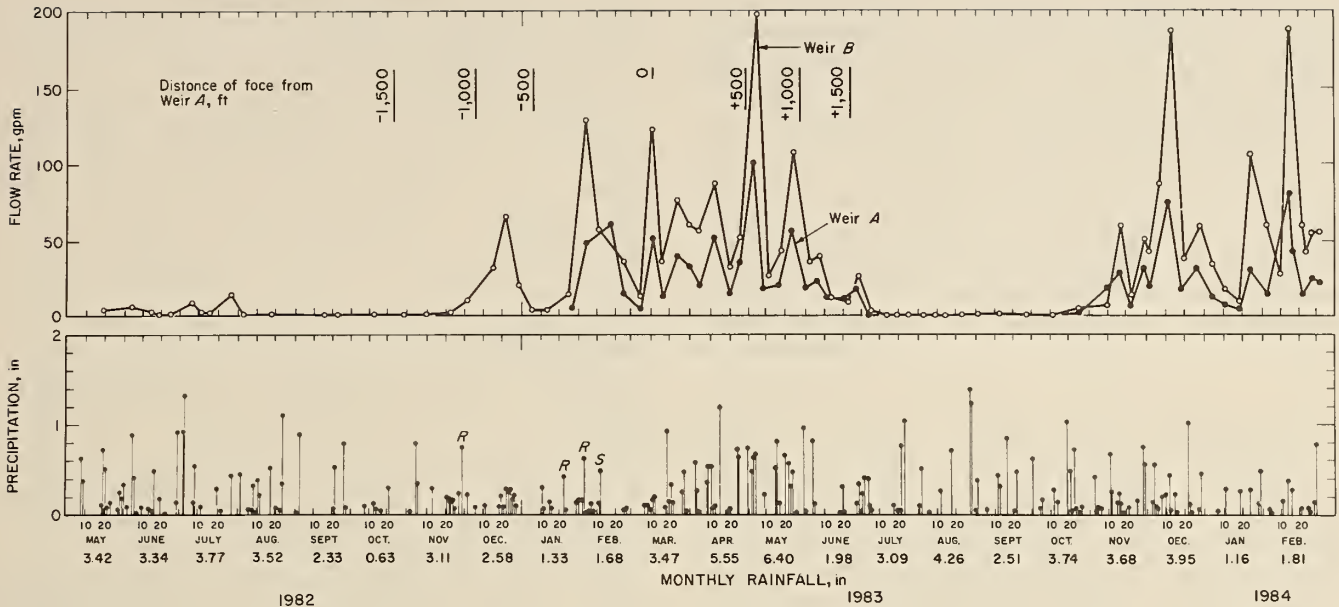


FIGURE 11. - Hydrograph at weirs A and B. R = rain; S = snow.

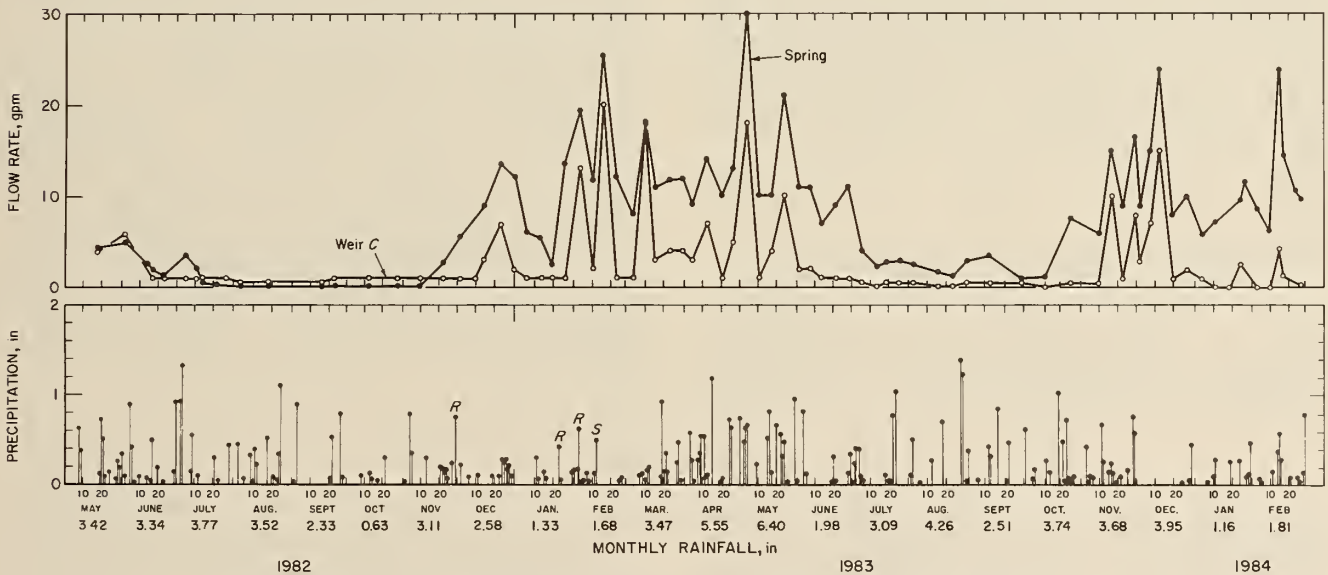


FIGURE 12. - Hydrograph at weir C and spring. R = rain; S = snow.

Weir B was located 1,450 ft downstream from weir A (fig. 2) and 1,100 ft outside the longwall panel rib line. The hydrograph for weir B is similar to that for weir A except that the peak flows are higher owing to minor augmentation along the 1,450-ft course between the two weirs and to more extended premining measurements. As with weir A, it was anticipated that some change in flow rates due to mining might be detected; however, the

only apparent changes are those easily attributed to seasonal effects. Thus, to date, no loss of flow rate due to mining in the source area can be determined at either weir A or B.

Another very small perennial stream located 600 ft off the monitoring profile A-A' and well outside the panel was monitored by weir C (fig. 2) for flow rate background data. The source area seepages that feed this stream probably

are far enough outside the panel to be free from any pronounced subsidence effects. This seems to be confirmed by the hydrograph (fig. 12), which shows the well-established cycle of peak flows during the winter-spring season of high infiltration and the low flow rates of the summer-fall season of high evapotranspiration. No effects of the mining and subsidence in the source area could be detected.

SUMMARY AND CONCLUSIONS

This report has described the short-term effects of mining a longwall panel on water resources in the immediate vicinity. Monitoring of these effects continued for about a year after the longwall face had passed the profile along which surface deformations and the water levels in five observation wells were measured. Two very small streams and a spring located in the vicinity were monitored to establish flow rate characteristics. This study was conducted under specific conditions existing at the site. The findings are not applicable to areas having different topography, geology, and hydrology.

The results of this study, while short term only, support the following conclusions:

1. Water levels in a 150-ft-deep well located near the centerline of the panel began to decline when the longwall face had approached within 500 ft of the well. The water levels continued to fall, and

A spring located about 400 ft north-east of weir C (fig. 2) was monitored to determine the flow rate characteristics. The hydrograph for this spring (fig. 12) is similar to that for weir C, but shows somewhat higher peak flows and a higher flow during the summer season. No subsidence effects were detected.

the well went dry about 2 months after the face had passed beneath it, at which time the face was 550 ft beyond the well. A temporary recovery of the water level was attributed to cascading, after which the well remained dry.

2. Water levels in two wells, located 100 and 300 ft outside the rib line of the panel, declined some 15 to 30 ft as a result of mining but recovered to near premining levels about 10 months after the longwall face had passed by.

3. Water wells located more than 500 ft outside the longwall panel rib line showed no detectable change in water levels as a result of mining. These wells also lie beyond the distance at the surface subtended by the 24° angle to the limit of detectable surface deformation.

4. No evidence of mining effects on the small streams or spring located within 1,200 ft of the panel could be detected.

REFERENCES

1. U.S. Code of Federal Regulations. Title 30--Mineral Resources; Chapter VII--Office of Surface Mining Reclamation and Enforcement, Department of the Interior; Subchapter K--Permanent Program Performance Standards; Part 817--Underground Mining Activities; July 1, 1984.
2. _____. Title 30--Mineral Resources; Chapter VII--Office of Surface Mining Reclamation and Enforcement, Department of the Interior; Subchapter G--Permanent Program Performance Standards; Part 783--Underground Mining Permit Applications--Minimum Requirements for Information on Environmental Resources; July 1, 1984.
3. Owili-Eger, A. S. C. Geohydrologic and Hydrogeochemical Impacts of Longwall Coal Mining on Local Aquifers. Soc. Min. Eng. AIME preprint 83-376, 1983, 16 pp.
4. Hill, J. G., G. J. Burgdorf, and D. R. Price. Effects of Coal Mine Subsidence on Ground Water Aquifers in Northern Appalachia (contract J0199063, SMC Martin Inc.). BuMines OFR 142-84, 1984, 149 pp., NTIS PB 84-236710.
5. Waite, B. A. Ground Water Monitoring of Underground Coal Mines. Min. Eng. (Littleton, CO), v. 34, 1982, pp. 170-171.

COMPARISON OF THE SUBSIDENCE OVER TWO DIFFERENT LONGWALL PANELS

By Paul W. Jeran¹ and Timothy M. Barton²

ABSTRACT

The subsidences over two longwall sections operating in the northern Appalachian coal region were monitored. The panels differed in dimensions, overburden thickness, and coalbed mined. Although

the final subsidence profiles differed, analysis of the data indicates that the same process of subsidence operated at each panel.

INTRODUCTION

Since 1960, when the first longwall with powered supports was installed in the United States, the use of the longwall system of mining by the coal industry has grown. In 1984, 21 U.S. coal companies were operating 112 longwalls.³ Eighty-four of these panels were in the northern Appalachian coal region, and the majority of these were 500 to 600 ft wide. In recent years, the trend has been to wider panels because of greater productivity allowed by changes in equipment.

One consequence of longwall mining is the subsidence of the ground surface above the panel. The Bureau has for several years monitored selected mining sites to obtain reliable and useful data on the reaction of the surface to mining. The ultimate goal of this work is to develop a surface subsidence predictive methodology based upon mining and geologic parameters.

The magnitude of subsidence of a point on the ground surface is proportional to the area of influence coincident with the zone of total extraction. In relatively flat-lying coalbeds the area of influence is typically circular in plan view. If the area of influence is entirely within the zone of extraction, then the maximum

possible subsidence will occur. If less, then the subsidence will be some fraction of the maximum subsidence. Figure 1 illustrates in cross-section the three typical geometries using a constant angle of draw and constant width of panel. The radius of the area of influence is dependent upon the thickness (H) of the overburden. Traditionally, the terms used to describe the three geometries are supercritical, where the radius of influence (RI) is less than half the width (w) of

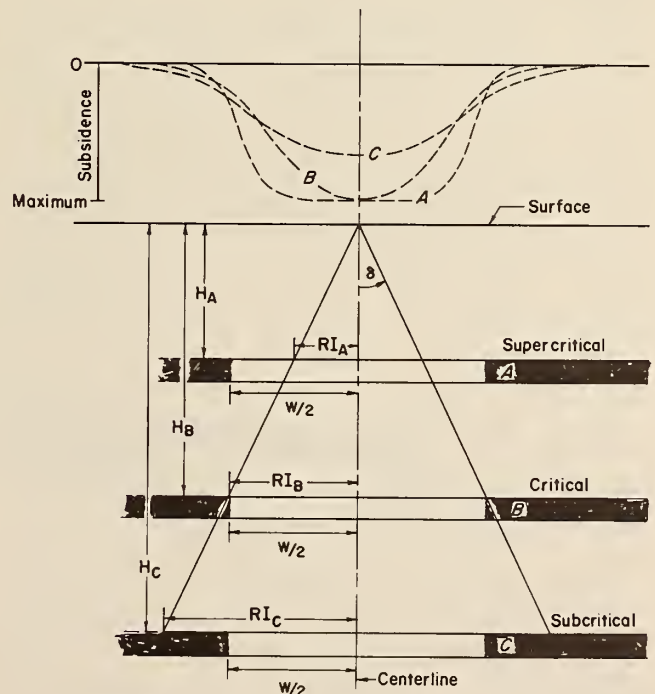


FIGURE 1. - Supercritical, critical, and subcritical geometries.

¹Geologist.

²Mining engineer.

Pittsburgh Research Center, Bureau of Mines, Pittsburgh, PA.

³Sprouls, M. W. Longwall Census 1984. Coal Min., v. 21, Dec. 1984, pp. 39-53.

the panel; critical, where the radius of influence is equal to half the width of the panel; and subcritical, where the half width of the panel exceeds the radius of influence.

The resulting subsidence curves for each of these geometries are shown in figure 1. The supercritical geometry results in a subsidence curve with multiple points of maximum subsidence. The critical case has one point of maximum subsidence. The subcritical case has a maximum point at the center, but this is less than the maximum possible subsidence. By inspection only the supercritical subsidence trough can be identified by its

multiple points of maximum subsidence. The remaining two cannot be differentiated without additional information because we cannot know if the maximum observed subsidence is the maximum possible subsidence.

Recently a very wide panel (950 ft wide) was monitored. The resultant subsidence exhibited multiple points of maximum subsidence. This differed from the subsidence troughs monitored over typical width (450 to 600 ft wide) panels which have but a single point of maximum subsidence. This report compares the data from this wide panel with data recently obtained from a typical width panel.

DISCUSSION

The two longwall panels used in this report are in the northern Appalachian coal region. The typical width panel, designated "E," is in southwestern Pennsylvania. It is 630 ft wide by 4,700 ft long. It was chosen because the average extracted thickness was the same as that at the wide panel, the subsidence was typical of the standard width panels we have monitored, and the data were obtained in the same manner as at the wide panel. The wide panel, designated "K," is in north-central West Virginia. This panel is 950 ft wide by 2,100 ft long.

At both panels, surface survey points were installed on 25-ft centers across two profiles and a centerline. The initial surveys were taken prior to mining, and the final surveys were taken a month after each panel was finished mining. Each panel was surveyed several times during mining. Figure 2 is a sketch of the survey lines relative to the panels.

Aside from their dimensions, the panels differed in coalbed mined and overburden. Panel E operated in the Pittsburgh Coalbed and extracted an average thickness of 6 ft. Panel K removed the same average thickness from the Lower Kittanning Coalbed. Figures 3 and 4 show the variation in overburden thickness for the centerlines and profiles at each of the panels.

Based upon drillers' logs of the core-holes drilled in the vicinity of each

panel, the overburden at each site averaged about 30 pct resistant strata (i.e., sandstones and limestones). Typical of Pennsylvanian age sediments, there is lateral variation and the range of resistant rock content is from 10 to 40 pct of the total thickness.

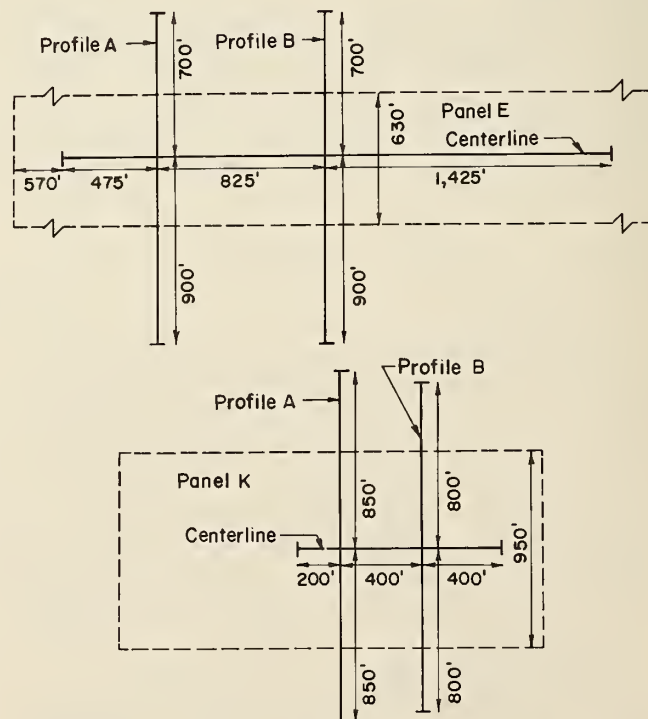


FIGURE 2. - Subsidence survey lines at panels E and K.

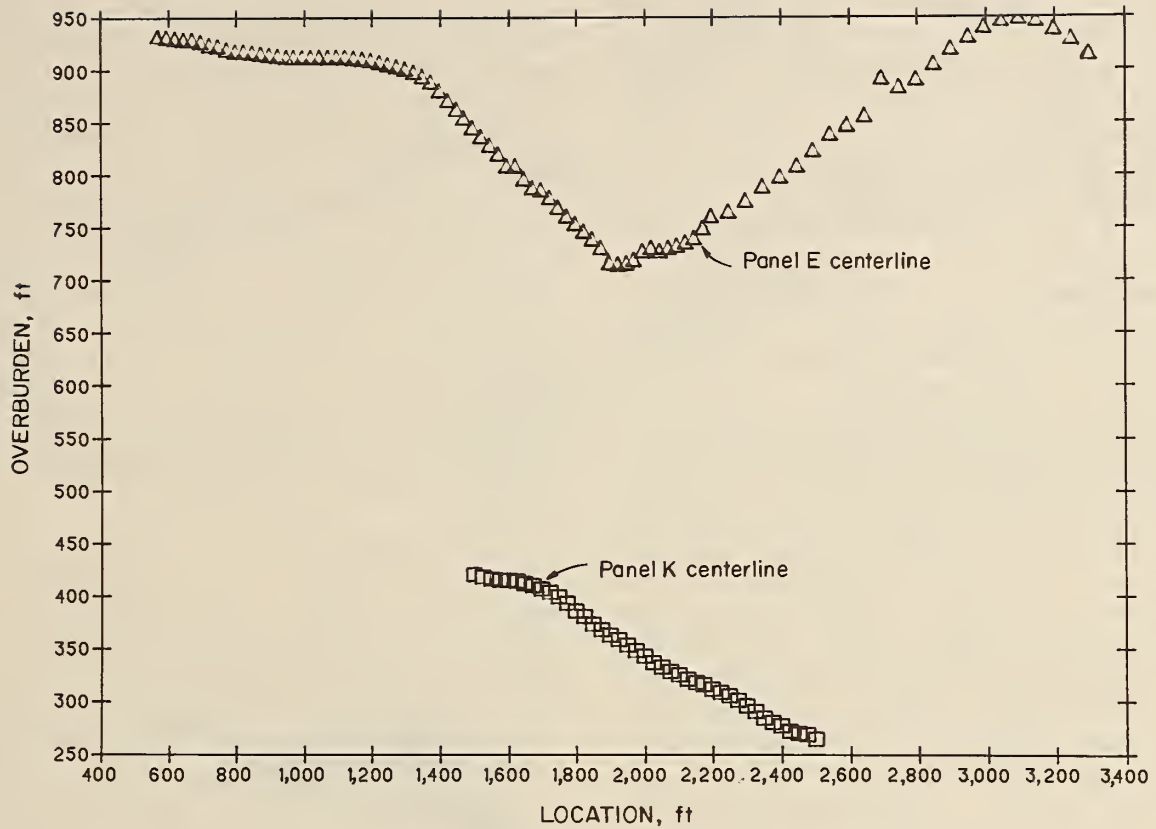


FIGURE 3. - Overburden thickness at centerlines.

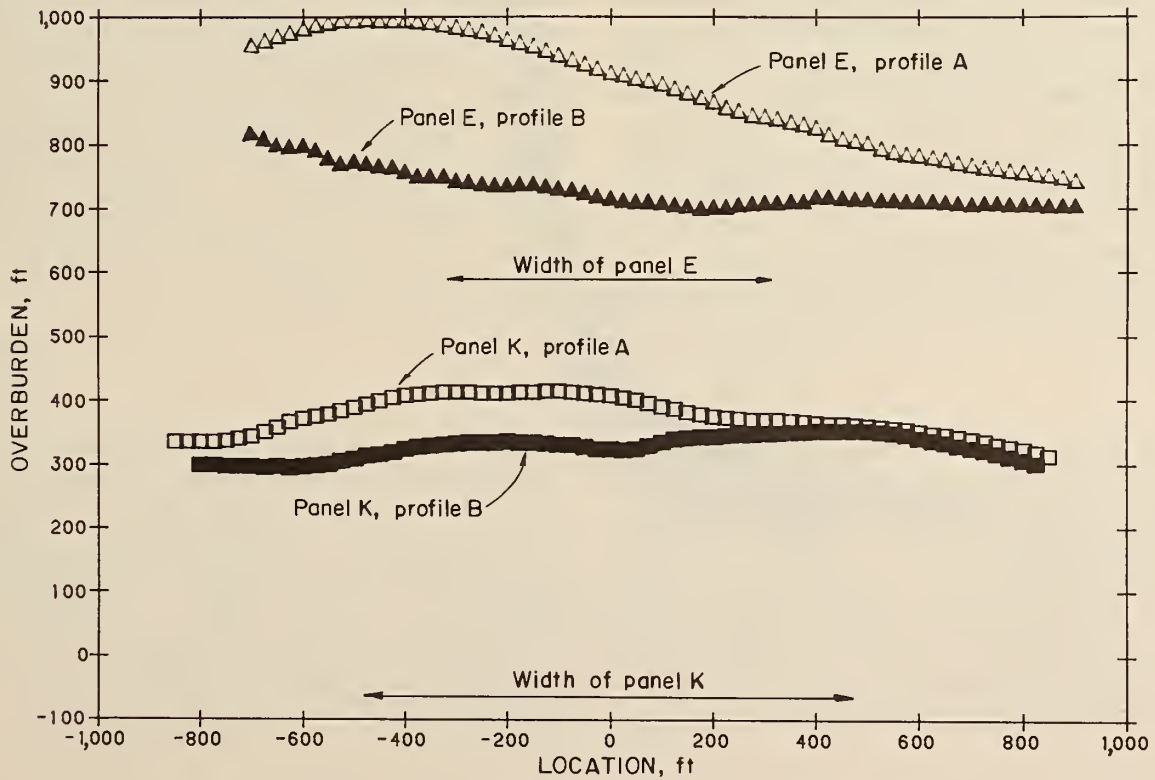


FIGURE 4. - Overburden thickness at profile lines.

The final subsidence of the centerline for each panel is shown in figure 5. Subsidence along each centerline was not uniform. Part of this variance may be attributed to one or more of the following: variation in overburden thickness, variation in extracted thickness, or variation in the lithologic composition of the overburden.

As the position of the face was recorded for each survey date, its position relative to each survey point during each survey is easily obtained. If the subsidence of a point at each survey is divided by the final measured subsidence of that point and these ratios are plotted against the relative face position, then a curve is obtained that shows the movement of the point relative to the movement of the face. By plotting these ratios from all points along the centerline for each panel, figure 6 and 7 result. These show that, at both panels, the surface exhibited some upheaval as the face approached some, but not all, of the survey points. Downward movement began as the face passed beneath each point. If the relative position of the face is divided by the overburden thickness at each point, then the response of the surface to the face position in terms of overburden thickness may be readily compared between the two sites. Figures 8 and 9 clearly show that, at both sites, the subsidence process was over 90 pct complete when the face had advanced the thickness of the overburden beyond the corresponding surface point.

The final subsidence profiles are shown in figure 10. Those from panel K exhibit

a broad flattish trough, indicating supercritical geometry. Profiles from panel E show the single point of maximum subsidence, which does not indicate the degree of criticality. Comparing profiles A and B at panel E, profile B, having the greater subsidence and thinner overburden, is closer to critical geometry than profile A, assuming all other factors are equal. At panel K, profile B exhibited a lesser magnitude of subsidence than did profile A. This may have resulted from the thinner overburden not compacting the gob as much as the thicker overburden. Differences in lithology and extracted thickness may also have played a part.

Inclinations between survey points were computed from the final profile survey data (fig. 11). At each panel, the greater inclination was created at the profile with the thinner overburden. Plotting the inclinations from the centerline data relative to face position as a function of overburden thickness (figs. 12-13) shows that for each panel, the maximum inclination occurred when the face was about a third the thickness of the overburden past the corresponding surface point. The maximum inclination over panel K exceeded that over panel E, which indicates that the potential for damage to surface structures is greater over thinner overburden. However, it should be noted that at both panels the maximum inclinations exceeded the limit of 15 mm/m established for protection of lowest priority surface structures in the Silesian coal basin.

SUMMARY

Subsidence over two longwall panels of different widths (630 and 950 ft) was monitored, and the data were compared. The subsidence profiles at the wider panel show the geometry to be supercritical. Those at the narrower panel indicate it is most likely subcritical. At both panels, the subsidence process relative to face position can be correlated to over-

burden thickness. Inclinations at both panels were in excess of 15 mm/m, and the thinner overburden exhibited the greater inclinations. In general, the similarity of the response of the overburdens to mining at each panel indicates that though the final subsidence troughs were differently shaped, the process of subsidence at each site was the same.

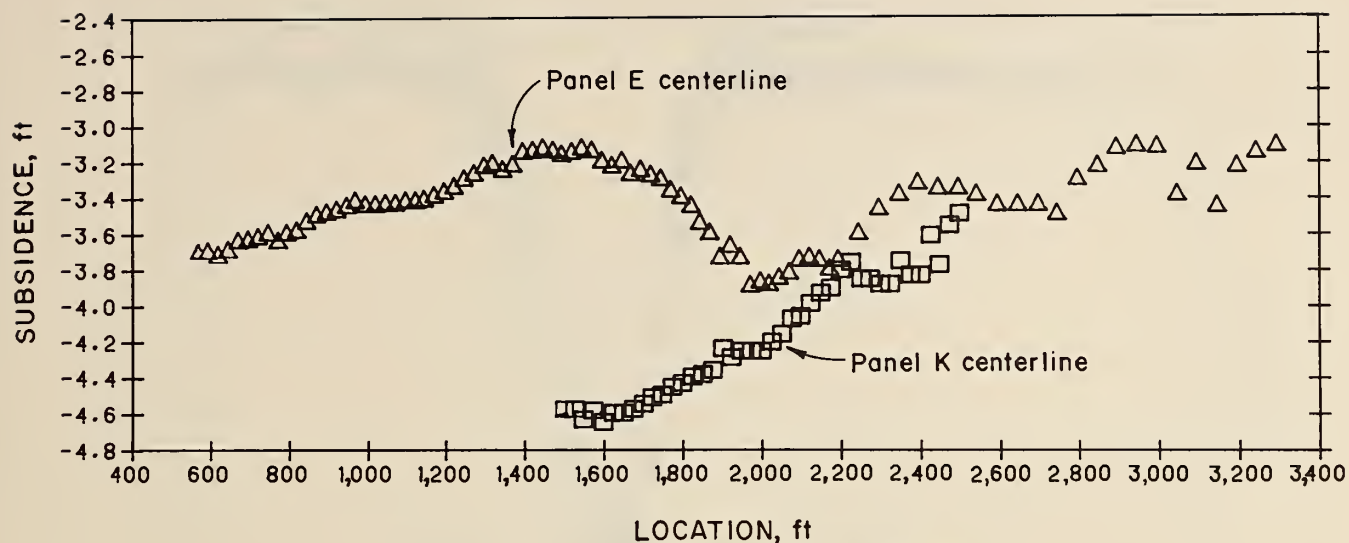


FIGURE 5. - Final subsidence for centerlines.

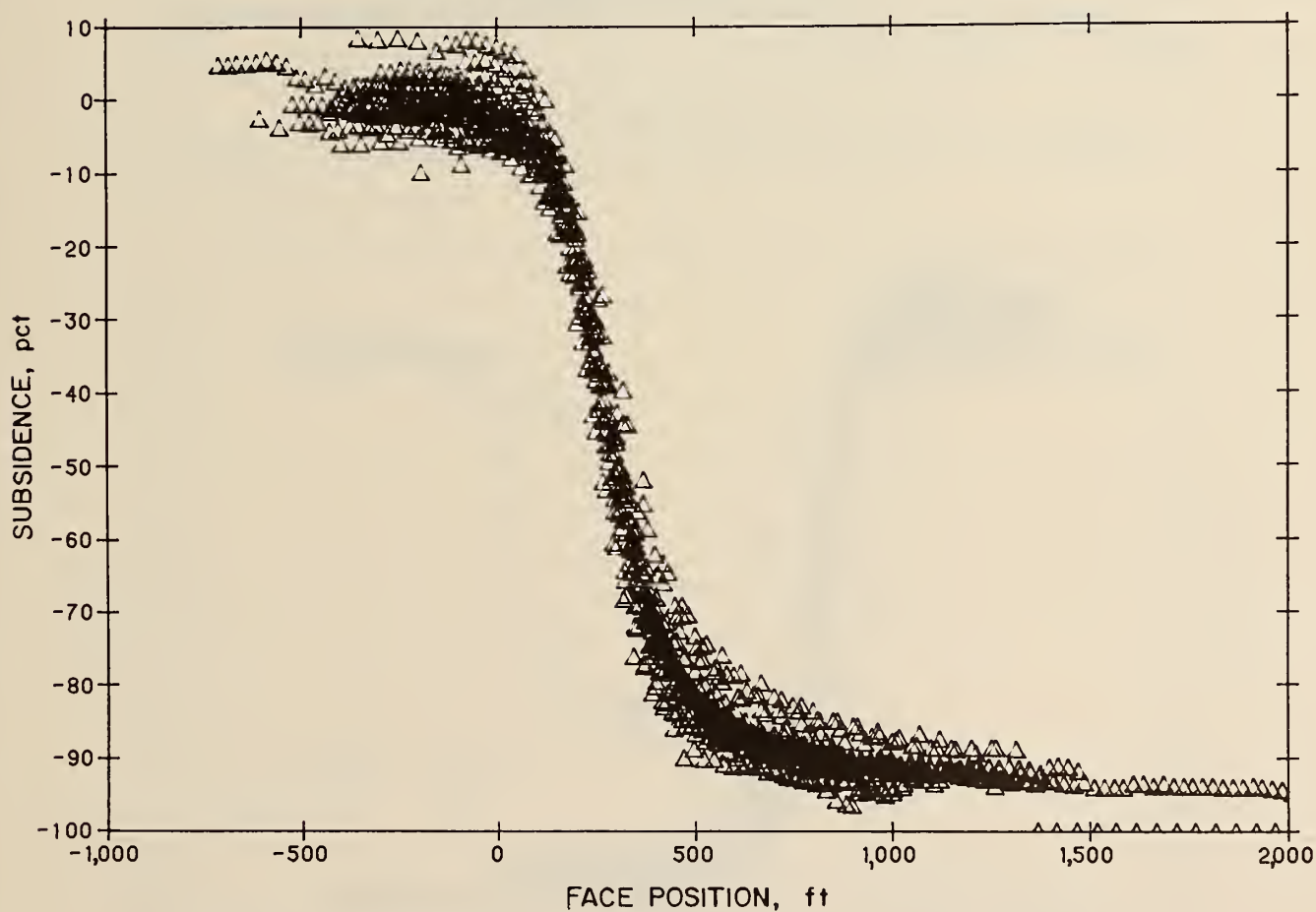


FIGURE 6. - Percent of final subsidence versus face position at panel E.

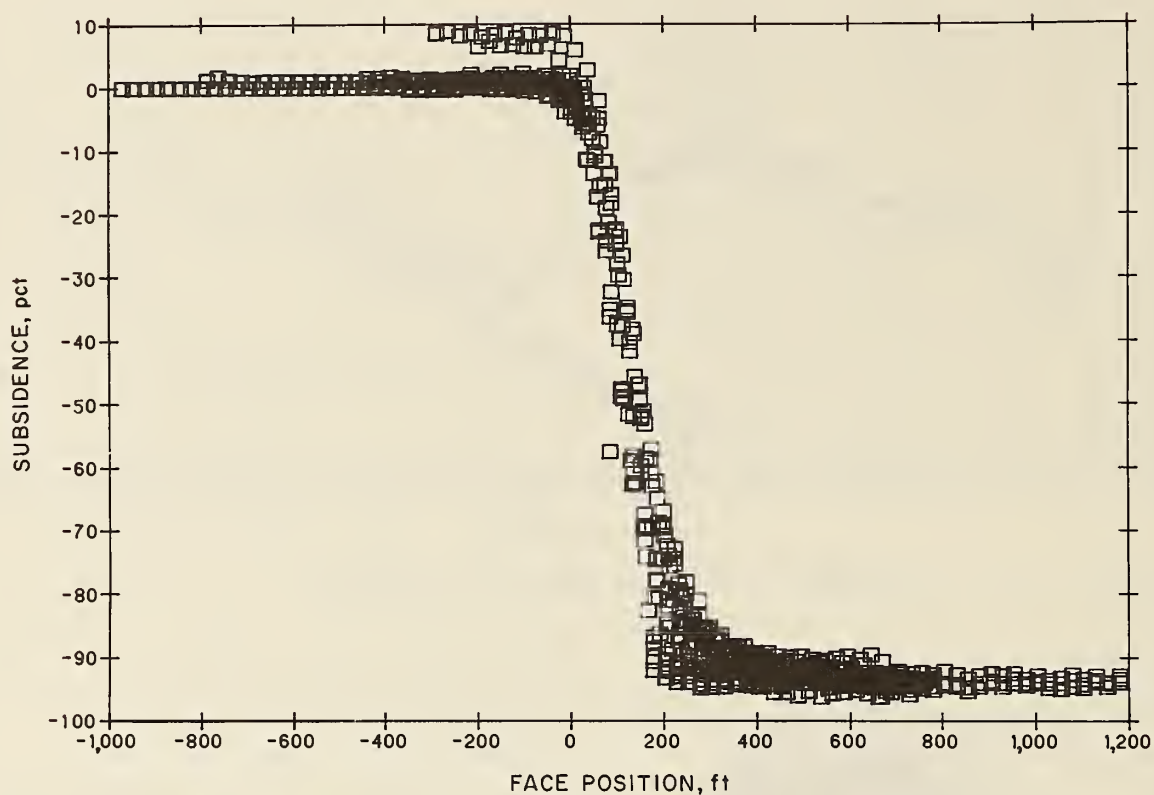


FIGURE 7. - Percent of final subsidence versus face position at panel K.

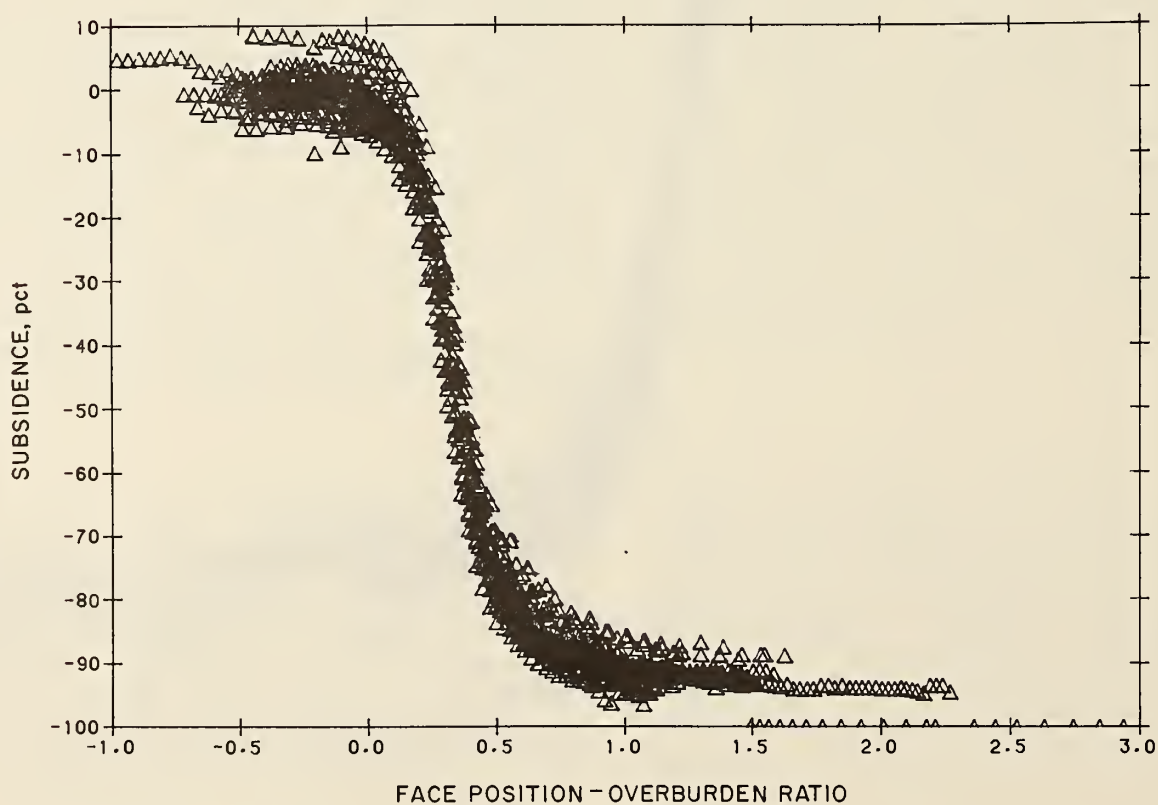


FIGURE 8. - Percent of final subsidence versus face position as a function of overburden thickness at panel E.

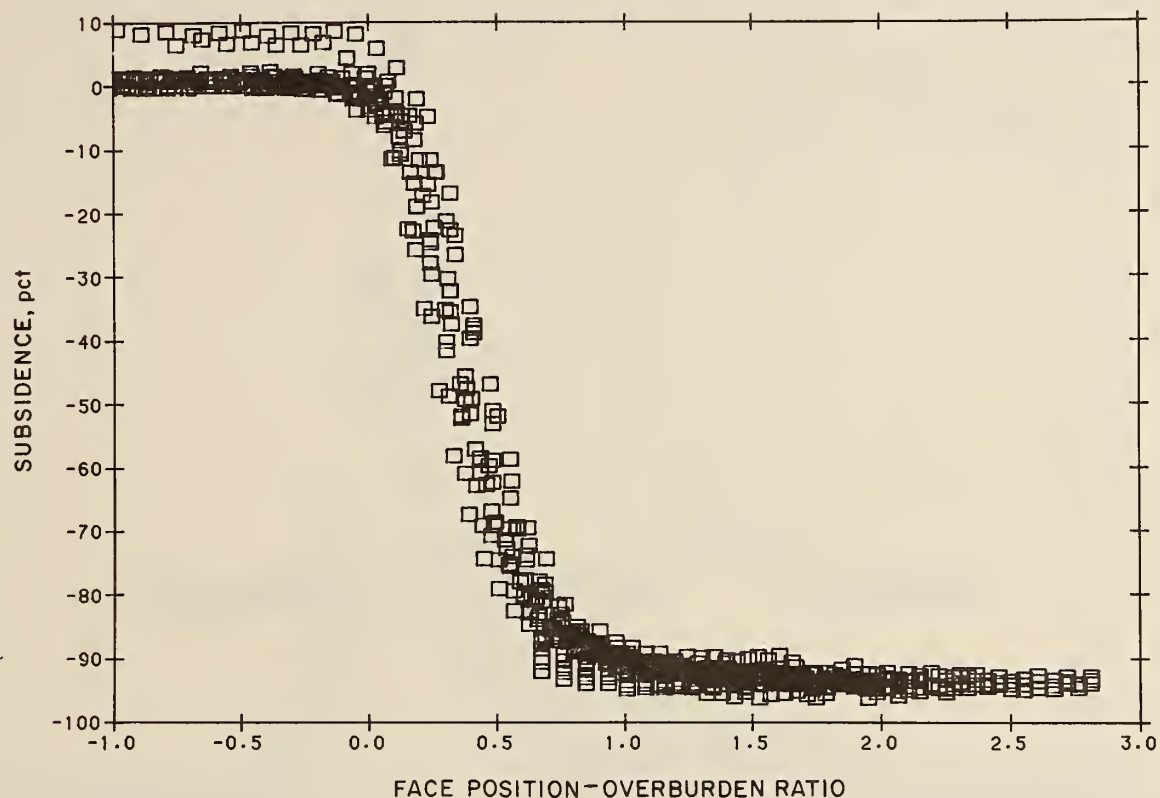


FIGURE 9. - Percent of final subsidence versus face position as a function of overburden thickness at panel K.

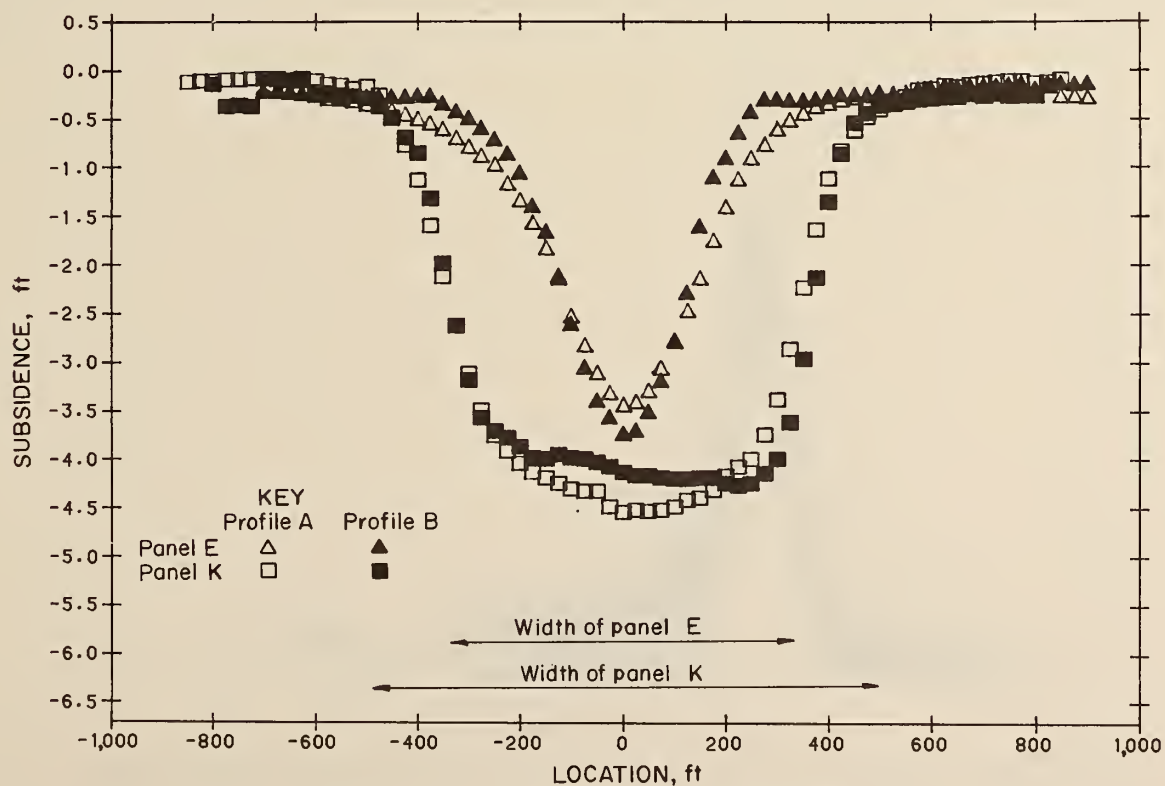


FIGURE 10. - Final subsidence profiles.

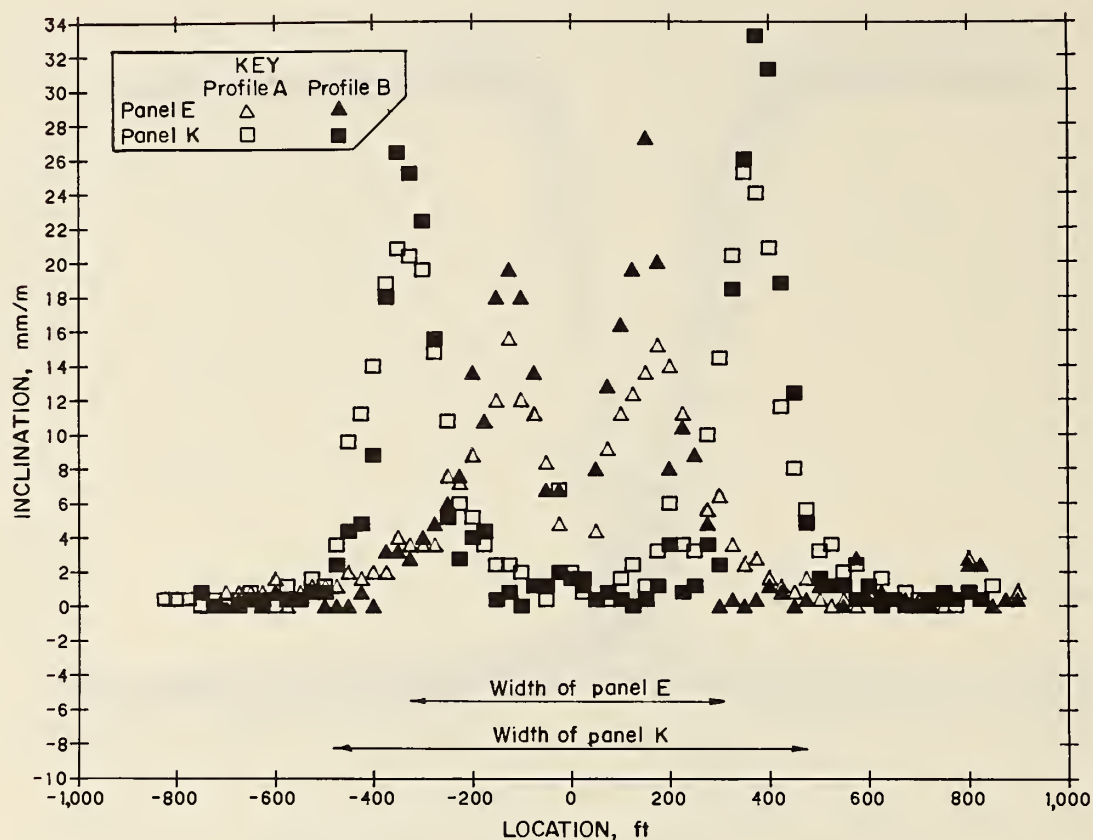


FIGURE 11. - Inclination across profiles.

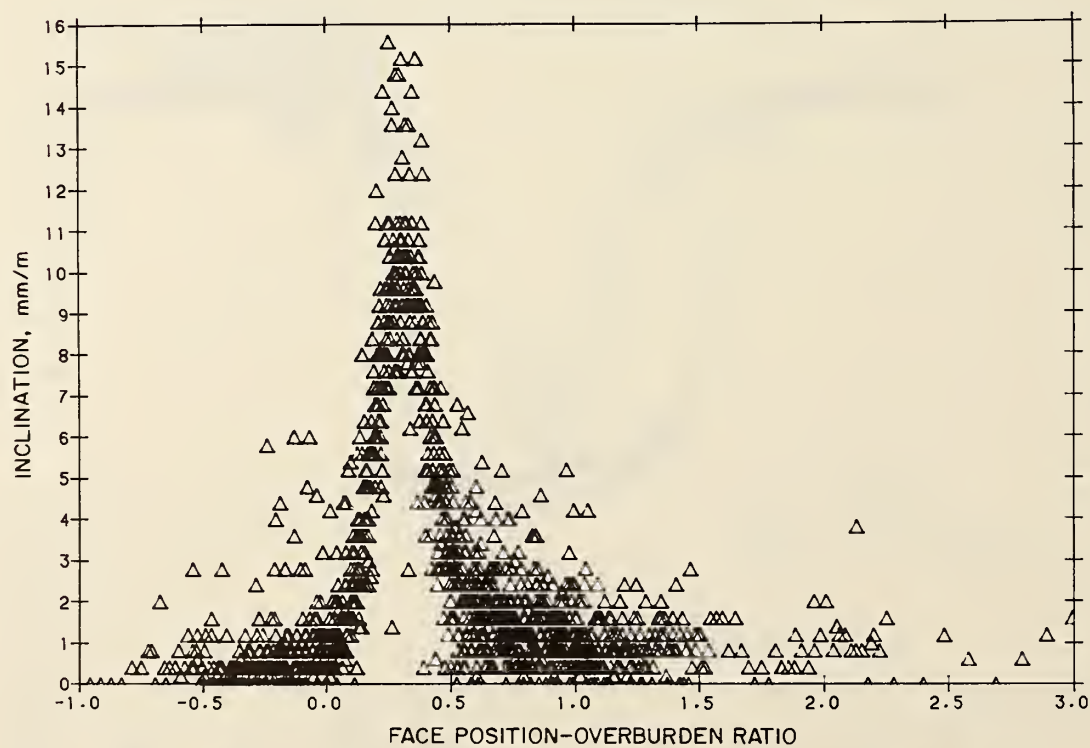


FIGURE 12. - Inclination versus face position as a function of overburden thickness, centerline panel E.

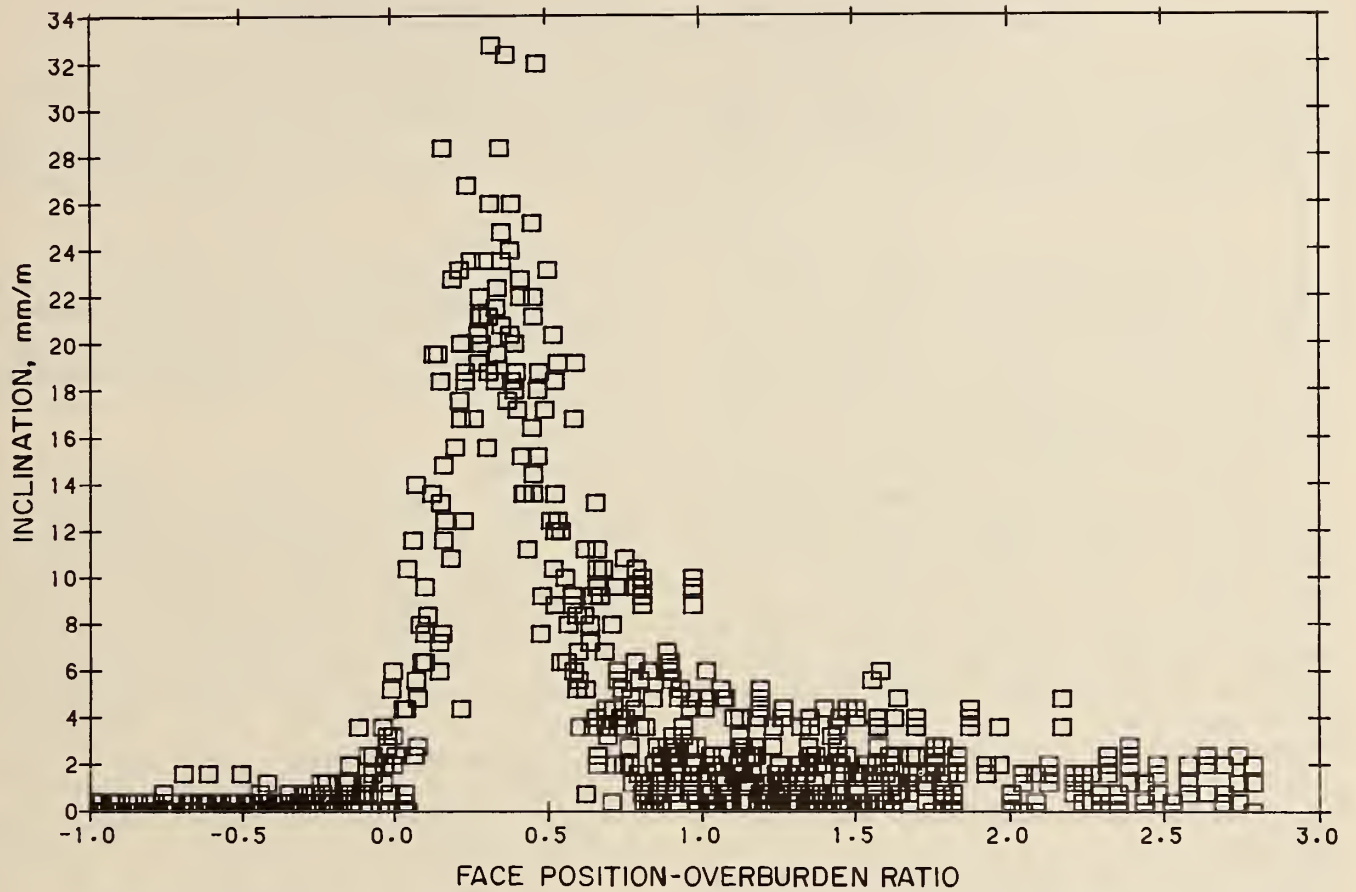


FIGURE 13. - Inclination versus face position as a function of overburden thickness, centerline panel K.

PRECALCULATION OF SUBSIDENCE OVER LONGWALL PANELS IN THE NORTHERN APPALACHIAN COAL REGION

By Vladimir Adamek¹ and Paul W. Jeran²

ABSTRACT

The specific lithological conditions over the Pittsburgh Coalbed, highly resistive limestone and sandstone units with relatively shallow overburden, prevent the use of any predictive method as developed for European conditions.

This paper describes the development of a subsidence precalculation methodology suitable to the mining and geological conditions in the northern Appalachian coal region.

It has been found that owing to lithological conditions over the Pittsburgh Coalbed, the subsidence coefficient varies within the area of the subsidence trough. This is different from the European conditions, where the subsidence coefficient is considered to be a constant.

The effects of lithology, in the form of a variable subsidence coefficient,

have been separated for each test site by introducing a correlation between hypothetically homogeneous overburden and existing lithological conditions, while providing for different mining conditions.

Field data from 11 Bureau longwall panel studies were used in the regression analysis. For each panel the characteristics of the variability of the subsidence coefficient along individual profile lines were defined. Regression analysis of the subsidence coefficients from all test sites on the location relative to the edge of the panel has yielded a third-degree polynomial equation with a coefficient of correlation of 0.9999.

All sensitivity tests have shown good results.

INTRODUCTION

The enactments of Surface Mining Control and Reclamation Act of 1977 and Public Law 95-87 made it mandatory that mine operators, prior to mining, define--

1. The aerial extent of surface movement.
2. The surface deformations resulting from both vertical and horizontal movements.
3. The time dependency of surface movements that will be caused by the proposed mining.

Since little or no experience in subsidence prediction existed in this country, the methods developed in Europe were applied to meet these requirements. It

quickly became apparent that none of the methods yielded acceptable results.

The Bureau of Mines began work on a project to develop a predictive model for subsidence caused by coal mining in this country. To date, field subsidence data have been collected from 11 longwall test sites via in-house monitoring programs. Analysis of these data verified the non-applicability of the existing methods to U.S. conditions.

The model presented in this paper is limited to predicting vertical movements over longwall panels and thus far has been investigated only for applications in the northern Appalachian coal region. It requires the operator only to input the geometry of the proposed mining and therefore can be used without prior knowledge or understanding of the subsidence process.

¹Mining engineer.

²Geologist.

Pittsburgh Research Center, Bureau of Mines, Pittsburgh, PA.

DEVELOPMENT OF SUBSIDENCE PRECOMPUTATION METHODOLOGY

Since the coefficient of subsidence and the angle of draw are important to the understanding of this model, a discussion of these follows.

COEFFICIENT OF SUBSIDENCE

For critical and supercritical situations, the coefficient of subsidence is defined as a ratio

$$a = \frac{s_{\max}}{m},$$

where s_{\max} = maximum subsidence measured

and m = extracted coal seam thickness,

For subcritical situations

$$a = \frac{s_{\max}}{me},$$

where e = the efficiency coefficient of the partial area of influence.

Practically, for all existing predictive methods, subsidence coefficient a is considered to be constant within the whole area of the subsidence trough.

The average coefficient of subsidence \bar{a} can be defined as

$$\bar{a} = \frac{VE}{VS}$$

VS = volume of the subsidence trough

VE = volume of the coal extracted.

For homogeneous overburden, or overburden behaving homogeneously from the point of view of subsidence, the values of a and \bar{a} should be about equal.

Moderate discrepancies between the values of a and \bar{a} can be caused by insufficient compaction of the gob area at the edges of the longwall panel, due to the resistance of chain pillars.

ANGLE OF DRAW

By definition, the angle of draw is identified as an angle between the line

connecting the top edge of a longwall panel with the nearest zero-movement point on the surface, and a vertical dropped from this point. The angle of draw serves at least two purposes as described below:

1. The angle of draw serves to delineate the surface area influenced by underground mining. The identification of a zero-movement point is a rather difficult task, depending on overall circumstances. For relatively shallow overburden and a smooth surface, good results are more probable.

In reality, in many cases, small surface subsidences (up to 0.2 to 0.3 ft) occur far beyond the edge of the panel, suggesting an unrealistically large angle of draw. These movements may not even be directly connected with underground mining activities, but can be caused by ground water movement, sliding, temperature changes, etc.

Therefore, it would be realistic to define the limit angle of draw as the angle between a vertical line and the line connecting the upper edge of the panel with the place on the surface where surface deformations do not exceed a certain limit. An example follows:

Vertical movement $S \leq 0.1$ ft

Inclination $I \leq 2$ mm/m

Horizontal strains $E \leq 1$ mm/m

2. The angle of draw serves as a functional parameter for predictive methodologies.

For a majority of predictive methods based on influence functions, the angle of draw is the functional parameter that, together with the underground geometry and overburden thickness, defines the characteristics of surface deformations.

For *homogeneous overburden* or overburden behaving homogeneously, the conception of the angle of draw as a functional parameter for predictive methodologies based on the principle of the area of the influence has been proven valid.

Individual theories developed on this conception (Keinhorst, Bals, Niemczyk,

Beyer, etc.) differ from each other very little, the differences being caused by assigning different values of influence to individual zones within the whole area of influence. Bals' theory has achieved the widest recognition and practical use in Europe. Its substance is the definition of the efficiency coefficient e . (See appendix.)

In accordance with Newton's law governing the attraction of masses, Bals

assumes that each differential part of mined-out area within the area of influence exerts an influence on the surface point inversely proportional to its distance from it.

Using the computer algorithm developed by the Bureau, it was possible to compute and tabulate the values of e for different mining conditions, i.e., underground geometry and overburden thickness (table 1).

TABLE 1. - Efficiency coefficients (e) for $\gamma = 25^\circ$

w/H	Distance inward from edge of panel as fraction of panel width										
	0.50	0.45	0.40	0.35	0.30	0.25	0.20	0.15	0.10	0.05	0.00
0.1.....	0.289	0.289	0.289	0.286	0.286	0.280	0.277	0.268	0.258	0.250	0.237
0.2.....	.473	.471	.468	.466	.460	.449	.440	.428	.415	.389	.361
0.3.....	.609	.609	.606	.599	.590	.577	.563	.542	.520	.487	.439
0.4.....	.722	.719	.714	.706	.692	.676	.654	.629	.594	.554	.487
0.5.....	.811	.808	.801	.788	.772	.749	.723	.686	.643	.588	.500
0.6.....	.879	.877	.868	.853	.833	.803	.765	.720	.667	.600	.500
0.7.....	.934	.931	.919	.899	.870	.833	.793	.744	.686	.609	.500
0.8.....	.973	.969	.952	.927	.896	.858	.818	.765	.703	.622	.500
0.9.....	.998	.988	.972	.949	.920	.882	.841	.786	.720	.633	.500
1.0.....	1.000	.999	.987	.967	.939	.903	.861	.804	.737	.644	.500
1.1.....	1.000	1.000	.977	.982	.957	.921	.879	.823	.751	.656	.500
1.2.....	1.000	1.000	1.000	.992	.972	.939	.896	.841	.765	.667	.500
1.3.....	1.000	1.000	1.000	.999	.983	.953	.913	.855	.780	.677	.500
1.4.....	1.000	1.000	1.000	1.000	.992	.966	.927	.870	.793	.686	.500
1.5.....	1.000	1.000	1.000	1.000	.999	.977	.939	.884	.804	.692	.500
1.6.....	1.000	1.000	1.000	1.000	1.000	.986	.952	.896	.818	.703	.500
1.7.....	1.000	1.000	1.000	1.000	1.000	.987	.963	.909	.828	.711	.500
1.8.....	1.000	1.000	1.000	1.000	1.000	.993	.972	.920	.841	.720	.500
1.9.....	1.000	1.000	1.000	1.000	1.000	.999	.979	.929	.851	.728	.500
2.0.....	1.000	1.000	1.000	1.000	1.000	1.000	.987	.939	.861	.737	.500
2.1.....	1.000	1.000	1.000	1.000	1.000	1.000	.992	.949	.870	.744	.500
2.2.....	1.000	1.000	1.000	1.000	1.000	1.000	.997	.957	.879	.751	.500
2.3.....	1.000	1.000	1.000	1.000	1.000	1.000	1.000	.964	.888	.758	.500
2.4.....	1.000	1.000	1.000	1.000	1.000	1.000	1.000	.972	.896	.765	.500
2.5.....	1.000	1.000	1.000	1.000	1.000	1.000	1.000	.978	.906	.772	.500
2.6.....	1.000	1.000	1.000	1.000	1.000	1.000	1.000	.983	.913	.780	.500
2.7.....	1.000	1.000	1.000	1.000	1.000	1.000	1.000	.988	.920	.786	.500
2.8.....	1.000	1.000	1.000	1.000	1.000	1.000	1.000	.992	.927	.793	.500
2.9.....	1.000	1.000	1.000	1.000	1.000	1.000	1.000	.996	.934	.799	.500
3.0.....	1.000	1.000	1.000	1.000	1.000	1.000	1.000	.999	.939	.804	.500
	Distance outward from edge of panel as fraction of panel width										
	0.00	-0.50	-0.10	-0.15	-0.20	-0.25	-0.30	-0.35	-0.40	-0.45	-0.50
0.1.....	0.237	0.222	0.213	0.201	0.191	0.184	0.180	0.177	0.171	0.166	0.160
0.2.....	.361	.332	.304	.288	.274	.261	.246	.234	.224	.214	.203
0.3.....	.439	.392	.357	.331	.305	.286	.263	.244	.227	.209	.194
0.4.....	.487	.418	.375	.333	.297	.263	.235	.207	.182	.159	.139
0.5.....	.500	.412	.356	.308	.263	.228	.196	.166	.139	.116	.094
0.6.....	.500	.400	.333	.280	.235	.196	.159	.130	.104	.080	.061

TABLE 1. - Efficiency coefficients (e) for $\gamma = 25^\circ$ --Continued

w/H	Distance outward from edge of panel as fraction of panel width--Continued										
	0.00	0.05	0.10	0.15	0.20	0.25	0.30	0.35	0.40	0.45	0.50
0.7.....	0.500	0.391	0.314	0.256	0.207	0.166	0.130	0.099	0.073	0.051	0.033
0.8.....	.500	.378	.297	.235	.182	.139	.104	.073	.048	.028	.013
0.9.....	.500	.367	.280	.214	.159	.116	.080	.051	.028	.012	.001
1.0.....	.500	.356	.263	.196	.139	.094	.061	.033	.013	.001	.000
1.1.....	.500	.344	.249	.177	.121	.077	.043	.018	.003	.000	.000
1.2.....	.500	.333	.235	.159	.104	.061	.028	.008	.000	.000	.000
1.3.....	.500	.323	.220	.145	.087	.046	.017	.001	.000	.000	.000
1.4.....	.500	.314	.207	.130	.073	.033	.008	.000	.000	.000	.000
1.5.....	.500	.308	.196	.116	.061	.022	.001	.000	.000	.000	.000
1.6.....	.500	.297	.182	.104	.048	.013	.000	.000	.000	.000	.000
1.7.....	.500	.289	.172	.091	.037	.007	.000	.000	.000	.000	.000
1.8.....	.500	.280	.159	.080	.028	.001	.000	.000	.000	.000	.000
1.9.....	.500	.272	.149	.071	.021	.000	.000	.000	.000	.000	.000
2.0.....	.500	.263	.139	.061	.013	.000	.000	.000	.000	.000	.000
2.1.....	.500	.256	.130	.051	.008	.000	.000	.000	.000	.000	.000
2.2.....	.500	.249	.121	.043	.003	.000	.000	.000	.000	.000	.000
2.3.....	.500	.242	.112	.036	.000	.000	.000	.000	.000	.000	.000
2.4.....	.500	.235	.104	.028	.000	.000	.000	.000	.000	.000	.000
2.5.....	.500	.228	.094	.022	.000	.000	.000	.000	.000	.000	.000
2.6.....	.500	.220	.087	.017	.000	.000	.000	.000	.000	.000	.000
2.7.....	.500	.214	.080	.012	.000	.000	.000	.000	.000	.000	.000
2.8.....	.500	.207	.073	.008	.000	.000	.000	.000	.000	.000	.000
2.9.....	.500	.201	.066	.004	.000	.000	.000	.000	.000	.000	.000
3.0.....	.500	.196	.061	.001	.000	.000	.000	.000	.000	.000	.000

In general, subsidence of any surface point above a longwall panel can be expressed as

$$s = s_{\max} f(x) = m a f(x).$$

The function $f(x)$ is a mathematical expression that relates to the physical setting and depends mainly on the underground geometry, overburden thickness, overburden properties, and relative position of the surface point toward the mined-out area.

The equation $s = m a f(x)$ is theoretically valid for any mining and geological conditions because of the broad meaning and flexibility of $f(x)$.

In this equation, there are three unknown: s , a , and $f(x)$. After acquiring a sufficient amount of field data (s), there still remain two unknown members in the equation, a and $f(x)$.

By alternately substituting a as a constant with computed values from field measurements

$$a = \frac{s_{\max}}{m} \quad \text{or} \quad a = \frac{s_{\max}}{m_e}$$

and substituting $f(x)$ with different existing predictive methodologies, one may verify the validity of individual methodologies for U.S. mining and geological conditions.

After analyzing data from 11 test sites, it has been found that none of the existing predictive methodologies based either on influence or profile function is applicable to U.S. mining geological conditions. The main reason is the extreme effect of lithology on the subsidence characteristics, namely highly resistant layers of limestone and sandstone with relatively shallow overburden. Figure 1 shows a typical subsidence profile as measured over the Pittsburgh Coalbed compared with precalculated profiles using the above-mentioned methods.

As a first step in developing a predictive model, the problem was approached by trying to establish the effect of

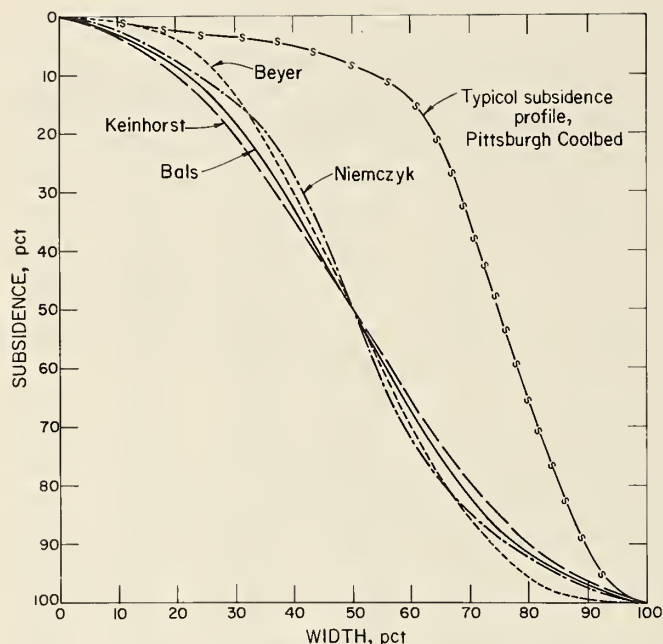


FIGURE 1. - Comparison of measured profile with some precalculated profiles for Pittsburgh Coalbed.

lithology on subsidence characteristics for each test site and also to define relative differences of this effect between individual test sites. This cannot be done by simple comparison of subsidence profiles. Different mining conditions and underground geometry including depth of cover must be taken into account.

The principle of this idea is to establish the difference in subsidence characteristics between hypothetically homogeneous overburden, i.e., overburden without the presence of resistive hard rock units, and existing lithological conditions. At the same time, one must provide for given mining conditions.

For computation of subsidences for homogeneous overburden, Bals' theory was used. Since one cannot define the exact value of the angle of draw, the whole process of computation for three concepts was repeated, namely, for $\gamma = 25^\circ$, for $\gamma = 15^\circ$, and also for a constant value of efficiency coefficient $e = 1$ for all points.

According to Bals, the subsidence of any surface point for homogeneous overburden is

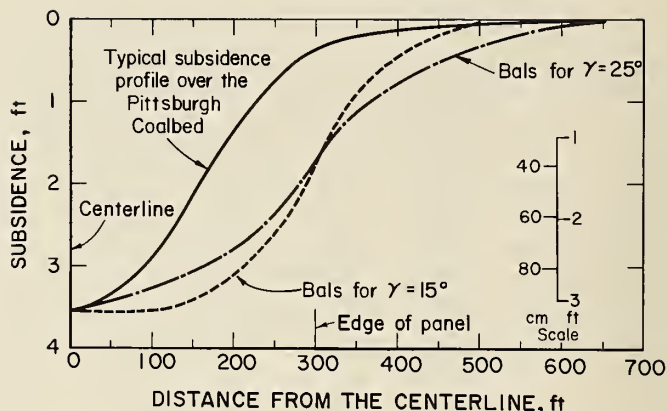


FIGURE 2. - Comparison of measured profile with Bals' predictive method.

$$s_i = m a e_i$$

with predetermined or estimated constant subsidence coefficient a .

Figure 2 shows precalculated profiles by Bals, using the values of the angle of draw $\gamma = 15^\circ$ and $\gamma = 25^\circ$ in comparison with measured profile. It is evident that there is no possibility of obtaining reasonable congruency between precalculated and measured profiles for any value of γ as a functional parameter. This leads to the conclusion that the conception of using the angle of draw as a functional parameter for direct precomputation of surface deformations is unsatisfactory for conditions where effect of lithology is as overwhelming as it is over the Pittsburgh Coalbed.

The specific lithological conditions over the Pittsburgh Coalbed, namely highly resistive limestone and sandstone units with relatively shallow overburden, prevent the use of any predictive method as developed for European conditions. Further, it is also justifiable to assume that the resistance of interbedded hard rock layers is strongest at the edge of the panel and diminishes toward the centerline.

Such a situation must lead to variability of the subsidence coefficient along the profile, otherwise considered to be constant for homogeneous overburden. This assumption is further supported by the discrepancy between the subsidence coefficient

$$a = \frac{s_{\max}}{m} \quad \text{or} \quad a = \frac{s_{\max}}{me}$$

and the average subsidence coefficient

$$\bar{a} = \frac{VS}{VE}$$

As mentioned before, for homogeneous overburden these two values should be about equal.

As shown in table 2, the values of a at the centerline of the panel, at each test site, are close to 0.6 and \bar{a} is about 0.35. Such discrepancy must have a decisive effect on the subsidence characteristics.

To obtain the congruency between pre-computed and measured data, the subsidence coefficient a_v was introduced as a variable:

$$a_{vi} = \frac{SF_i}{me_i}$$

where SF_i = measured subsidence.

For each surface point at all test sites the value of a_v has been defined. Figures 3-8 show the characteristics of a_v for $\gamma = 25^\circ$ and $\gamma = 15^\circ$ and for constant $e = 1$ along all profiles.

If the assumption about the validity of Bals' theory for homogeneous overburden is correct--and no reason has been found to doubt it--then each of these curves represents a lithological effect on subsidence characteristics, expressed in the form of the variable subsidence coefficient. The dispersion of individual curves shows the differences of lithological effect between individual test sites.

The usefulness of this approach for subsidence precalculation depends on two possibilities:

1. The lithological effect on subsidence characteristics differs at each site beyond acceptable limits, as would be demonstrated by a large dispersion of individual curves.

2. The lithological effect at each site is acceptably similar. Then the

TABLE 2. - Overview of basic parameters at various test sites

Mine	H, ft		m, ft	w, ft	s_F at centerline, ft	a at centerline for $\gamma = 25^\circ$	\bar{a} (VS/VE)	$\frac{w}{H}$
	Range	At centerline						
1	520-706	650	5.5	460	-2.62	0.513	0.30	0.71
2	677-700	700	5.5	600	-3.25	.597	.35	.86
3	645-700	700	5.5	600	-3.25	.597	.32	.86
4	509-624	615	5.5	605	-3.65	.664	.44	.98
5	652-781	652	5.5	605	-3.55	.645	.39	.93
6	740-795	795	5.5	600	-3.09	.587	.32	.75
7	732-795	795	5.5	600	-3.09	.587	.32	.75
8	913-995	913	6.0	630	-3.42	.614	.40	.69
9	803-913	913	6.0	630	-3.42	.614	.38	.69
10	802-855	855	6.0	630	-3.12	.547	.34	.74
11	717-780	717	6.0	630	-3.72	.623	.34	.88
12	702-719	717	6.0	630	-3.72	.623	.34	.88
13	368-402	402	6.0	940	-4.04	.673	.37	2.34
14	345-402	402	6.0	940	-4.04	.673	.39	2.34
15	700-845	845	5.5	600	-2.95	.571	.31	.71
16	747-866	747	5.5	510	-2.79	.547	.34	.68

H = Height of the overburden.

m = Effective coal seam thickness.

w = Width of the panel.

s_F = Subsidence measured.

a = Subsidence coefficient s_{\max}/me .

\bar{a} = Average subsidence coefficient.

VS = Volume of the subsidence trough.

VE = Volume of the coal extracted.

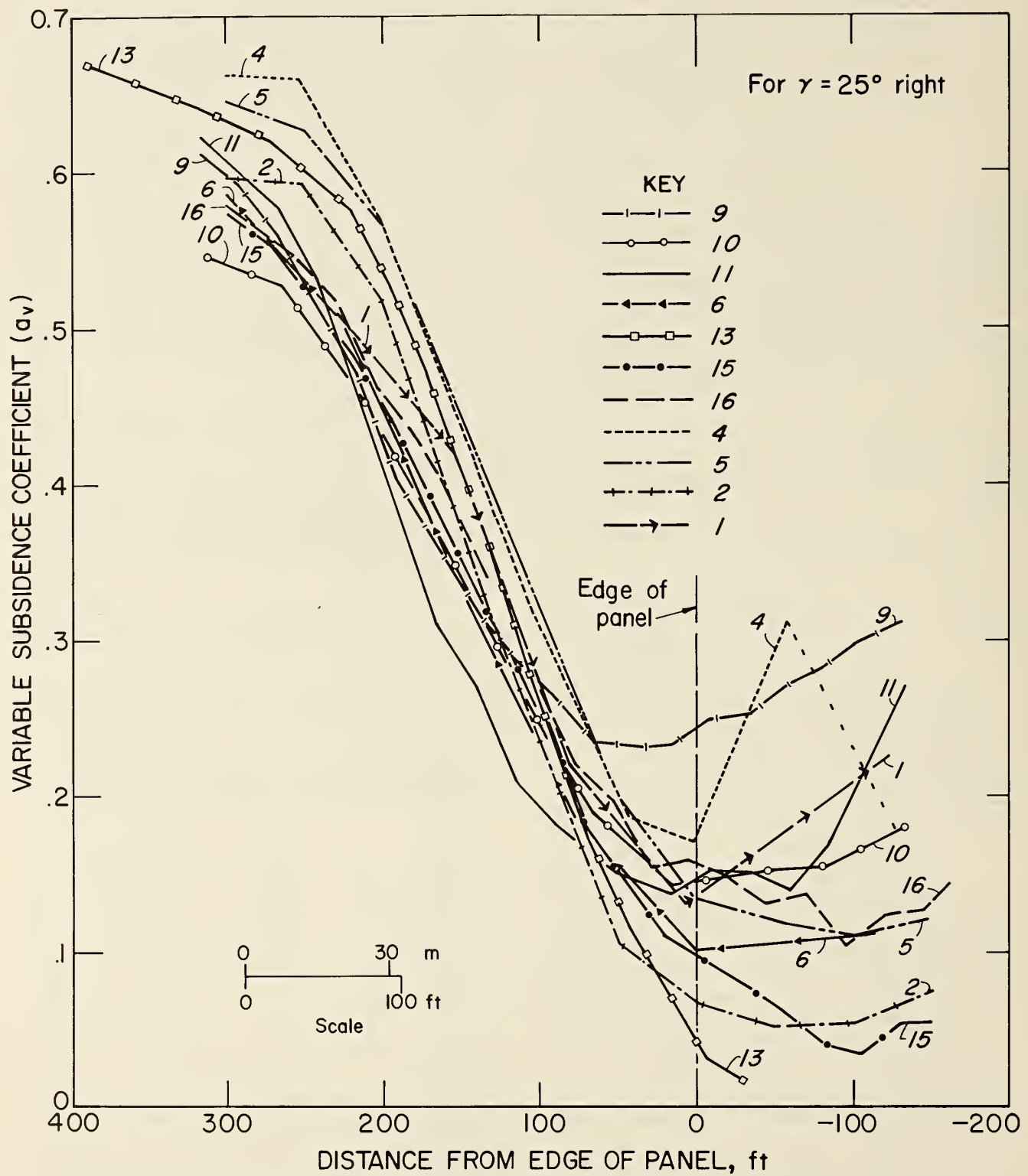


FIGURE 3. - Variable subsidence coefficient for $\gamma = 25^\circ$ right.

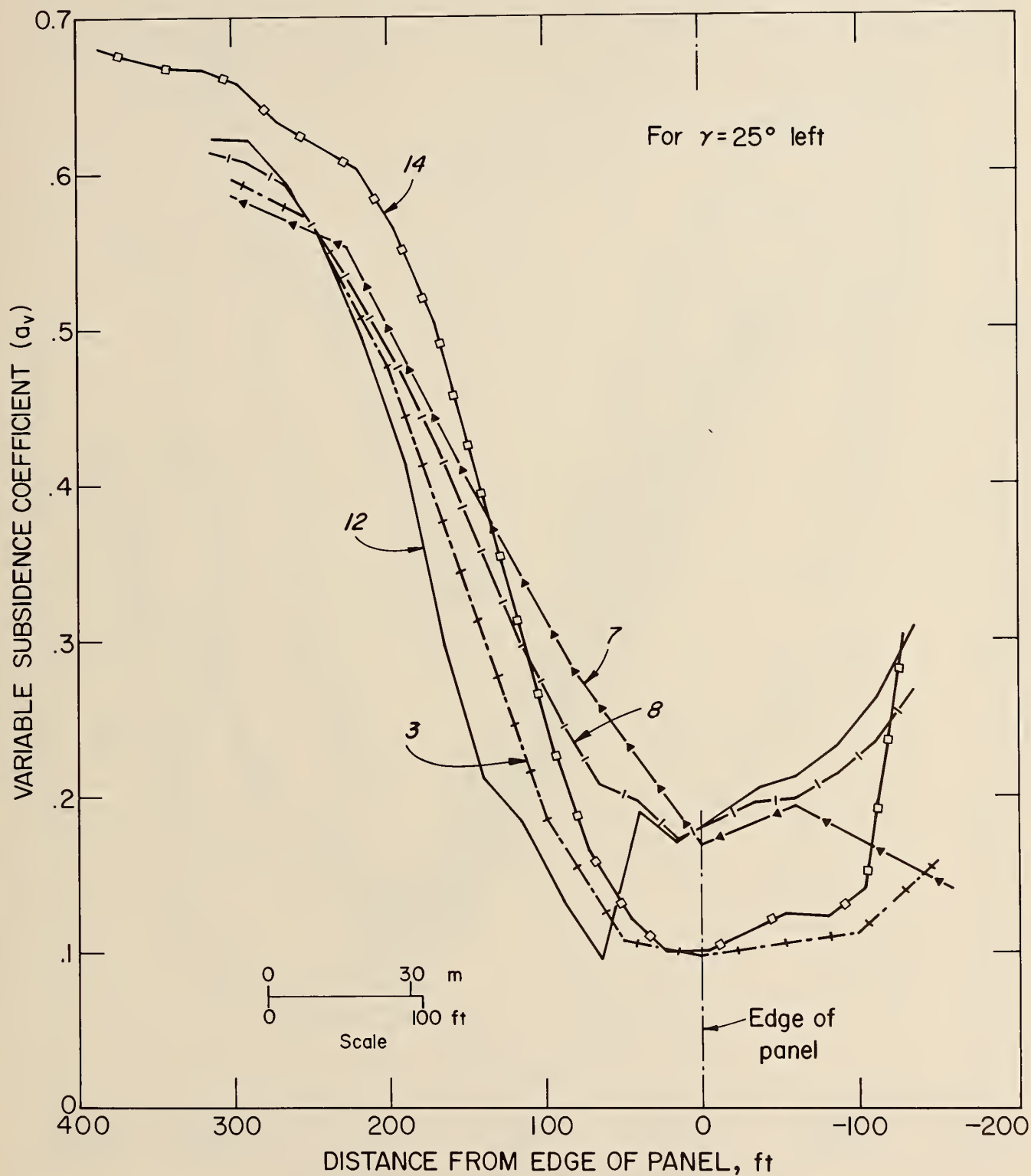


FIGURE 4. - Variable subsidence coefficient for $\gamma = 25^\circ$ left.

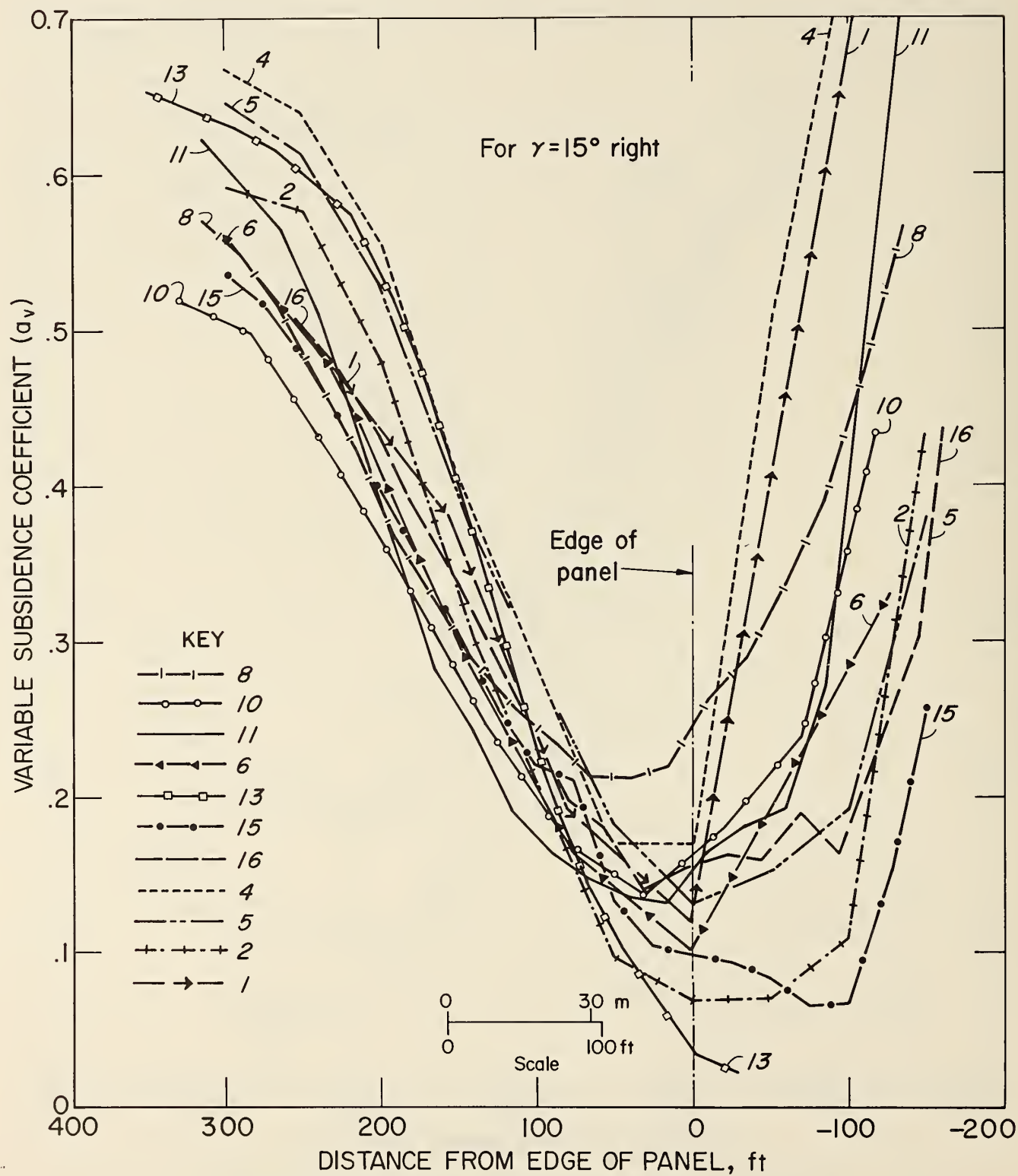


FIGURE 5. - Variable subsidence coefficient for $\gamma = 15^\circ$ right.

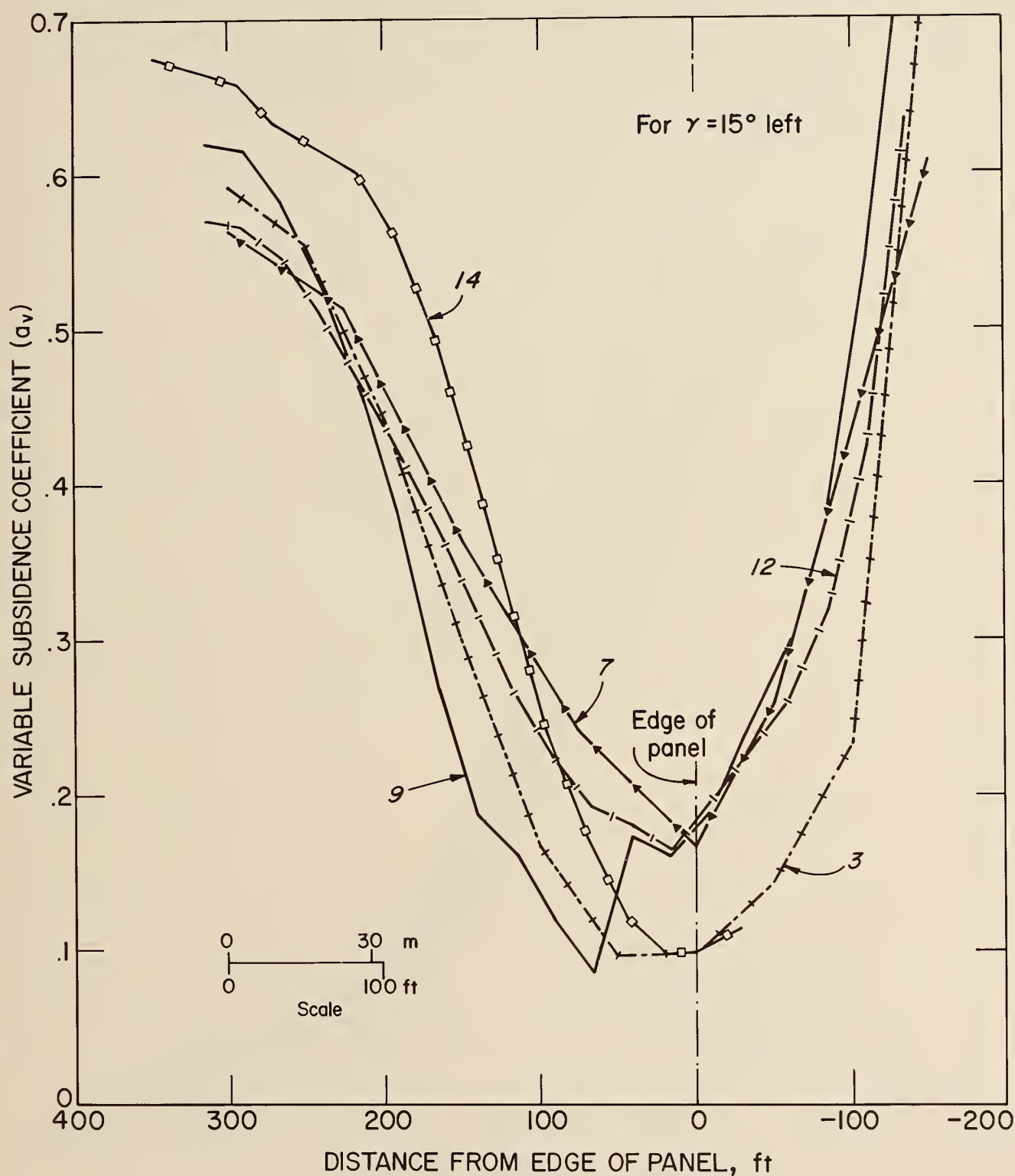
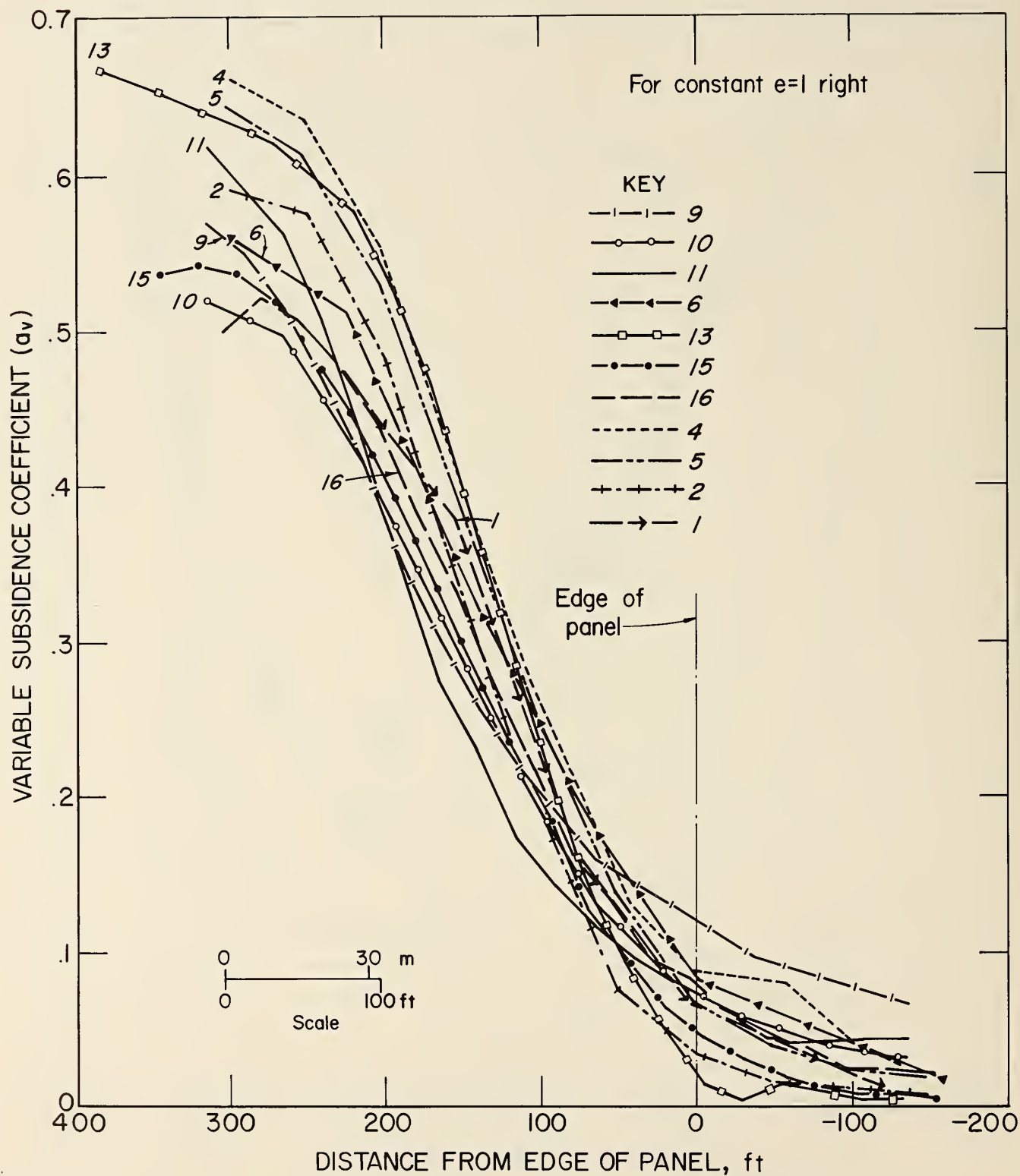


FIGURE 6. - Variable subsidence coefficient for $\gamma = 15^\circ$ left.

FIGURE 7. - Variable subsidence coefficient for $e = 1$ right.

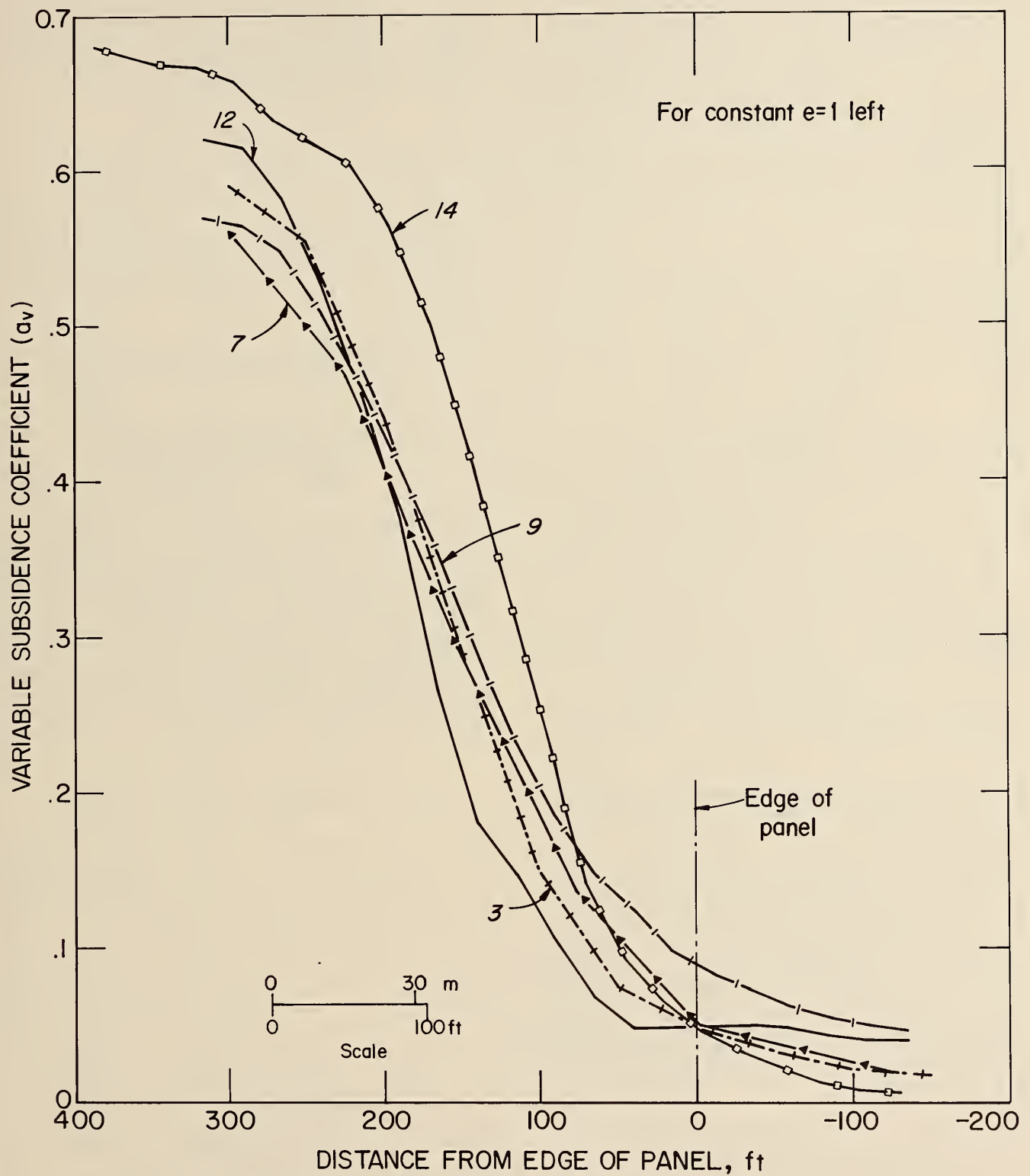


FIGURE 8. - Variable subsidence coefficient for $e = 1$ left.

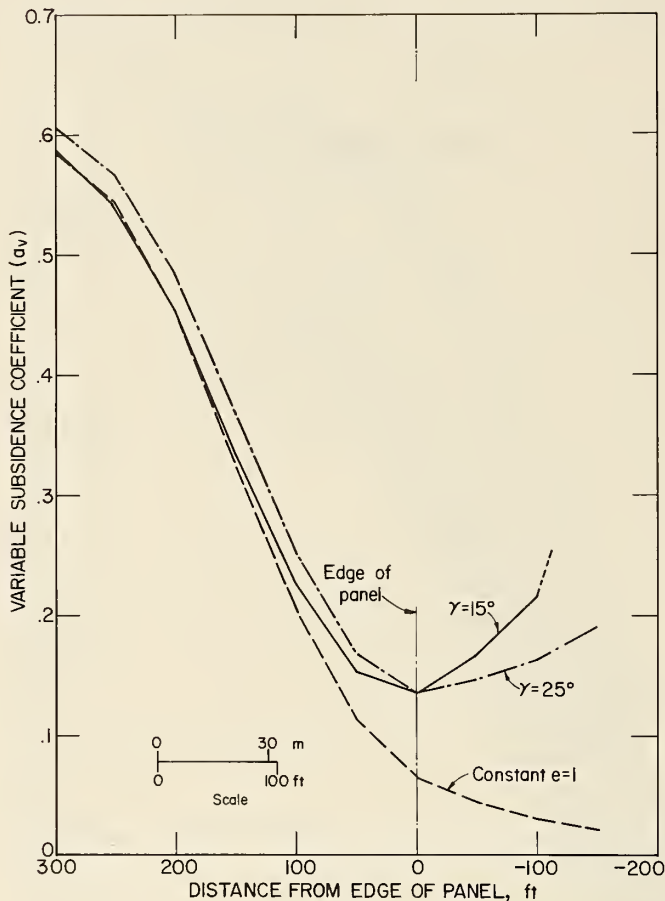


FIGURE 9. - Averaged values of variable subsidence coefficients.

standard deviations to the averaged values of subsidence coefficients would be satisfactory.

Figure 9 shows averaged values of the subsidence coefficient a_v for $\gamma = 25^\circ$ and $\gamma = 15^\circ$ and for constant value of efficiency coefficient $e = 1$ for all points.

Regression analysis of the subsidence coefficients from all sites on the location relative to the edge of the panel has yielded a third-degree polynomial equation with a coefficient of correlation of 0.9999.

For $\gamma = 25^\circ$

$$a_v = -3.587 \times 10^{-8} X^3 + 1.628 \times 10^{-5} X^2 - 9.105 \times 10^{-5} X + 1.359 \times 10^{-1}$$

where X is the distance in feet from the edge of the panel toward the centerline.

For the points located outwards of the edge of the panel, $X = 0$.

Then, the subsidence of any point toward the centerline will be

$$s_i = m e_i \times a_{vi}$$

and outwards $s_i = m e_i \times 0.1359$.

Efficiency coefficients e_i are tabulated in table 1 for different mining conditions. Interpolation will be necessary, where the ratios

$$\frac{W}{H} = \frac{\text{width of the panel}}{\text{thickness of the overburden}}$$

$$\frac{X}{W} = \frac{\text{distance in feet from the edge of the panel}}{\text{width of the panel}}$$

do not match the values in the table.

As an example, given a point located 100 ft inside the edge of a 600-ft-wide panel, calculate the subsidence if the overburden is 684 ft thick and extracted thickness is 5.5 ft.

Using table 1, first determine the values of w/H and X/W where

w = width of panel,

H = thickness of overburden,

and X = distance inside edge of panel.

$$w/H = 600/684 = 0.88 \quad X/w = 100/600 = 0.17$$

The closest values in the table are

		x/w	
		0.20	0.15
w/h	0.8	0.818	0.765
	0.9	0.841	0.786

By interpolation, the efficiency coefficients for $X/w = 0.17$ at $w/H = 0.8$ and $w/H = 0.9$ are calculated:

$$((0.818 - 0.765)/5) \times 2 + 0.765 = 0.786;$$

$$((0.841 - 0.786)/5) \times 2 + 0.786 = 0.808.$$

From these, the efficiency coefficient for $w/H = 0.88$ and $X/w = 0.17$ can be interpolated:

$$((0.808 - 0.786)/10) \times 8 + 0.786 = 0.803.$$

Using the Bals algorithm to compute the precise efficiency coefficient for the above point, a value of 0.8017 is obtained. The use of either value in the regression equation yields a predicted subsidence of 1.12 ft.

Coefficient a_v can be defined directly from figure 10 for any point identified by the distance in feet from the edge of the panel.

As shown in table 2, the majority of the field data on which the analyses are based comes from longwall panels with a width of about 600 ft or less. Only one panel is 940 ft wide.

To avoid any guesswork, the polynomial equation has been developed for points with maximum distance 300 ft from the edge of the panel or up to the centerline, whichever comes first. Only for panels much wider than 600 ft and overburdens in excess of 800 ft would subsidences around the centerline have to be adjusted to the shape of the precomputed partial profile.

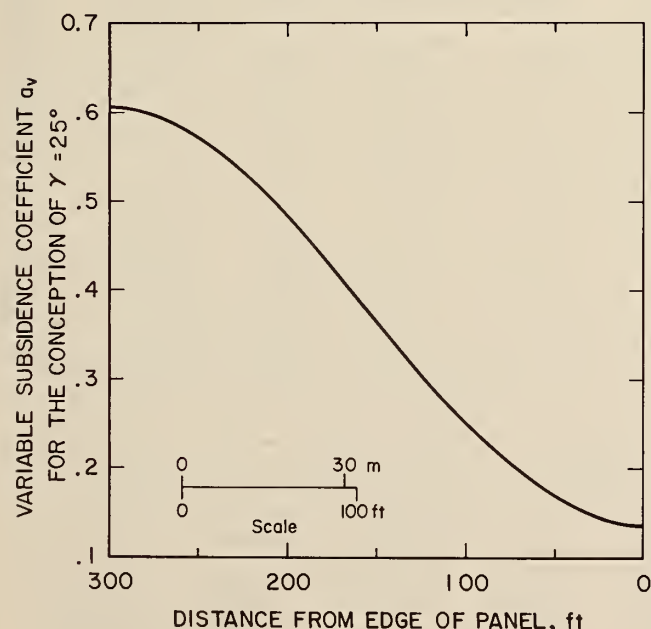


FIGURE 10. - Variable subsidence coefficient for $\gamma = 25^\circ$.

The equation $s_i = m e_i a_v$ for subsidence precomputation is a combination of principles on which both influence and profile functions are based.

Efficiency coefficient e represents the principles of influence functions, and a_v represents the principles of profile functions. Such a combination seems to be justified by at least two logical reasons:

1. Whatever mining geological conditions are involved, only a certain mined-out area influences the movement of a surface point. Coefficient e provides for that and also for variable mining conditions, namely for $\frac{w}{H}$ ratio.

2. At the same time, geological conditions vary for different mining areas. The introduction of a variable subsidence coefficient seems to be the only logical solution to the problem for mining areas where lithological effect on subsidence characteristics is so overwhelming.

As previously stated, the regression analysis of the variable coefficient a_v has been performed for the angles of draw $\gamma = 25^\circ$ and $\gamma = 15^\circ$ and for constant $e = 1$. The reason is as follows:

One cannot define the exact value of the angle of draw for hypothetically homogeneous overburden, i.e., overburden without the presence of highly resistive hard rock units. Only by comparing results from several conceptions can the most appropriate be chosen.

Table 3 contains the computed values of a_v along each profile with averaged values of \bar{a}_v and standard deviations.

It must be emphasized that the magnitude of standard deviations to a_v only cannot determine which conception is the best. They are influenced by corresponding efficiency coefficients, which differ for each point and different mining conditions.

For a better understanding, a practical case was analyzed, namely the profile for No. 2 Mine. The width of the panel is $w = 600$ ft, and the coal seam thickness is $m = 5.5$ ft.

Table 4 shows, for all three conceptions, the comparison between measured and precomputed subsidences and comparison of standard deviations $\pm \sigma_i$ in feet

TABLE 3. - Variable subsidence coefficients (a_v) along individual profiles with averaged values (\bar{a}_v) and standard deviations ($\pm\sigma_v$)

Mine	Distance inward, ¹ ft						Edge of panel (0)	Distance outward, ¹ ft		
	300	250	200	150	100	50		-50	-100	-150
$\gamma = 25^\circ$										
1....	NA	NA	0.480	0.410	0.275	0.182	0.135	0.170	0.210	0.240
2....	0.597	0.590	.515	.370	.235	.207	.068	.053	.055	.075
3....	.597	.571	.475	.335	.186	.106	.098	.105	.110	.150
4....	.662	.655	.565	.435	.308	.205	.175	.295	.230	.230
5....	.645	.627	.565	.440	.318	.200	.135	.120	.112	.124
6....	.587	.530	.445	.335	.230	.155	.100	.105	.112	.115
7....	.586	.564	.502	.405	.315	.235	.167	.190	.170	.150
8....	.600	.530	.425	.335	.270	.234	.245	.265	.295	.320
9....	.610	.571	.487	.380	.267	.200	.180	.196	.225	.225
10....	.542	.505	.430	.340	.245	.175	.145	.153	.165	.190
11....	.610	.545	.410	.285	.193	.152	.145	.145	.200	.300
12....	.622	.571	.445	.250	.154	.150	.180	.210	.248	.248
13....	.635	.600	.535	.405	.255	.130	.042	.015	NA	NA
14....	.660	.621	.572	.432	.250	.128	.100	.122	.137	.300
15....	.575	.525	.450	.350	.255	.152	.098	.065	.065	.055
16....	NA	.540	.460	.375	.265	.192	.157	.135	.110	.135
\bar{a}_v609	.570	.485	.368	.251	.169	.136	.147	.163	.191
$\pm\sigma_i$033	.043	.053	.054	.045	.041	.050	.074	.070	.083
$\gamma = 15^\circ$										
1....	NA	NA	0.438	0.365	0.225	0.128	0.065	0.039	0.021	0.006
2....	0.591	0.576	.482	.327	.189	.075	.035	.016	.011	.009
3....	.591	.555	.442	.293	.149	.075	.049	.033	.022	.018
4....	.662	.633	.547	.398	.260	.128	.088	.081	.043	.018
5....	.645	.613	.529	.387	.253	.138	.069	.039	.025	.018
6....	.562	.529	.455	.344	.245	.158	.084	.062	.042	.020
7....	.562	.501	.407	.287	.185	.108	.051	.039	.027	.015
8....	.558	.487	.378	.275	.203	.151	.120	.093	.078	.062
9....	.566	.523	.430	.315	.203	.133	.089	.066	.052	.045
10....	.513	.473	.387	.288	.192	.117	.074	.048	.037	.030
11....	.603	.529	.382	.242	.153	.104	.073	.046	.044	.045
12....	.617	.548	.410	.213	.121	.056	.049	.049	.041	.040
13....	.635	.603	.537	.400	.234	.101	.022	.013	.006	.005
14....	.658	.620	.570	.437	.253	.102	.049	.025	.009	.006
15....	.537	.489	.404	.296	.198	.102	.048	.023	.008	.005
16....	NA	.501	.440	.340	.209	.126	.079	.044	.025	.022
\bar{a}_v593	.545	.452	.325	.205	.113	.065	.045	.031	.023
$\pm\sigma_i$046	.053	.063	.061	.040	.028	.024	.022	.019	.017
Distance inward, ¹ ft							Edge of panel (0)	Distance outward, ¹ ft		
300								-50	-100	
250										
200										
150										
100										
50										
CONSTANT e = 1										
1....	NA	NA	0.435	0.365	0.240	0.165	0.120	0.400	0.690	
2....	0.590	0.575	.480	.330	.210	.095	.068	.070	.110	
3....	.590	.555	.445	.300	.166	.096	.098	.145	.235	
4....	.665	.640	.555	.405	.285	.170	.169	.525	.700	
5....	.645	.612	.526	.393	.281	.180	.131	.152	.190	

NA Not applicable.

¹From edge of panel.

TABLE 3. - Variable subsidence coefficients (a_v) along individual profiles with averaged values (\bar{a}_v) and standard deviations ($\pm\sigma_j$)--Continued

Mine	Distance inward, ¹ ft						Edge of panel (0)	Distance outward, ¹ ft	
	300	250	200	150	100	50		-50	-100
CONSTANT e = 1--Continued									
6....	0.562	0.500	0.410	0.298	0.207	0.142	0.103	0.195	0.285
7....	.565	.530	.465	.365	.280	.216	.168	.310	.430
8....	.560	.486	.385	.300	.245	.213	.247	.320	.440
9....	.570	.525	.440	.340	.240	.185	.185	.250	.325
10....	.505	.445	.365	.277	.200	.150	.163	.215	.360
11....	.607	.535	.385	.256	.175	.140	.153	.189	.400
12....	.620	.550	.415	.220	.135	.140	.180	.325	.480
13....	.632	.600	.535	.400	.232	.112	.038	.030	.030
14....	.660	.620	.575	.440	.255	.135	.100	.120	.140
15....	.535	.481	.396	.305	.220	.135	.098	.083	.067
16....	NA	.500	.430	.335	.238	.170	.155	.165	.180
\bar{a}_v593	.544	.453	.333	.226	.153	.136	.218	.316
$\pm\sigma_j$047	.057	.065	.059	.042	.036	.052	.131	.202

NA Not applicable. ¹From edge of panel.

for a given case. The distribution of σ_j (ft) = $m\epsilon_j\sigma_j$ for each conception is the decisive factor for their evaluation. It shows which conception reflects best the reality in situ. Despite the relatively small differences between σ (ft), the conception for $\gamma = 25^\circ$ clearly shows the best results.

Small differences between individual conceptions are due to the nature of the data from which they were derived. As shown on table 2, the range of differences between mining conditions (width of the panels, overburden thickness) at individual test sites is relatively small. It means that for mining conditions similar to those at the test sites, all three conceptions could be used for subsidence precomputation with good results. The question remains, which one would yield the best results, should it be used for precomputation at a site with substantially different mining conditions? For example, let us assume that we have to precompute subsidences over a longwall panel 350 ft wide with 1,800 ft of overburden and coal seam thickness of 6 ft. The results are shown on figure 11. The difference between individual conceptions is obvious.

From the logical point of view, the conception for constant $e = 1$ is out of

competition, since it virtually neglects different mining conditions and the magnitude of maximum subsidence becomes only a function of the width of the panel. More difficult is the choice between the conceptions $\gamma = 15^\circ$ and $\gamma = 25^\circ$. The question can be answered only after having sufficient field data.

From available data the conception of $\gamma = 25^\circ$ shows the best results. Therefore, this conception is considered as the most applicable.

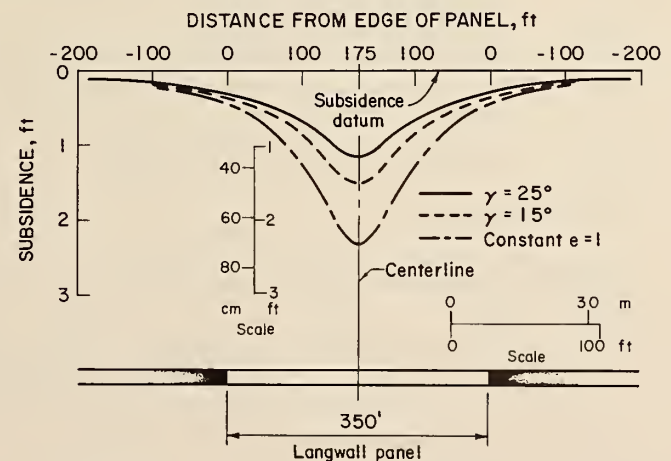


FIGURE 11. - Precomputed subsidence profiles for $\gamma = 25^\circ$ and $\gamma = 15^\circ$ for $e = 1$. ($H = 1,800$ ft, $w = 350$ ft).

TABLE 4. - Comparison of precomputed values for $\gamma = 25^\circ$, $\gamma = 15^\circ$, and $e = 1$

Values ¹	Distance inwards, ² ft						Edge of panel (0)	Distance outward, ² ft		
	300	250	200	150	100	50		-50	-100	-150
	$\gamma = 25^\circ$									
\bar{a}_v	0.606	0.567	0.485	0.368	0.251	0.169	0.136	0.146	0.163	0.190
$\pm\sigma_i$032	.042	.053	.054	.045	.041	.055	.074	.070	.083
e_i990	.971	.933	.878	.802	.692	.500	.309	.198	.121
$\sigma_i e_i$032	.041	.049	.047	.036	.028	.027	.022	.014	.010
$\pm\sigma_i$ft..	.18	.22	.27	.26	.20	.16	.15	.13	.08	.060
sF.....ft..	3.25	3.17	2.65	1.80	1.04	.41	.19	.09	.06	.050
sP.....ft..	3.30	3.04	2.47	1.77	1.12	.64	.37	.23	.15	.090
$\pm\Delta_i$ft..	.05	-.13	-.18	-.03	.08	.23	.18	.14	.09	.040
$\gamma = 15^\circ$										
\bar{a}_v	0.588	0.540	0.453	0.333	0.226	0.153	0.136	0.218	0.316	NA
$\pm\sigma_i$046	.057	.065	.059	.042	.036	.052	.131	.202	NA
e_i	1.0	1.0	1.0	.976	.899	.766	.5	.235	.101	NA
$\sigma_i e_i$046	.057	.065	.058	.038	.038	.026	.03	.02	NA
$\pm\sigma_i$ft..	.25	.31	.36	.32	.21	.16	.14	.17	.11	NA
sF.....ft..	3.25	3.17	2.65	1.80	1.04	.41	.19	.09	.06	NA
sP.....ft..	3.24	2.97	2.49	1.78	1.11	.64	.37	.28	.18	NA
$\pm\Delta_i$ft..	-.01	-.20	-.16	-.02	.05	.17	.18	.19	.12	NA
CONSTANT $e = 1$										
\bar{a}_v	0.587	0.545	0.452	0.325	0.205	0.113	0.065	0.045	0.031	0.023
$\pm\sigma_i$05	.053	.063	.061	.04	.028	.024	.022	.019	.017
$\pm\sigma_i$ft..	.28	.29	.35	.34	.22	.15	.13	.12	.1	.09
sF.....ft..	3.25	3.17	2.65	1.80	1.04	.41	.19	.09	.06	.05
sP.....ft..	3.23	3.	2.49	1.79	1.13	.62	.36	.25	.17	.13
$\pm\Delta_i$ft..	-.02	-.17	-.16	-.01	.09	.21	.17	.16	.11	.08

NA Not applicable.

¹Nomenclature explanations:

\bar{a}_v = averaged variable subsidence coefficient as computed for individual conceptions ($\gamma = 25^\circ$, 15° , $e = 1$).

σ_i = standard deviations to the averaged values of the subsidence coefficient \bar{a}_v for individual conceptions.

e_i = efficiency coefficients.

σ_i (ft) = $m e_i \sigma_i$.

sF (ft) = subsidences as measured in the field.

sP (ft) = precomputed subsidences $SP = m.e_i a_{vi}$ (inwards)
 $SP = m.e_i 0.1359$ (outwards).

Δ_i (ft) = differences between measured and precomputed subsidences.

²From edge of panel.

SENSITIVITY TESTS

The subsidences of all 16 half profiles from 11 test sites with the total of 189 surface points involved in the regression analysis have been computed using the polynomial equation developed for $\gamma = 25^\circ$.

Figure 12 shows the distribution of deviations between computed and directly measured subsidences with regard to the distance from the edge of the panel. Table 5 shows that for 89 pct of all points the deviation is between 0.00 and 0.29 ft, and for 74 pct it is between 0.00 and 0.19 ft.

Such results must be considered satisfactory, especially if the possible sources of these deviations are considered:

1. The effect of lithology on subsidence characteristics is not absolutely the same at all investigated sites.

TABLE 5. - Summary of the distribution of deviations

Deviations ft	Number of points	Pct of total
0.00-0.09.....	81	43
.10- .19.....	57	31
.20- .29.....	29	15
.30- .39.....	14	7
.40- .49.....	4	2
.50- .59.....	4	2
Total.....	189	100

2. If the estimate of the extracted coalbed thickness is inaccurate, the full value of the error affects the precalculation.

TIME COEFFICIENT

Figures 13 and 14 show characteristics of time coefficient, involving the subsidence process. Ninety-five pct of total subsidence usually occurs within 2

months of passing of the longwall face. Residual subsidences may occur during several more months. In no case have they lasted for more than 1 year.

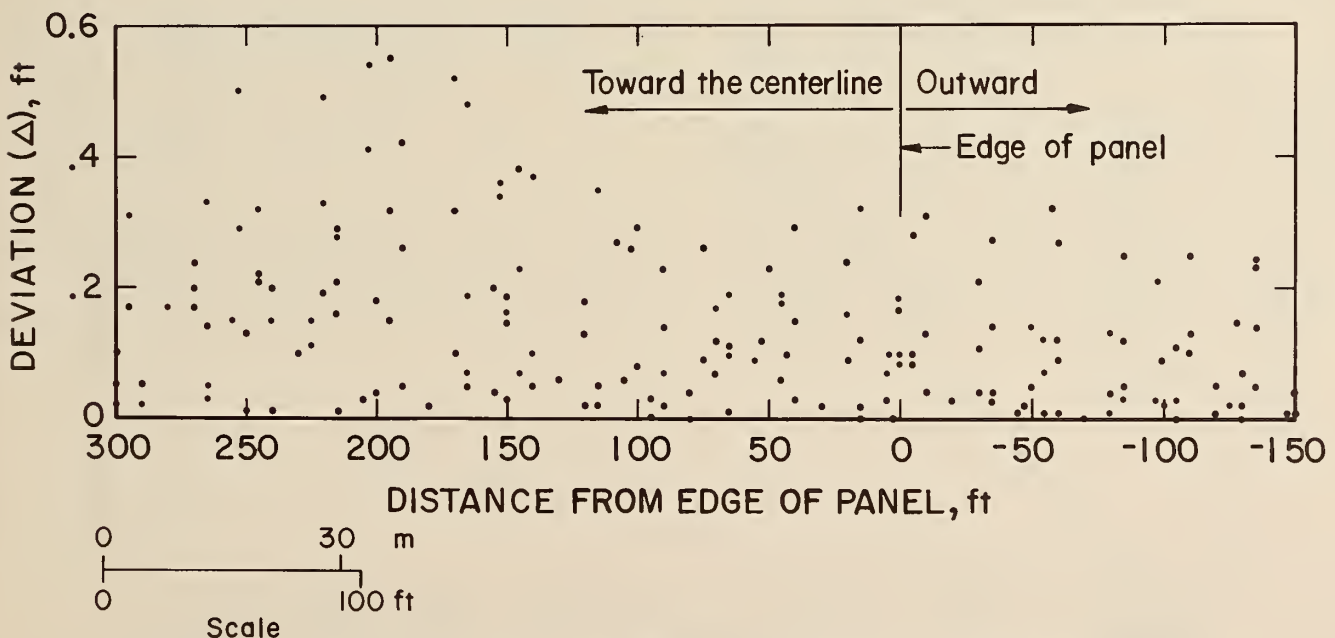


FIGURE 12. - Distribution of deviations between computed and measured subsidences.

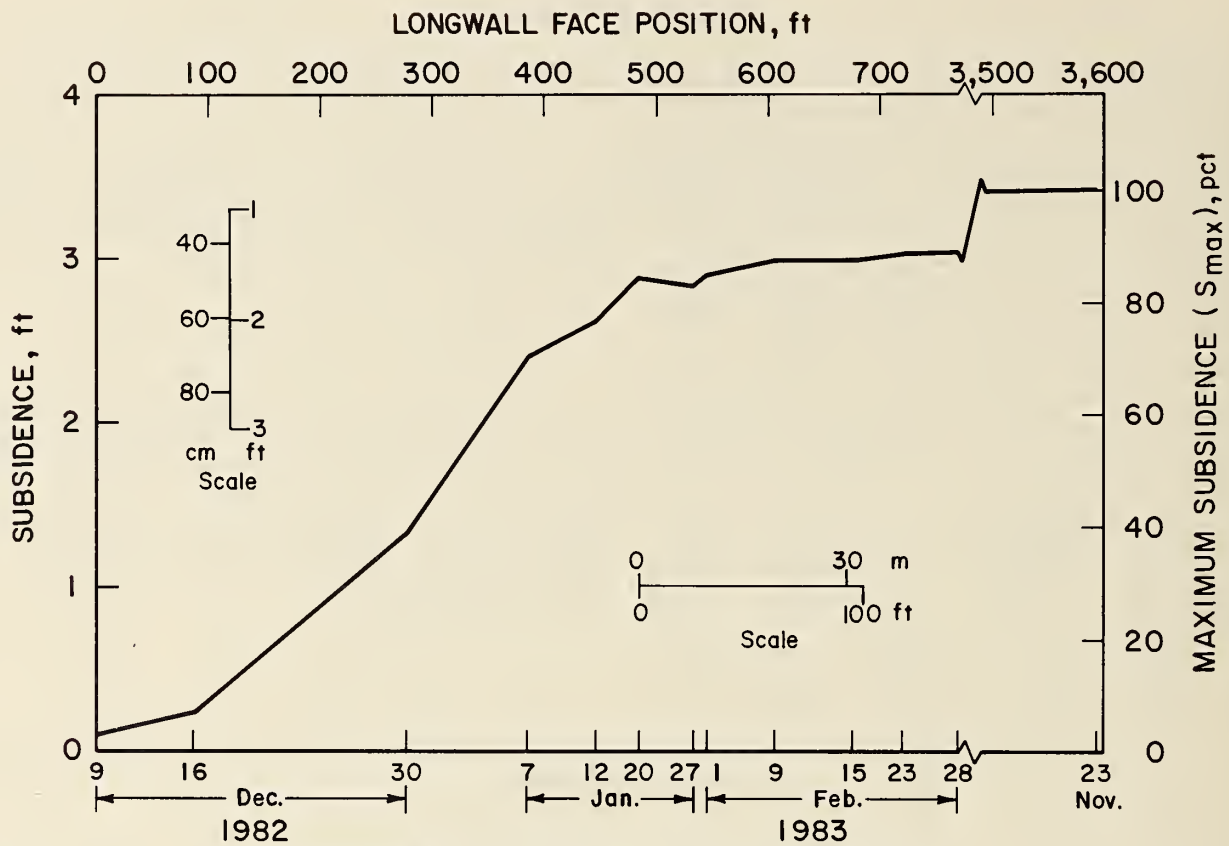


FIGURE 13. - Characteristics of time coefficient.

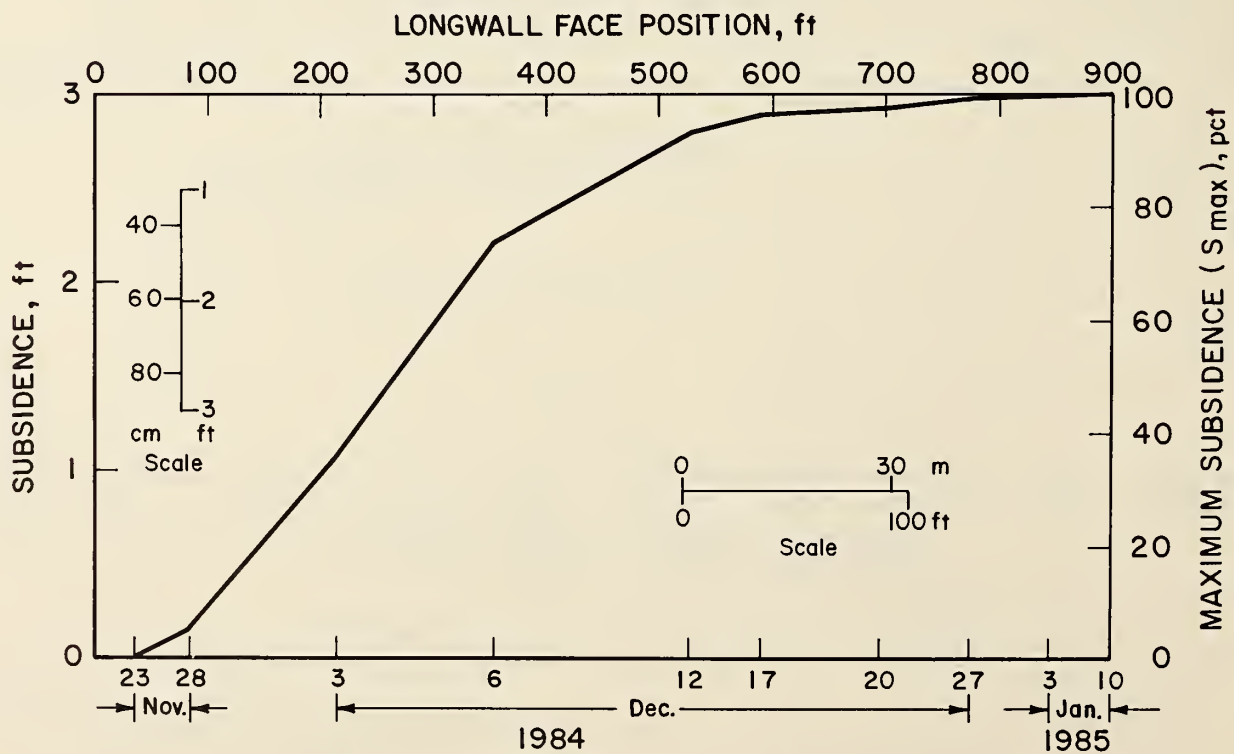


FIGURE 14. - Characteristics of time coefficient.

The extremely low average subsidence coefficient

$$\bar{a} = \frac{VS}{VE} = \frac{\text{Volume of subsidence trough}}{\text{Volume of the coal extracted}} = 0.35$$

in comparison with $a = 0.6$ to 0.8 in European conditions may be a cause for some concern. It means that about 65 pct of the volume of extracted coal has been left as underground voids. This is due to high resistance of hard rock units, decreasing toward the centerline of the panel.

At this time, it is difficult to predict whether such a new equilibrium within the overburden is permanent or not. On the test sites that were remeasured 2 years after mining activities had finished, no additional subsidences had occurred.

CONCLUSION

Good results for subsidence precomputation by the developed formula have been proven by the sensitivity tests.

Despite this fact, the methodology must be considered to be a preliminary one. The regression analysis is based on a still limited amount of field data with relatively similar mining conditions. Its applicability in other mining areas has to be tested. The advantages of the developed methodology are--

1. It can be used by persons without any previous knowledge of the theory of subsidence.

2. It is relatively simple and fast in comparison with existing predictive methods.

3. It eliminates the use of inaccurately estimated functional parameters (maximum subsidence, location of the inflection point, etc.), necessary for existing predictive methods.

BIBLIOGRAPHY

Adamek, V., and P. W. Jeran. Evaluation of Existing Predictive Methods for Mine Subsidence in the U.S. Paper in Proceedings First Conference on Ground Control in Mining, ed. by S. S. Peng. West Virginia University, July 1981, pp. 209-219.

_____. Evaluation of Surface Deformation Characteristics Over Longwall Panels in the Northern Appalachian Coal Field. Paper in Proceedings International Symposium on Ground Control in Longwall Coal

Mining and Mining Subsidence - State of the Art (Honolulu, Hawaii, 1982). AIME, 1982, pp. 183-197.

Bals, R. Beitrag zur Frage der Vorausberechnung Bergbaulicher Senkungen (Contribution to the Problem of Precalculating Mining Subsidence). Mitt. aus dem Markscheidewesen 1931/1932, pp. 98-111 (in German).

Niemczyk, O. Bergschadenkunde (Study of Mine Damages). Verlag Gluckauf, G.m.b.H., 1949, p. 107 (in German).

APPENDIX

To facilitate the use of this precalculation methodology, a basic computer program was written for use on a personal computer. The program prompts the user for the values of point location (distance from the edge of the panel in feet), overburden thickness, extracted coalbed thickness, and width of the panel. It then computes the efficiency coefficient, e , using an algorithm based on Bals' theory. This value is used in the developed regression equation to calculate the subsidence of the input point. The result is output to the screen.

Values of the efficiency coefficients e cannot be tabulated within the area of $H \tan 25^\circ$ from the beginning and the end of the panel, since within this area there are irregular partial areas of influence. Therefore, the values of coefficient e for surface points within this area have to be individually calculated.

As previously stated, the definition of efficiency coefficient e is based on an assumption that the extracted area consists of an infinitely large number of small particles i , each of them influencing the movement of a surface point by a force inversely proportional to the square of its distance f from it. The full area of influence is defined by a conical section with its base at the top of the coal seam and the apex at surface reference point P (fig. A-1). The angle of draw γ is equal to one half of the interior angle of the cone. For flat seams, the area of influence is a circle.

Only that part of the full area of influence that overlaps the extracted area influences the magnitude of displacement of investigated point P .

Based on previously expressed assumptions, the acting force on point P for the full area of influence is

$$K = \int_{\gamma_0}^{\gamma_1} \frac{i}{f^2} \gamma_1 \cdot$$

Since $f = \frac{H}{\cos \gamma}$ (H = overburden thickness)

$$K = \frac{i}{H^2} \int_{\gamma_0}^{\gamma_1} \cos^2 \gamma_1 d\gamma_1.$$

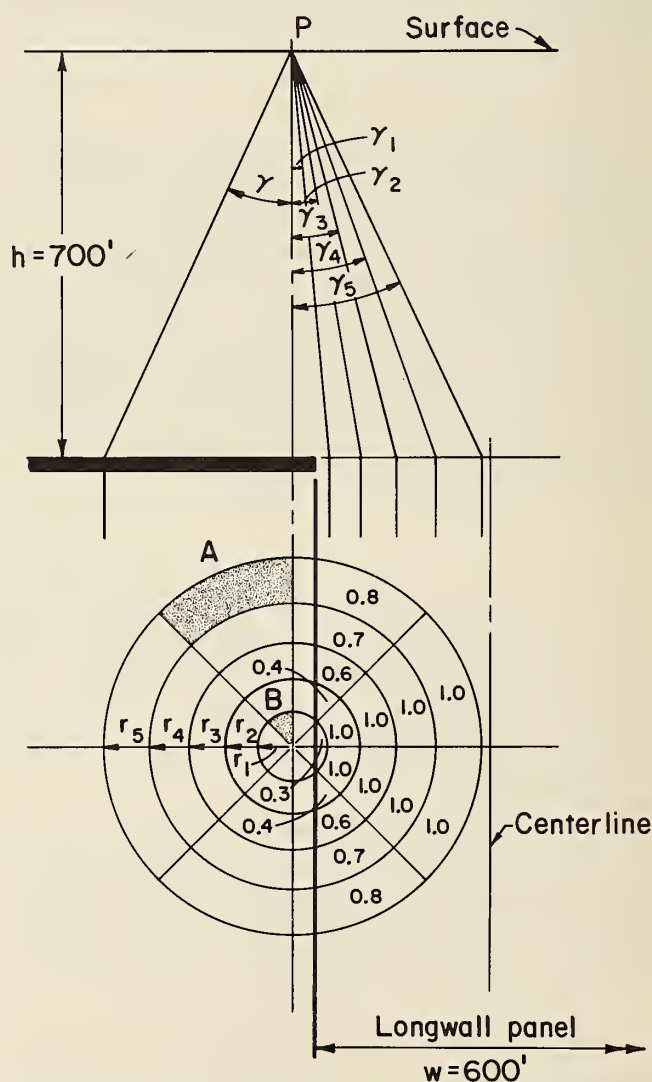


FIGURE A-1. - Graphic definition of subsidence by Bals' theory.

After neglecting $\frac{i}{H^2}$ for flat coal seams and for $\gamma_0 = 0$ to γ_1

$$K = \frac{1}{2} [(\sin \gamma \cos \gamma + \gamma)]_0^1$$

$$= \frac{1}{4} (\sin 2\gamma_1 + 2\gamma_1).$$

The expression $2\gamma_1$ in the equation is in radians.

Example: For $\gamma = 25^\circ$ and after neglecting constant factors $1/4$

$$K = \sin 50^\circ + 50^\circ = 0.766 + \frac{50^\circ \pi}{360^\circ}$$

$$= 0.766 + 0.872 = 1.638$$

Figure A-2 shows the curve $\sin 2\gamma + 2\gamma$ for K from $\gamma = 0^\circ$ to 35° .

To define the coefficient of efficiency e for an area that is only a part of the full area of influence, Bals' theory divides the full area into a certain (theoretically unlimited) number of areas of equal influence, by annular circles and diameters.

For better understanding and practical use, this is demonstrated in the following example (fig. A-1):

Efficiency coefficient e has to be defined for point P.

Width of the panel $w = 600$ ft.

Thickness of the overburden $H = 700$ ft.

Angle of draw $\gamma = 25^\circ$.

By experience, reasonable accuracy can be obtained by dividing the full area of influence into 40 sections, by 4 diameters and 5 concentric circles. Then each section bears 2.5 pct of the total influence. The influence of section B is equal to the influence of the larger but more distant section A.

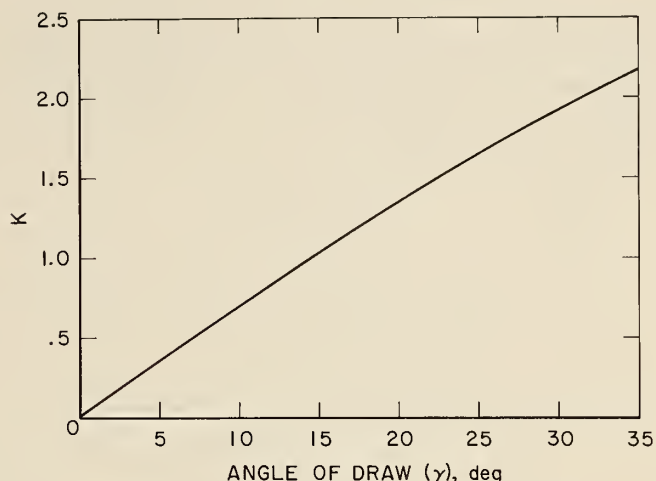


FIGURE A-2. - The curve $\sin 2\gamma + 2\gamma$ by Bals.

First, one must define values of radii of single-zone areas:

For $\gamma = 25^\circ$, the radius of the full area is

$$r = r_5 = 700' \times \tan 25^\circ = 700'$$

$$\times 0.466 = 326'$$

and $K = 1.638$.

To obtain single-zone areas of equal influence, a particular k must be assigned to each of them.

For five zones,

$$k_1 = \frac{K}{5} \times 1; k_2 = \frac{K}{5} \times 2; \text{etc.}$$

For each k_i , the corresponding zone angle γ_i is determined from the curve $\sin 2\gamma + 2\gamma$ (fig. A-2):

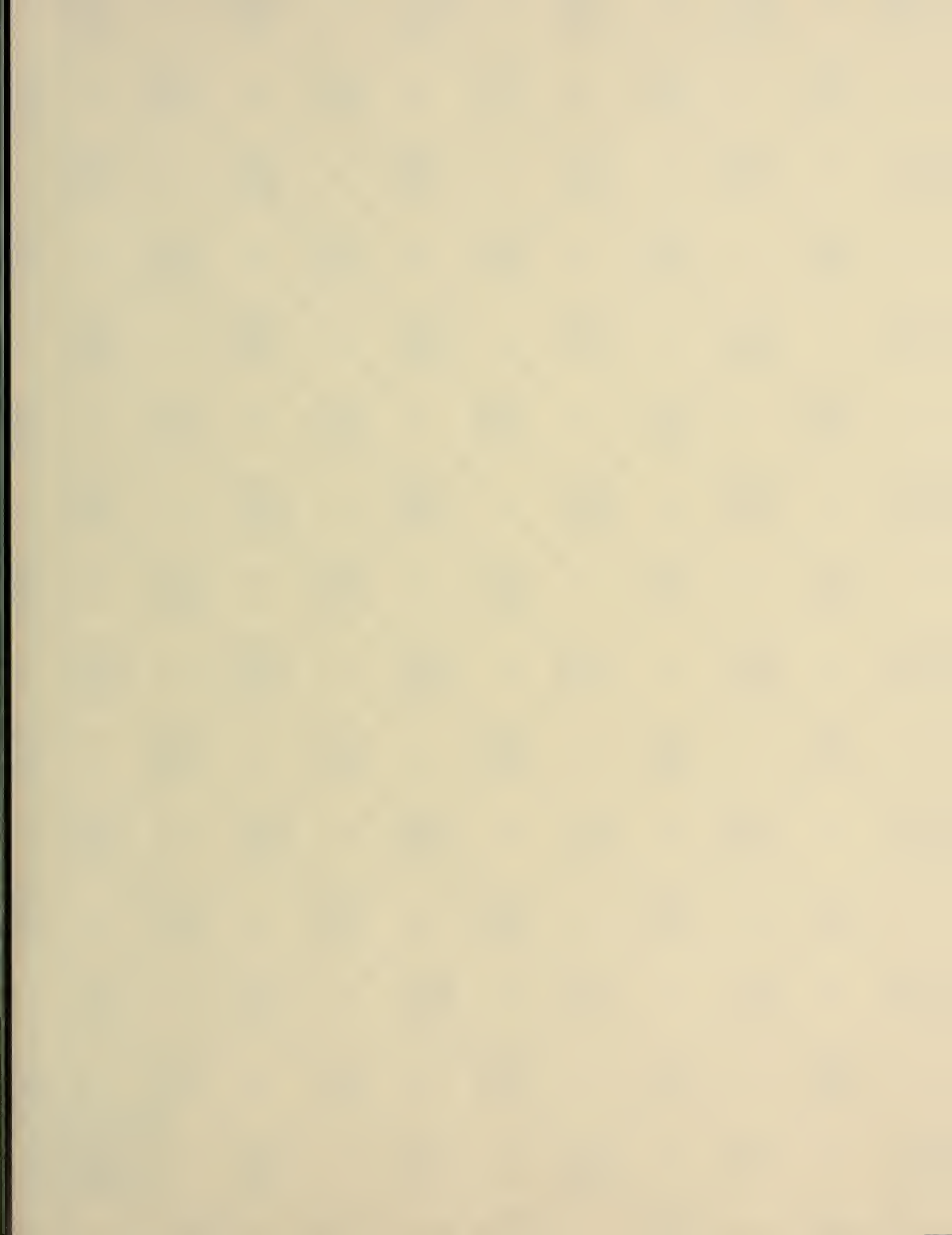
Zone	k_i	γ_i , deg	$r_i = H \tan \gamma_i$, ft
1.....	0.3276	4.6	56.3
2.....	.6552	9.5	117.1
3.....	.9828	14.4	179.7
4.....	1.3104	19.5	247.9
5.....	1.6380	25	326

Each zone area is divided by diameters into eight sections for better estimation of extracted area. Parts of sections can be measured by planimeter or simply estimated:

<u>Zone</u>	<u>Sections</u>
1	NA 0.3 + 0.3 NA = 0.6
2	0.4 + 1.0 + 1.0 + 0.4 = 2.8
3	.6 + 1.0 + 1.0 + .6 = 3.2
4	.7 + 1.0 + 1.0 + .7 = 3.4
5	.8 + 1.0 + 1.0 + .8 = 3.6
	Total = 13.6
	13.6 × 2.5% = 34%
NA Not applicable.	

Efficiency coefficient e for point P is 0.34. For cases that do not require high accuracy, single radii of concentric circles can be determined by dividing radius of the influence area into five equal parts. This method is not limited as to the shape of the extraction area.

H 71 86





HECKMAN
BINDERY INC.

JAN 86

N. MANCHESTER,
INDIANA 46962

LIBRARY OF CONGRESS



0 002 955 970 3